North Carolina Agricultural and Technical State University

Aggie Digital Collections and Scholarship

2019

Multi-scale Interactions Between the Diurnal Cycle, the MJO, and Convectively Coupled Equatorial Waves over the Maritime Continent

Lakemariam Yohannes Worku
North Carolina Agricultural and Technical State University

Recommended Citation

Multi-scale Interactions Between the Diurnal Cycle, the MJO, and Convectively Coupled Equatorial Waves over the Maritime Continent

Lakemariam Yohannes Worku

North Carolina A&T State University

A dissertation submitted to the graduate faculty
in partial fulfillment of the requirements for the degree of
DOCTOR OF PHILOSOPHY
Program: Energy and Environmental Systems
Concentration: Atmospheric Science
Major Professor: Dr. Ademe Mekonnen

Greensboro, North Carolina
2019

The Graduate College
North Carolina Agricultural and Technical State University

This is to certify that the Doctoral Dissertation of

Lakemariam Yohannes Worku

has met the dissertation requirements of
North Carolina Agricultural and Technical State University

Greensboro, North Carolina
2019

Approved by:

Dr. Ademe Mekonnen
Major Professor

Dr. Yun-Lang Lin
Committee Member

Dr. Solomon Bililign
Committee Member

Dr. Carl Schreck III
Committee Member

Dr. Jing Zhang
Committee Member

Dr. Niroj Aryal
Graduate Faculty Representative

Dr. Keith Schimmel
Program Director

Dr. Clay S. Gloster, Jr.
Interim Dean, The Graduate College

Biographical Sketch

Lakemariam Yohannes Worku was born in Gondar, Ethiopia, and grew up in a small town called Kimrid Dingay, Ethiopia. He went to elementary and secondary school in Kimir Dingay, Ethiopia. And later, he attended college preparatory school in Debre Tabore, 30 km away from Kimir Dingay. In 2003 he went to study meteorology science for his undergraduate study at Arba Minch University and graduated in July 2007.

In 2011, while he was working at the National Meteorological Agency (NMA) of Ethiopia, he started his graduate school at Bahir Dar University in Water Resource Engineering (Specialization in Engineering Hydrology) and graduated in January 2014. In January 2016, he started a new challenge, which is starting his Ph.D. program at North Carolina A&T State University in Greensboro, North Carolina.

Professionally he has been meteorologist, infrastructure expert, hydrology lecturer, and weather and climate consultant for over eight years. In November 2007, he joined National NMA as a meteorologist. He worked at NMA for almost seven years as a junior meteorologist and senior meteorologist. He worked in agrometeorology, hydrometeorology, and development meteorology departments of NMA. In 2015, he started his teaching career at Arba Minch University as a hydrology lecturer in Hydraulics and Water Resource Engineering department. Within that same year, he was also working as a weather and climate consultant for a regional Non-Governmental Organization (NGO) called Horn of Africa Regional Environmental Center and Network (HoAREC&N) in Gambella, Ethiopia. Since January 2016, he worked as a graduate research assistant and graduate teaching assistant at North Carolina A&T State University.

Dedication

I would like to dedicate this work to my heroes: my late grandma Emahuay Kirikim

Tsegaye, my late mom Yengusie Dinkayehu, and my late aunt Zewdalem Dinkayehu.

Acknowledgments

I would like to thank God for giving me all the blessings and the strength to overcome so many challenges in life. I am blessed with the spiritual support, guidance, and protection of St. Virgin Mary, St. Hana, St. Arsema, Archangel Gabriel, Archangel Michael, and all saints and angels.

All my family has been supportive throughout this journey, and I would like to thank them from the bottom of my heart. My children Blen, Soliana, Danat, and Caleb have been the guiding light through all the trials and tribulations of my journey. They are my ultimate motivation in life.

I would like to thank my advisor Dr. Ademe Mekonnen for giving me this fantastic opportunity. He has been so gracious from the start, and I learned a lot of academic and social skills from him. In addition to my principal advisor, I would like to thank Dr. Carl Schreck for co-advising me and his continued support in improving my coding, writing, and organizing skills, as well as for sharing his filtering data.

Dr. Keith Schimmel, director of Applied Science and Technology PhD program, was so supportive to this date on so many levels, and I appreciate his kindness. My professors and committee members Dr. Lin, Dr. Billilign, and Dr. Zhang, thank you for all the great advice and lessons you gave me for the past four years. Finally, I also would like to thank Dr. Aryal for his willingness to be part of my dissertation committee. Thank you all!

Table of Contents

List of Figures

List of Abbreviations

CCEWs	Convectively Coupled Equatorial Waves
CFSv2	Climate Forecast System version 2
CLAUS	Cloud Archive User Services
CLIVAR	Climate Variability and Predictability
CTP	Cloud-top Pressure
ECMWF	European Center for Medium-Range Weather Forecasting
ENSO	El Nino Southern Oscillation
ERA	ECMWF Re-Analysis
IR-WS	Infrared Weather State
ISCCP	International Satellite Cloud Climatology Project
LST	Local Standard Time
MC	Maritime Continent
MJO	Madden-Julian Oscillation
NCEP	National Center of Environmental Prediction
NESM	Naval Earth System Model
OLR	Outgoing Longwave Radiation
PFs	Precipitation Features
PNG	Papua New Guinea
SST	Sea Surface Temperature
Tb	Brightness Temperature
TD-Type	Tropical Depression
TMPA	TRMM Multispectral Precipitation Analysis
TRMM	Tropical Rainfall Measurement Mission

WSs   Weather States

Abstract

Given the Maritime Continent's (MC's) critical role in the global climate, examining

variations in diurnal cycle and its interaction with the Madden–Julian Oscillation (MJO), Kelvin

and Equatorial Rossby waves may lead to improved sub-seasonal forecasts. This study used

satellite data of TRMM, TRMM Precipitation Features (PFs), and convective classifications

from ISCCP. The convection becomes more organized through the afternoon and evening,

leading to peak rainfall over the islands around 1800–2100 local standard time (LST). Over the

next few hours, some of that rainfall transitions to stratiform rain over land. The convection then

propagates offshore overnight with rainfall peaking along the coast around 0300–0600 LST and

over oceans around 0600–0900 LST. The coastal and oceanic diurnal ranges also seem to be

larger in stratiform rainfall, in contrast to the land where convective precipitation dominates.

The diurnal cycle of rainfall and convection may influence by the presence of the MJO,

Kelvin waves, and Equatorial Rossby (ER) waves. The presence of MJO phases does not

modulate the morning rainfall over land rather it moderately modulates afternoon rainfall. The

MJO exerted a more significant impact on rainfall over the coast and ocean compared to land.

Well-organized convection is marginally higher in the afternoon than in the morning over the

MC. However, non-organized scattered convection peak over the coast and sea. The MJO

impacts the variability of both well-organized and scattered convection more than it does to

rainfall.

We classified wave phases into four types: wet, dry, increasing, and decreasing wave

phases. The wet wave phase is associated with active convection and high rain rate while the dry

wave phase is characterized by suppressed convection and less rainfall. Decreasing and

increasing phases serve as a transition between wet and dry phases. Rainfall over the MC peaks

during MJO wet phases and is minimum during dry phases. But Kelvin and ER wave phase effects on rainfall is weaker than the MJO. Kelvin wave dry and decreasing phases increase the organized deep convection over land but not much over the coast and sea. However, when an ER wave is in the wet and increasing phase, it shows a strong influence over all regions. There are shallow convection peaks when MJO and Kelvin wave phases are wet and decreasing while it is minimum during the dry wave phase. It peaks over land and coast when the ER wave phase is dry and increasing, respectively.

CHAPTER 1

Introduction

The Maritime Continent (MC) is a region located between the Indian and Pacific Oceans. This region consists of thousands of small and large islands surrounded by shallow seas and peninsulas (Fig. 1). The region is situated adjacent to an area of warmer sea surface temperatures (SSTs) and often referred to as the warm pool region (Birch et al. 2016; Sobel et al. 2011; Virts et al. 2013). Larger landmasses of the MC include Sumatra, Papua New Guinea (PNG), Borneo, and Java islands. Larger islands exhibit mountain peaks extending well over 2000 m above sea level. The complex terrain is mostly oriented southeast-northwest and has an essential effect in the organization of convection into different temporal and spatial scales (Mori et al., 2004; Sobel et al., 2011). Studies show that the high mountains and their orientation modulates rainfall (Ramage 1971) and atmospheric waves such as the Madden-Julian Oscillation (MJO; Zhang 2005; Wang and Liu 2011). In addition to obstructing wave propagation, the high terrain has a significant influence on large-scale circulations that have a far and broader impact on a global scale (Neale and Slingo 2003). The MC is a tropical region where multi-scale interaction between the diurnal cycle, intraseasonal scale variabilities (the MJO), and synoptic scale variability (Kelvin waves, and Equatorial Rossby waves) observed.

In this study, the intraseasonal variability is defined as variability between 30 and 120 days. The MJO is typical of the intraseasonal variability that varies between 30 - 90 days. Synoptic scale variability is defined as variability between 2 and 20 days. Equatorial waves such as Kelvin waves (2.5 - 17 days variability) and equatorial Rossby waves (6 - 32 days variability) are considered as synoptic-scale variability. Studies show that the MJO starts over the western Indian ocean in boreal winter and propagates eastward toward the West Pacific but sometimes

stalls or terminates over the MC (Hendon and Salby 1994; Birch et al. 2016; Majda and Yang 2016) due to its interaction with the high terrain. The diurnal cycle associated with the high terrain may play a role in influencing the MJO propagation (e.g., Hagos et al. 2016). On the other hand, the MJO can have a strong influence on the timing and amplitude of the diurnal cycle (e.g., Innes and Slingo 2006; Hagos et al. 2016), suggesting a two-way interaction. The two-way interaction between the diurnal cycle and the MJO and CCEWs convection over the MC is largely understudied.

1.1. Background

This section presents a background discussion of the diurnal cycle, MJO, Kelvin waves, and Equatorial Rossby waves to help interpretation in Sections 3 and 4.

1.1.1 Diurnal cycle

The most important modes of variability in the Tropics, generally, and in the MC, in particular, are the diurnal cycle and seasonal cycle (Yang and Slingo 2001). The diurnal cycle is related to differential heating, while the seasonal cycle is related to Earth's tilt away from or toward the sun. It is a dominant feature in the atmospheric variations and also a significant source variability of convection and precipitation over tropics (Mori et al. 2004; Yokoi et al. 2017; Kikuchi and Wang 2008). Diurnal variability explains about 40% of the total convective variability in the tropics (e.g., Yang and Slingo 2001). Several studies on the diurnal cycle of precipitation and convection show that the diurnal cycle over land exhibits substantial variability, while it is weak over the ocean. The diurnal cycle of rainfall has a two-peak period: a late afternoon sharp peak over land and a late night to an early morning weaker peak over the coast and ocean regions (Birch et al. 2016; Collier and Bowman 2004; Mori et al. 2004; Nitta and

Sekine 1994; Sato et al. 2009; Yokoi et al. 2017). The role of the diurnal cycle in total

convection and its seasonal variability is discussed below.

Figures 2 and 3 show mean convection: the amplitude of total convection, and the

contribution of the diurnal cycle to the total convection during boreal winter (December -

January – February; DJF) and boreal summer (June-July-August; JJA). Deep convection

dominates the MC during DJF. Deep convection during JJA is located to the north of the MC,

suggesting seasonal shift associated with changes in the intertropical convergence zone (ITCZ)

and arrival/withdrawal of the Asian summer/winter monsoon (Yang and Slingo 2001).

The diurnal cycle over the MC is one of the strongest in global tropics, and it is

associated with significant scale differential heating between land and sea. It has an essential role

in the organization of convection and precipitation (Lin et al., 2000; Neale and Slingo, 2003;

Sorooshiam et al., 2002). The convective variability in winter is higher where deep convection is

stronger (Figs. 2c and 3c). It is interesting to note, the diurnal variance (variance < 1 day) is

smaller over coastal and ocean areas (~15-20%) compared to land (30-40%). That suggests the

land-based diurnal cycle is the most basic mode of variability compared to ocean areas. This

difference is primarily because of the difference in specific heat between land and ocean where

land warms much more quickly than the ocean. Synoptic-scale systems explain most of the deep

convective variability over coastal and ocean areas (e.g., easterly waves, Kelvin and equatorial

Rossby waves) and intraseasonal scale systems such as the MJO (Yang and Slingo 2001).

1.1.2 Intraseasonal Variability - MJO

Discovered by Madden and Julian in the 1970s, the MJO noticed in a regular oscillation

of winds and pressure over the West Equatorial Pacific (Madden and Julian: 1971, 1972, 1994).

The MJO manifests itself in enhanced or suppressed phases. The enhanced and suppressed

phases have opposite effects on convection and rainfall. Different MJO phases are also aggregated into different phases, phases 1-8, across the globe (Wheeler and Hendon 2004; Madden and Julian 1972). Different phases influence convection and rainfall differently around the world.

As documented in past works, the MJO is a major part of the tropical intraseasonal variability and an essential component of atmosphere-ocean circulation system (e.g., Wu and Hsu 2009; Schreck et al. 2013). The MJO defined as the variability in the range between 30 to 90 days and wave speed of ~5 m s-1 (Madden and Julian: 1971, 1972 and 1994; Zhang 2005). It is linked with various weather events and onset, breaks, and wet monsoon periods over south Asia. The MJO propagation precedes the onset of large-scale deep convection over the Indian Ocean (e.g., Straub 2013). It propagates with an enhanced phase (substantial rainfall intensity) initially over the central Indian Ocean. It later dissipates as a suppressed phase (less rainfall intensity) over the western Pacific Ocean (Gottschalck et al. 2010; Zhang 2005). Several studies relate the onset of summertime Indian monsoon rainfall to the enhanced MJO passage over the eastern Indian Ocean (Singh and Bhatla 2019; Teng and Wang 2003; Joseph et al. 2009).

The MJO characterized by enhanced and suppressed convections that propagate eastward over the MC and well into the West Pacific. Figure 4 presents an idealized lifecycle of the MJO through the vertical cross-section at the equator of cloudiness, zonal winds, and vertical wind streamlines and sea level pressure (Madden and Julian 1972). The MJO convection that forms over the western Indian Ocean propagates eastward and decays near the dateline in the central Pacific. Enhanced MJO convection is associated with lower surface pressure, surface wind convergence, and vertically upward motion. It should be noted that low-level convergence is also associated with moisture convergence, and this fuels convection. As seen in Figs. 4 and 5,

enhanced convection is associated with the upper-tropospheric divergence, which helps maintain the MJO convection (e.g., Rui and Wang 1990). Note that the letters in Fig. 4 correspond to different enhanced phases of MJO. Enhanced MJO saw over the western Indian Ocean (Phase F equivalent to Phase 2). The enhanced phase moves eastward and now located over the MC (near Indonesia; Letter G equivalent to Phase 3). The eastward propagation identified by letters correspond to different phases in the recent literature (F=Phase 2; G = Phase 3; H=Phase 4; A = Phase 5; B = Phase 6; C=Phase 7; D=Phase 8; E= Phase 1).

The other aspect of MJO is its seasonal activity. The MJO variance (a measure of activity) during boreal winter (austral summer) is stronger than boreal summer, as shown in Figs. 6a and 6b. During boreal winter, peak MJO activity dominates the region between the MC and north of Australia. During boreal summer, the peak MJO activity shifts to the north in the region of the eastern Indian Ocean and northern MC (Fig. 6a and 6b). Wheeler and Kiladis (1999) computed the MJO variance by filtering the outgoing longwave radiation data (a proxy for dep convection) in time from 30-96 days and eastward wave number 1-5 (see Wheeler and Kildais 1999 for details). Wheeler and Kildais (1999) also found that the MJO explains about 10% of the total variance between the eastern Indian and western Pacific regions.

1.1.3 Synoptic scale variability (Kelvin waves and Equatorial Rossby waves)

Convectively Coupled Equatorial Waves (CCEWs) are equatorially trapped waves. CCEWs have a significant impact and control of a substantial fraction of rainfall variability within the tropics (Roundy and Frank 2004). The synoptic scale convectively coupled equatorial wave modes such as Kelvin waves (KWs) and Equatorial Rossby (ER) waves. They exert a substantial influence on diurnal cycle of rainfall and convection (Kiladis et al. 2009; Van Der Linden et al. 2016; Kim and Alexander 2013).

As discussed in Kiladis et al. (2009) Kelvin waves are important equatorial wave modes with eastward and westward propagation, as seen in Figure 7. Convectively coupled KWs are characterized by a typical phase speed in the range 12-25m/s, wavelength about 5000km, and 2.5-to-17-days wave period. Kelvin waves are characterized by an eastward propagation and defined by a zero component in the meridional wind while ER waves are described as westward propagating waves with zonal wind dominant near the equator (Kiladis et al. 2009).

Past works show that Kelvin waves (Figure 7) are considered relatively fast-moving waves compared to the slow-moving and large-scale MJO envelopes. Kelvin waves also identified as the synoptic-scale convectively active cells within the MJO system. Kelvin waves span a global propagation near the equator. They propagate through the MC in association with the MJO,which later propagate toward eastern Pacific and South America (Kiladis et al. 2009).

As discussed earlier, Kelvin Waves (Figure 8a) are primary CCEWs wave modes that form near the equator. The pioneering work by Matsuno (1966) shows that expression for KWs can be derived assuming a shallow fluid near the equator on a rotating planet. Equatorial KWs defined as waves that get trapped about the equator. Thus, the meridional perturbation may be ignored, and the solution for KWs will be similar to that for ordinary shallow-water gravity wave for a fluid system of mean depth given by:

$c = (gh)^{1/2}$ where c is the phase speed of the wave, g is gravity and h is mean depth.

On equatorial β −plane, the Coriolis parameter (measure of rotation) may be approximated as:

$f \approx \beta y$, where f is the Coriolis parameter, y is the distance from the equator, and

$\beta = \frac{2\Omega}{a}$, Ω is the angular velocity of the Earth and a is the radius of the Earth.

Using linearized momentum and continuity equations (see also Holton 1973; Matsuno 1966), the KW solution can be derived and can be shown as trapped waves around the equator. The Kelvin mode solution takes the following expression:

$$\hat{u} = u_0 exp(-\frac{\beta y^2}{2c})$$

Where u_o is the amplitude of the zonal perturbation velocity. For the solution to exist, the phase speed must be positive (c > 0). Thus, KWs propagate eastward with zonal and geopotential perturbations that are latitude dependent. As the meridional distance from the equator (y) increases $\hat{u}$ rapidly decreases, and the equation converges.

Figure 9a depicts (in schematics) a horizontal velocity geopotential height structure associated with the Kelvin wave. Convection favored near convergence zone between the low-pressure area to the east and a high-pressure area to the west. In other words, convection is associated with strong zonal westerlies to the west of the convective center and easterlies to the east of the convective center.

ER waves are one of the dominant modes of convective activity in tropics. As shown in figure 8b, ER waves are an equatorial-bound wave that propagates westward with an average phase speed of ~ 4.5 m s-1, less than Kelvin waves phase speed. ER variance is stronger over warm pool regions (typically West Pacific) and Asian monsoons than other CCEWs. The ER waves also have a broader impact on Australian-Indonesian monsoons (Kiladis et al. 2009; Gottschalck et al. 2013). Kiladis et al. (2009) Also discussed was that analysis of ER waves as complicated than other CCEWs due to its slow speed, mixed up with some eastward MJO envelopes, and broad spatial scales. Equatorial Rossby (ER) waves feature a pattern that straddles the equator expressed by alternating high-and-low-pressure cells. Figure 9b presents an idealized ER wave mode where stronger winds are located near the equator. Low-level

divergence is located between low pressure to the east and high pressure to the west, while convergence zones are found between high pressures to the east and low-pressure centers to the west. The convergence/divergence pattern at the equator indicates the increase and decrease in mass on the equator, resulting in the westward propagation of ERs. This study will investigate the multi-scale interaction between diurnal cycle and MJO, Kelvin waves, and ER waves.

1.2. Objective

The principal objective of this study is to better understand the multi-scale interaction between the diurnal cycle, MJO, and equatorial waves (Kelvin waves and Equatorial Rossby waves). First, the diurnal cycle of rainfall and convection over the MC was analyzed by comparing the datasets from Tropical Rainfall Measurement Mission (TRMM) Multi-Satellite Precipitation Analysis (TMPA), Weather States (WSs) from International Satellite Cloud Climatology Project (ISCCP), and TRMM Cloud and Precipitation Features (PFs). Then, we analyzed the MJO and equatorial waves over the MC and the interaction with the diurnal cycle of rainfall and convection. The study aims to achieve the objective by analyzing a suite of data sets indicated above and additional information sources such as cold-cloud brightness temperature. Another aim is to understand the variability of near-surface rain and deep convection over the MC. The following key scientific questions will lead our investigation:

1. What are the relationships between the diurnal cycle of rainfall, precipitation features, and convection over the MC?

2. How are the diurnal cycles of rainfall and convection modulated by the MJO, Kelvin waves, and ER waves? Also, the plan is to accomplish the objective by subdividing the effort into two phases: (i) Study of the diurnal cycle of rainfall and convection over the MC, and (ii)

Investigation of the complex interaction of the diurnal cycle with MJO, Kelvin waves, and Equatorial Rossby waves.

      This study consists of four chapters. In Chapter 2, there is a brief survey of the data sources and methodologies applied to investigate the diurnal cycle over MC (Chapter 3) and the multi-scale interaction between the diurnal cycle and the MJO, Kelvin and equatorial Rossby waves (Chapter 4). Finally, the general summary of the study and final remarks are discussed.
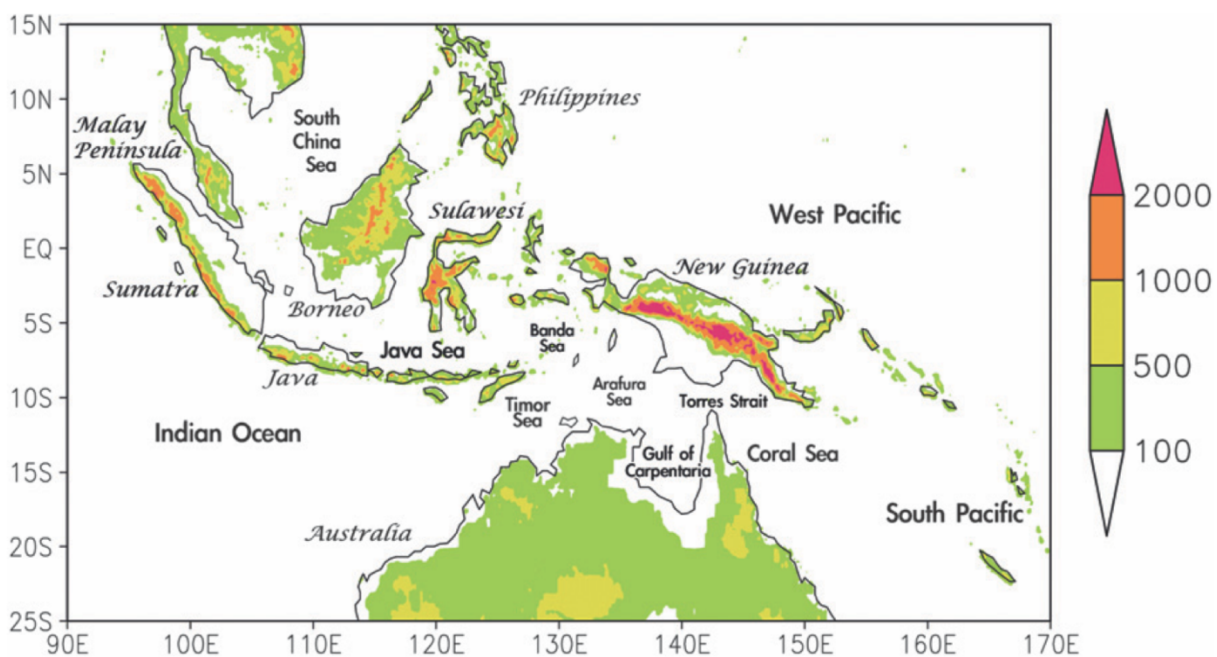
Figure 1. The Maritime continent topographical map. From Wu and Hsu (2009)
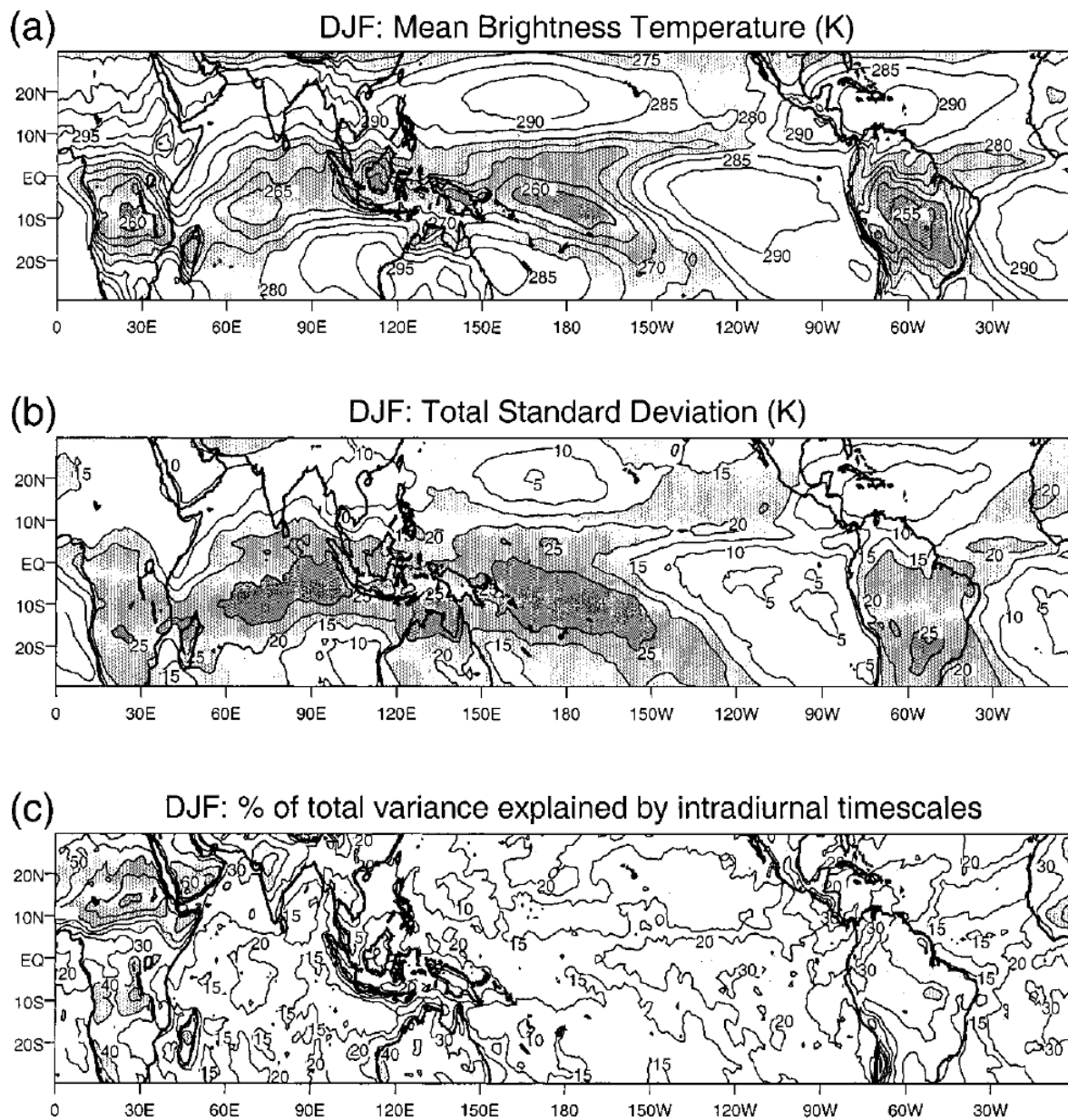
Figure 2. Boreal winter (DJF) Seasonal (a) mean brightness temperature (K), (b) total standard deviation of temperature (K), and (c) fraction of total variance represented in intradiurnal timescales. (See Yang and Slingo 2001; Fig. 1a-c)
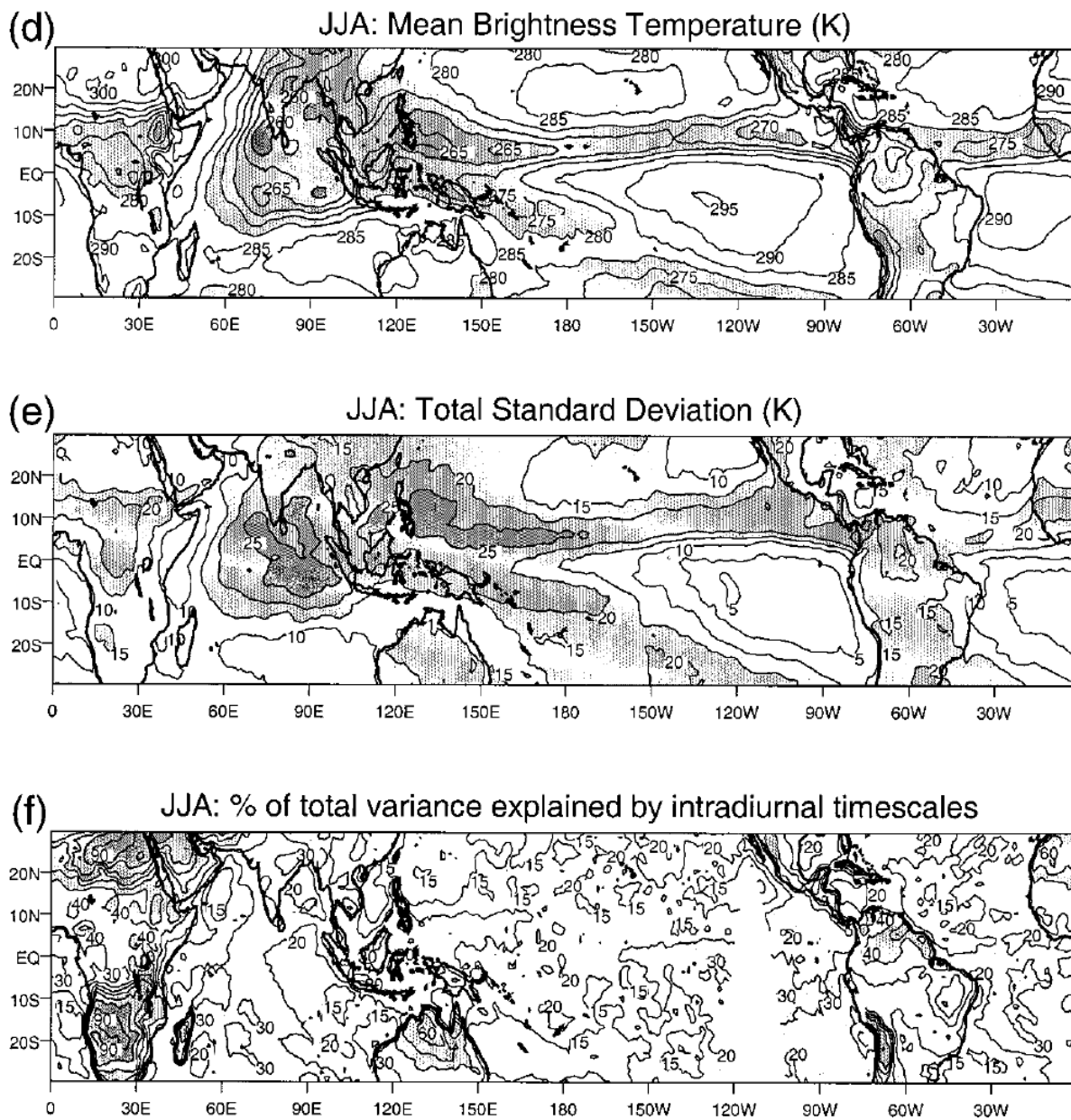
Figure 3. Same as fig. (2) but for JJA season (See Yang and Slingo 2001; fig. 1d-f)

EAST LONGITUDE   WEST LONGITUDE
20° 60° 100° 140° 180° 140° 100° 60° 20°

Tropopause

F

Sea Level Pressure

G

H

A

B

C

D

E

AFRICA   INDONESIA   S. AMERICA
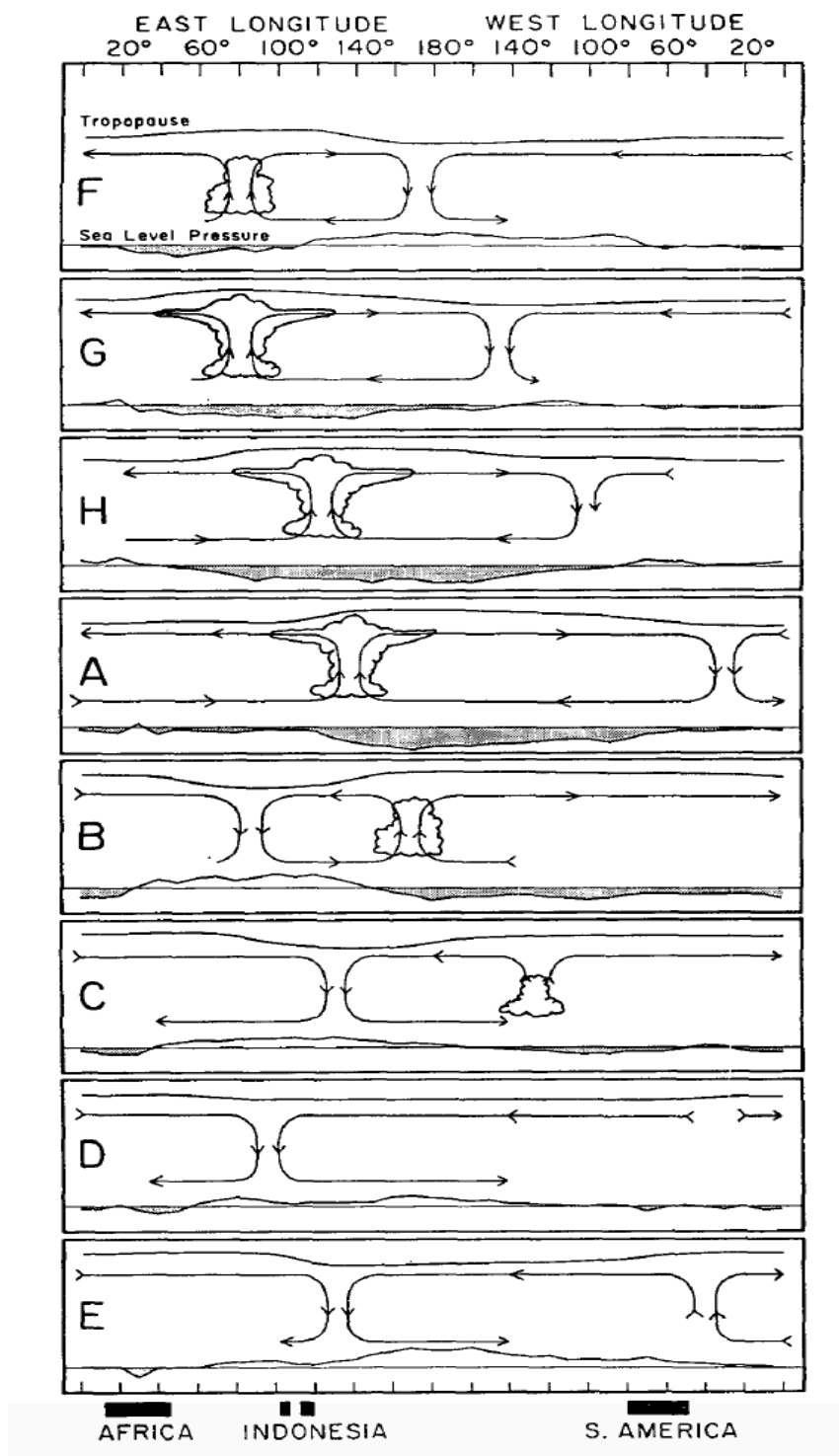
Figure 4. The time and space variations of the disturbance associated with MJO. The letters on the left of each chart correspond to dates associated with the MJO. From Madden and Julian (1972).
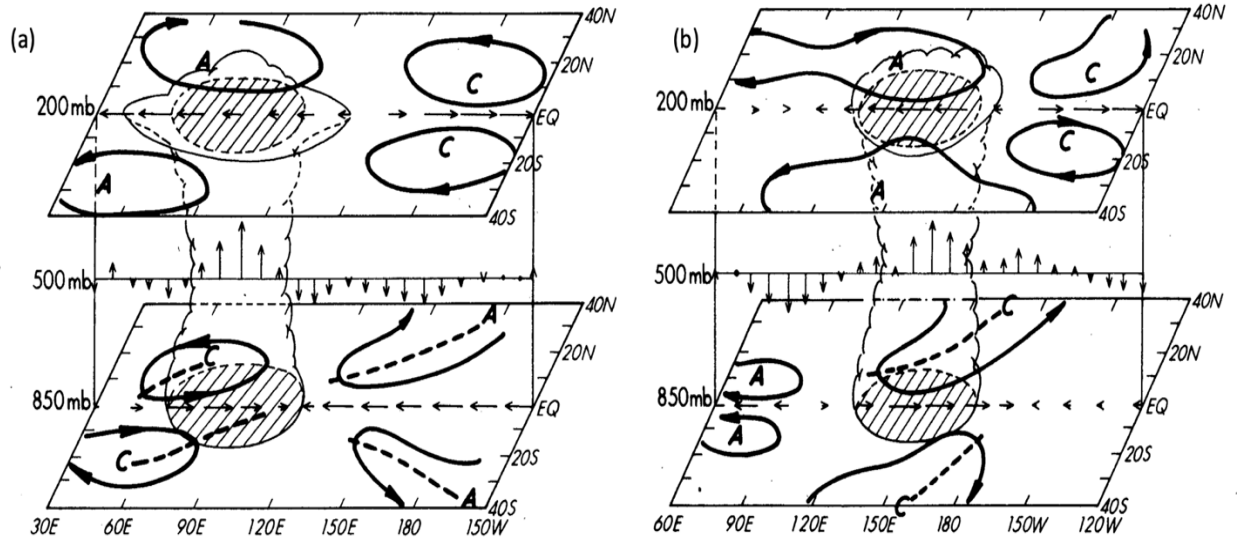
Figure 5. The structural characteristics of intraseasonal low-level frequency waves (MJO) at (a) phase 3 and (b) phase 5. The shaded region represented areas where OLR anomalies are less than -7.5 W m^{-2}. Bold letter A and C stands for Anti-cyclonic and Cyclonic circulation centers. From Rui and Wang (1990).
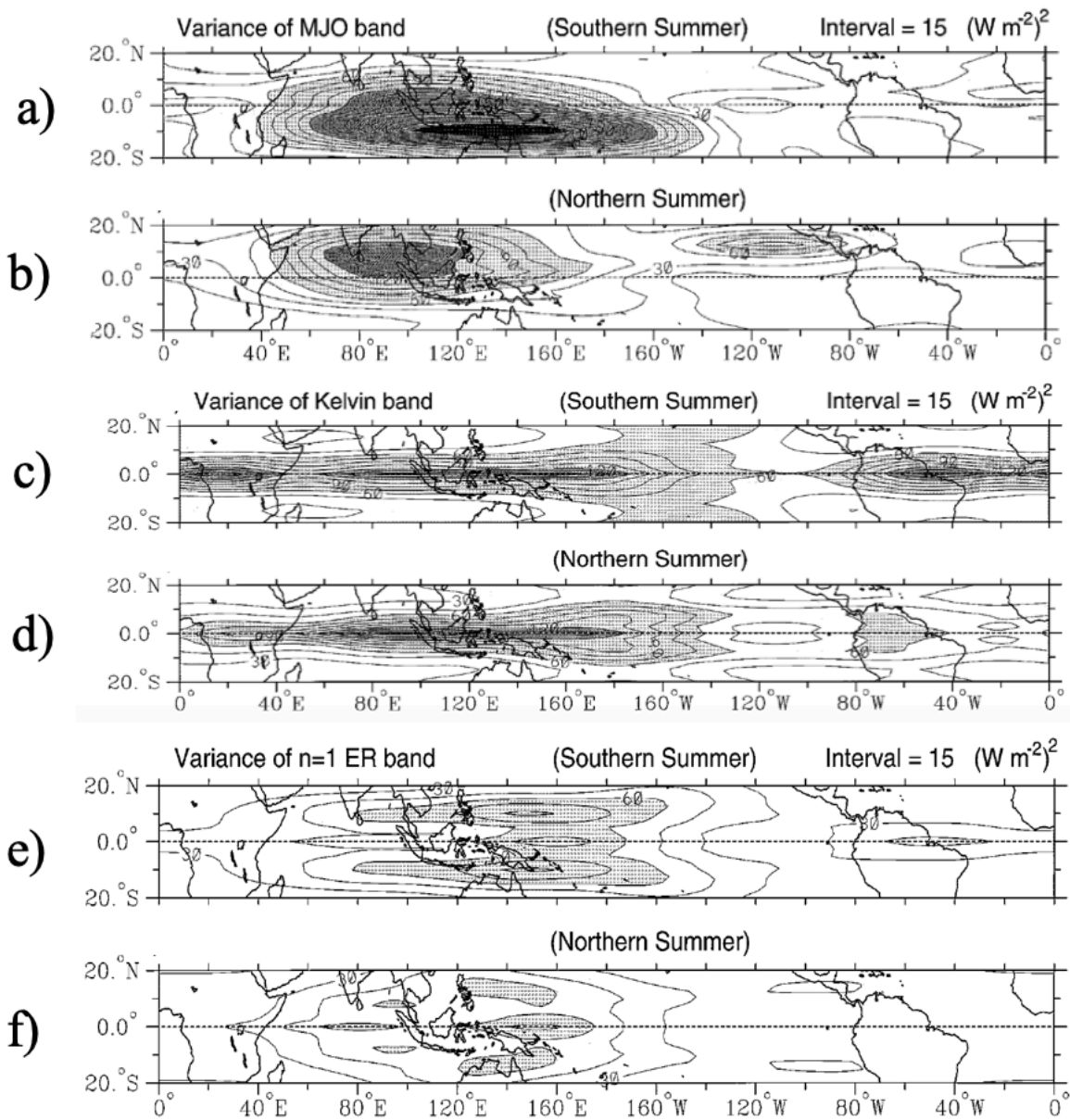
Figure 6. OLR variance for various parts of the wave number-frequency domain interest (a) and

(b) the MJO-filtered band, (c) and (d) the Kelvin wave-filtered band, and (e) and (f) the ER

wave-filtered band in Southern summer (Northern winter) and Northern summer respectively.

From Wheeler and Kiladis (1999).

OBSERVATIONS OF KELVIN WAVES AND THE MJO
Time–longitude diagram of CLAUS Tb (2.5S–7.5N), January–April 1987
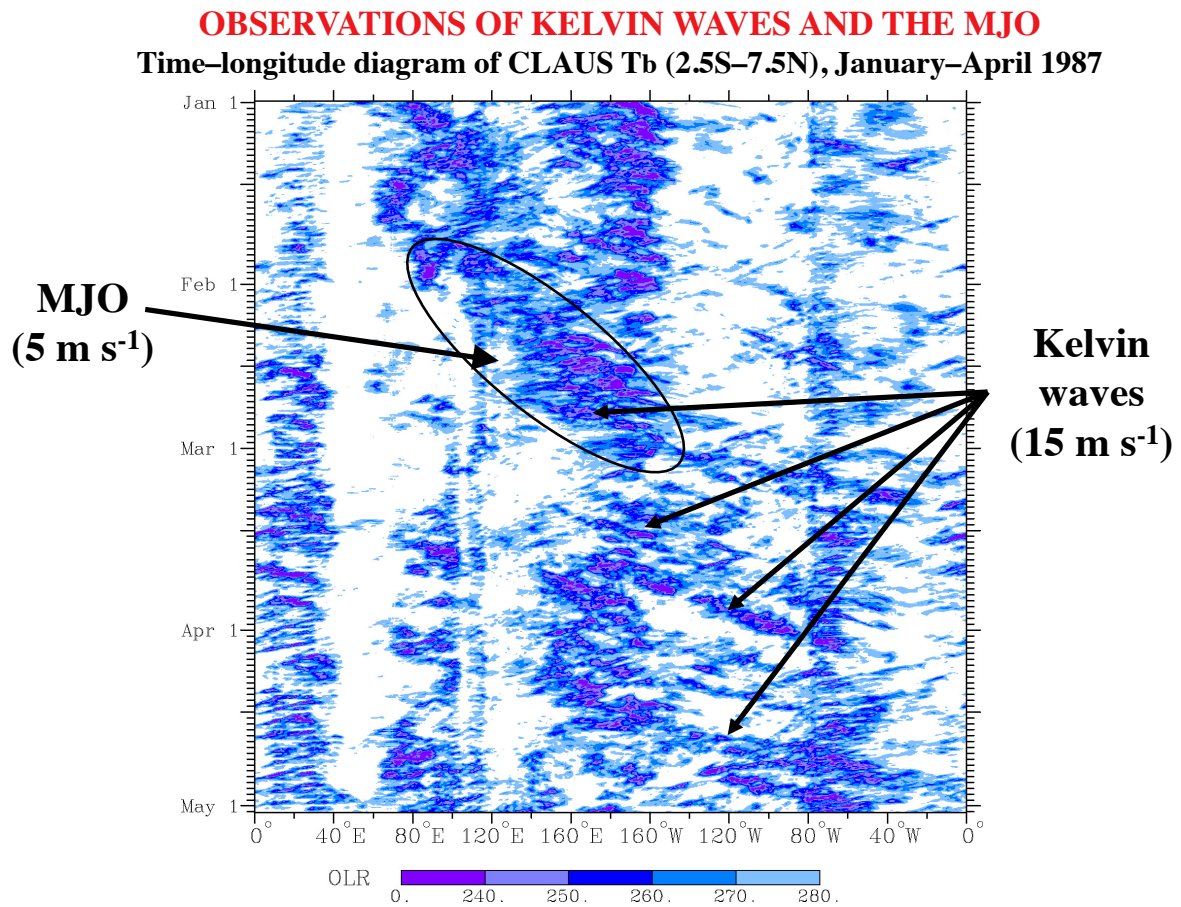
Figure 7. Observation of Kelvin waves embedded within MJO envelope at a higher zonal speed (15 m/s) than the MJO zonal speed (5 m/s). From George N. Kiladis lecture (2006).
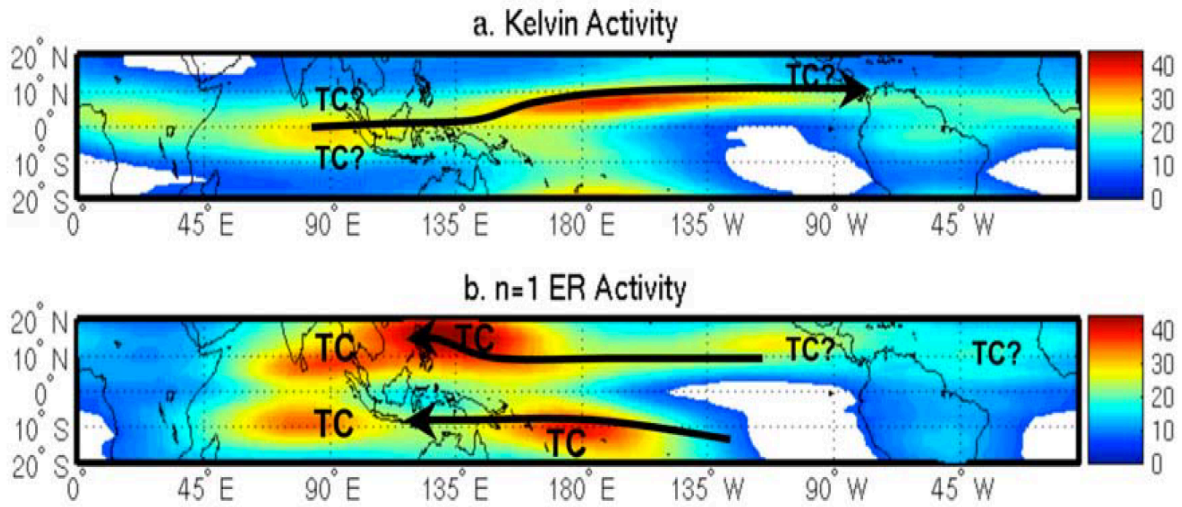
Figure 8. Distribution of space-time filtered annual mean variance of Cloud Archive User Services (CLAUS) Brightness Temperature (Tb) and their impact over tropics for (a) Kelvin Waves and (b) ER waves. From Kiladis et al. (2009).

Figure 9. Schematic depiction of (a) Kelvin wave speeds and (b) Equatorial Rossby waves respectively in dry and wet situations. From (UCAR/COMET, 2017).

CHAPTER 2

Data and Methodology

In this chapter section, we provide a brief survey of data sets used and the methodologies that are applied for our investigation.

2.1. Data sources

2.1.1 Rainfall from TMPA, Version 7

Tropical Rainfall Measurement Mission (TRMM) was a joint mission between the National Aeronautics and Space Administration (NASA) of the United States and the National Space Development Agency (NASDA) of Japan. TRMM was proposed in the late 1980s to be the first-ever space-borne weather radar accompanying by multi-channel (nine) passive microwave radiometer and an AVHRR (Advanced Very High-Resolution Radiometer) (Simpson et al. 1988).

The TRMM Multi-Satellite Precipitation Analysis (TMPA) provides a calibration-based sequential scheme for combining precipitation estimates from multiple satellites, as well as gauge analyses where feasible, at fine scales of 0.25^0 X 0.25^0 spatial and 3-hr temporal resolution from the wide variety of modern satellite-borne platforms (Huffman et al. 2007). The three primary rainfall instruments onboard are passive microwave radiometer or TRMM Microwave Imager (TMI), the Precipitation Radar (PR), Lightning Imaging System (LIS), and the Visible and Infrared Radiometer System (VIRS) (Kummerow et al., 1998). We used TMPA version 7 from December 1997 to November 2014, which is the lifespan of the TRMM satellite.

2.1.2 ISCCP Infrared Weather State (IR-WS)

The ISCCP provides various satellite observed datasets that describe clouds, the atmosphere, and its surface properties, including a joint histogram distribution of cloud-top pressure (CTP) and cloud optical thickness (τ). Pattern analysis using the k-means cluster

analysis method of CTP- τ identifies distinct histogram distributions of cloud properties, referred

to as weather states (WSs) for various regions of the globe. Pattern analysis of CTP-τ for the

global tropics within $\pm15^o$ latitude produces identifies six WSs (Mekonnen and Rossow 2011;

Rossow and Schiffer 1999; Rossow et al. 2005). Three of the six WSs for the tropical regions

identified as convectively active. The rest are convectively inactive WSs. A similar analysis for

the extended global tropics within ±35 latitude identifies eight different characteristics of WSs

(e.g., Mekonnen and Rossow 2011). Three of the eight WSs (referred to as WS1, WS2, WS3)

represent convectively active. The remaining five (WS4-WS8) represent convectively inactive

(suppressed) WSs (Fig. 10). WSs data are reported on a 2.5^0 X 2.5^0 grid at a 3-hourly interval

during the day. Figure 10 shows the eight WS distinct patterns of joint histograms of CTP-τ

distributions of various cloud properties for 35^0S-35^0N. The fractional coverage of mesoscale

domains (identified by colors) denote area coverage by each WS: the larger the cover, the larger

the fraction of the 2.5^o map grid. Optically thicker (τ >23) and higher-topped (CTP< 440 hPa)

clouds are associated with deep convection, seen on the upper right side of the histograms.

Moderately thick and higher topped clouds are related to mesoscale anvil clouds. Higher topped

and optically thin clouds on the upper left are cirrus clouds.

The relative frequency of occurrences (RFO) for each WSs category are shown at the top

right corner of each histogram. It describes the frequency of each WS relative to the extended

tropical area (35^0S-35^0N). As shown in Fig. 10, WS1 is less frequent in the tropics (RFO ~

5.9%). Still, it occupies the largest area covered by deep convective clouds dominated by

mesoscale cloud systems (brighter colors tending to yellow on the right-hand side). WS2 with

mesoscale anvil clouds is more frequent than WS1 but with fewer deep convective clouds. WS3

is the most frequent convective system (RFO=17.3%) with much less deep convection. WS3 is

the small size (blue shades on the upper right-hand corner) equivalent to isolated cumulonimbus clouds. WS3 represented isolated and shallow deep convection. WS1-WS3 in the top panel represents different types of deep convection. WS4 (RFO=9.6%), optically thin, and high-topped clouds, represent cirrus clouds. WS5-WS8 represents shallow boundary layer clouds over the ocean areas and dry subtropical areas. WS4-WS8 represents convectively suppressed cloud regimes. Rossow et al. (2013) showed that large and high-intensity rainfall (rain > 2mm/hr) in the tropics is related to WS1 and moderate rainfall (rainfall < 2mm/hr) is associated with WS3 type of deep convective systems.

WSs are available only for the daytime when τ is defined, and thus, WS data is not suitable for diurnal cycle studies. Another dataset called Infrared WSs (IR-WSs) was used to analyze the diurnal cycle of convection over the MC. It is noted that CTP histograms that use infrared (IR) retrievals are available for all times of day in the ISCCP data archive. CTP-IR retrievals are used to extend for nighttime (Tan et al. 2013). By compositing the CTP histograms for each daytime, WS defined by CTP- τ, Tan et al. (2013) found three distinct convectively active and four convectively suppressed regimes. Their convectively active weather states, named as CD, CC, and IM, correspond to the three daytime WS regimes described above WS1, WS2, and WS3, respectively. IR weather states exhibit similar RFO values. The work by Tan et al. (2013) also includes thin cirrus (named IC), equivalent to WS4, and three low-level cloud regimes indicating suppressed conditions. Therefore, the weather regimes identified by Tan et al. (2013) are WSs extended for nighttime. For consistency, the following is used for terminology: IR-WS1 = CD, IR-WS2 = CC, IR-WS3 = IM, IR-WS4 = IC, IR-WS (5+6+7+8) = SP (suppressed convection). The IR-WS dataset is available at 2.5°, 3-hourly from 1983-2009 for the extended tropics (35°S-35°N). In this study, the three convectively active states, namely IR-

WS1, IR-WS2 and IR-WS3 are the weather state we are going to investigate. IR-WS data is

available at the Earth System Sciences and Remote Sensing Technologies Center, The City

College of New York (https://www.noaacrest.org/rscg/Products/WS/tircluster.html).

To show that IR-WS represents tropical convection, the July-September cloudiness in

Fig. 11 is shown. The higher frequencies of the convectively active cloud systems (IR-WS1, 2,

and 3) coincide with the seasonal location of the deep convective zone over Africa and southern

Asia and tropical oceans. Higher frequencies of the suppressed cloud systems are concentrated

outside of the seasonal deep convective zone. Note, IR-WS1 and IR-WS2 are much less frequent

than IR-WS3, but most of the rainfall is associated with them (Rossow et al. 2013).

2.1.3 TRMM Precipitation Features (PFs)

The TRMM Precipitation Features were identified using data from two instruments of the

TRMM satellite. The instruments are near-surface Precipitation Radar (PR) and TRMM

Microwave Imager (TMI) 85.5-GHz polarization corrected temperature (PCTs). The PFs

database constructed with an event-based analysis of satellite sensors that can target the same

object but still provide a measurement of its characteristics with different information (Nesbitt et

al. 2000). They identified three precipitation characteristics: 1) PFs without ice scattering 2) PFs

with ice scattering and without Mesoscale Convective Systems (MCSs) 3) PFs with MCSs. PFs

with and without ice scattering may be characterized as features contain four or more contiguous

data bins with an area >= 75 km2 while PFs with MCSs contains 108 or more contiguous data

bins with an area >= 2000 km2. The PFs were stored by size and intensity from shallow features

(~ 75 km^2) to large scale MCSs (Nesbitt et al. 2000; Nesbitt and Zipser, 2003).

The TRMM PR detects most of the rainfall in the tropics near-surface and most of the

vertical structure of storms amount (Barnes and Houze 2013; Liu et al. 2008). We chose to use

PR data over TMI because it provides near-surface rainfall measurement with vertical radar echo

and also has less error over the ocean than TMI. Nesbitt et al. (2000) suggested using the TMI

ice scattering method results in a significant uncertainty during estimation of light or heavy

rainfall occurring at small spatial scales. Convective, Stratiform, and volumetric rainfall are three

variables from the radar precipitation feature (RPF) used for the investigation of the diurnal cycle

of rainfall. This data is available at the University of Utah (http://trmm.chpc.utah.edu/) and

Texas A&M University (http://atmos.tamucc.edu/trmm/data/).

2.2. Methodology

2.2.1 Land-sea Masking

The defining attribute of the MC's diurnal cycle is the contrast between the cycles over

the islands and the ocean. Similar to Mori et al. (2004), we partition the MC into three groups:

land, ocean, and coastal areas (Fig. 12 a and b). Land and ocean were identified using the Naval

Oceanographic Office (NAVOEANO) 1-km Very High-Resolution land/sea tag map with

distance from land (https://www.ghrsst.org/ghrsst-data-services/tools/).

TRMM PF and TMPA data binned into 0.25° latitude-longitude grids. They were

classified according to the distance from the center of each grid box to land (Fig. 12a). Pixels

over land were considered land (orange), those within 50 km of land were considered as coast

(blue), and those farther than 50 km classified as the ocean (gray).

The ISCCP data have a much coarser 2.5° latitude-longitude resolution, so each grid box

was binned according to the fraction of the box that contained ocean (Fig. 12b). If more than

50% of the grid box consisted of the ocean, then it was classified as ocean (gray). If 94% of the

box contained land, then it was classified as land (orange). The remaining pixels were considered

as coast (blue). These thresholds were selected to provide the best qualitative match with the

TRMM mask. It is not perfect; several large landmasses lack coastal pixels, medium-sized

islands often flagged as only coasts, and tiny islands are often considered ocean. However, the results should not be overly sensitive to reasonable variations in these definitions.

2.2.2 Identification of MJO and Convectively Coupled Equatorial waves

The MJO amplitude and phase was identified using a pair of principal components time series called real-time multivariate MJO index series 1 (RMM1) and 2 (RMM2) proposed by Wheeler and Hendon (2004). Wheeler and Hendon (2004) developed an independent index for monitoring the MJO based on a pair of empirical orthogonal functions (EOFs) of combined zonal winds and Outgoing Longwave Radiation (OLR) data. The MJO events were isolated using wave number-frequency filtering (Wheeler and Kiladis 1999; Wheeler and Weickmann 2001). The MJO phases selected, where the enhanced MJO wave amplitude is greater than or equal to one (>=1). In this study, we use RMM index available at North Carolina Institute for Climate Study (NCICS), North Carolina State University,(https://ncics.org/portfolio/monitor/mjo/rmm/).

Kelvin waves and Equatorial Rossby waves also identified through Fourier filtering as well. Wavenumber frequency filtering can be achieved through the inverse transform process of space-time spectral analysis, as discussed in Wheeler and Kiladis (1999). Further, after identifying amplitude and phases of waves, our work will focus on the interaction between the diurnal cycle, the MJO, and equatorial waves (e.g., Kelvin wave) over the MC.

Figure 13 and 14 shows symmetric wavenumber-frequency spectrum for the MJO, Kelvin waves, and ER waves (Schreck et al. 2011; Wheeler and Kiladis 1999; Janiga et al. 2018). We used daily averaged TMPA (1998-2015) and OLR (to identify days with) data for space-time filter. The wave number k and period used in Janiga et al. (2018): MJO (k =0:9, p = 20:100 days), Kelvin (k = 1:14, p = 2.5:20 days), and ER (k = -10:-1, p = 10:100 days). They filter relatively without restriction to allow diversity in the propagation characteristics.

The four-wave characteristics we identified with wavenumber frequency filter are wet, dry, decreasing and increasing wave phases. Wet, dry, decreasing, and increasing wave phases in previous studies characterized as trough, ridge, northerlies, and southerlies, respectively (Janiga and Thorncroft, 2016; Thompson et al., 1979; Reed and Recker 1971). Chang et al. (2016) explained these four wave phases as wet, dry, dry-to-wet, and wet-to-dry wave phases respectively but their calculation is different than what was done. Wet wave phase associated with an active convection and moist air with high rain rate while dry wave phase shows a suppressed convection and dry air where rain rate is less. Decreasing (wet-to-dry) and increasing (dry-to-wet) wave tendencies are transition wave phases between wet and dry phases (Riley et al. 2011).

The Fourier analysis applied after reducing spectral noise by reducing the beginning and end of time series using normalization factor. Then Fourier transform will be performed in time and space, and power calculated for all coefficients. After filtering the TRMM data for each MJO events, then the composite analysis will follow (Thayer-Calder and Randall 2009). OLR is better at identifying dates with convection that used to select ISCCP dates. The wave phases filtered with wave amplitude greater than 1.5.

We will identify which MJO events that propagate across the MC, and those do not. Then we will investigate which MJO events modulate the diurnal cycle of rainfall and convection while propagating east and transitioning over the MC. Besides, investigation of the modulation of diurnal cycle of rainfall and convection by Kelvin wave will be studied.

2.2.3 Statistical Analysis

Results are summarized using box-and-whisker plots (Tukey 1977; box plots for short). Box plots, Figure 15, have an appeal because they do not assume a normal distribution, and the

statistics are not affected by extremes in the data. Box plots also allow comparison of different datasets and lend themselves to easy interpretation. It is an important statistical tool to summarize the location (median), spread (IQR; Interquartile Range), and skewness (relative position of box, upper and lower quartile) of data (Willmott et al. 2007; Hoaglin et al. 2009). Boxplot has the edge over standard deviation and mean in terms of explaining the distribution of weather and climate-related variabilities. The box plot can clearly show the distribution and as well as available extremes and median values of dispersion. Briefly, boxes represent the middle 50% of ranked data ranging from the 25th percentile to the 75th percentile. Here, the range between the 25th and 57th percentile referred to as the Interquartile range (IQR). In Fig. 15 the whiskers represent the 10th percentile at the lower end and the 90th percentile at the top end. Outliers are excluded to emphasize distributions related to maxima (90th percentile), minima (10th percentile), median (50%), and IQR spread. The box plots were developed using satellite data of TMPA rainfall, and ISCCP weather states (OLR were used to identify convective dates). The boxplot for wave phases of the MJO, Kelvin, and ER waves used data that were filtered temporally over 100^0E and then applied to the whole region based on the selected dates.
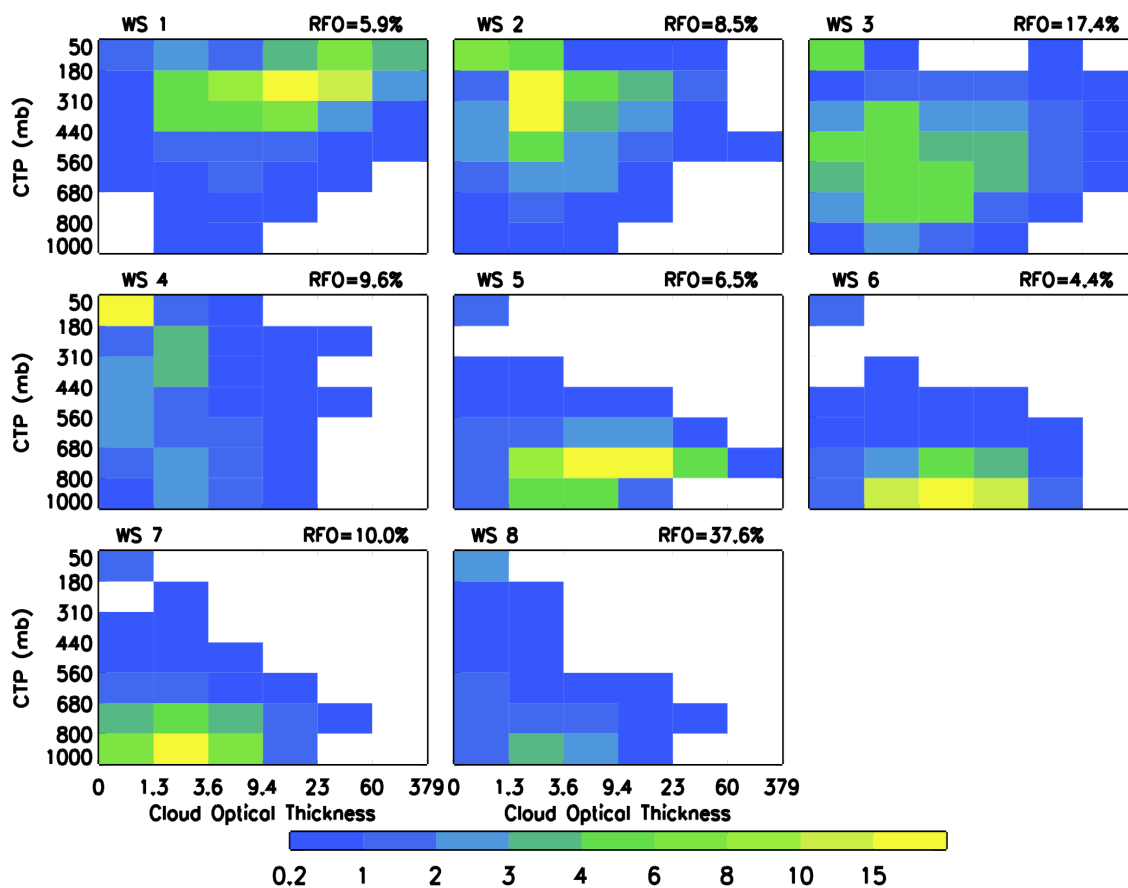
Figure 10. Mean CTP–τ patterns of eight weather states (WSs) from 3-hrly ISCCP D1 data (colors in legend indicate fractional coverage of the 2.5º map grid cell). The histogram is the 1983-2004 average for latitudes 35ºS-35ºN. The WS, numbered 1-8, describe from (top) most convectively active to (middle, bottom) least convectively active states. The WS relative frequencies of occurrence (RFO; in %) are shown on the top-right corner of each plot (From Mekonnen and Rossow 2011).
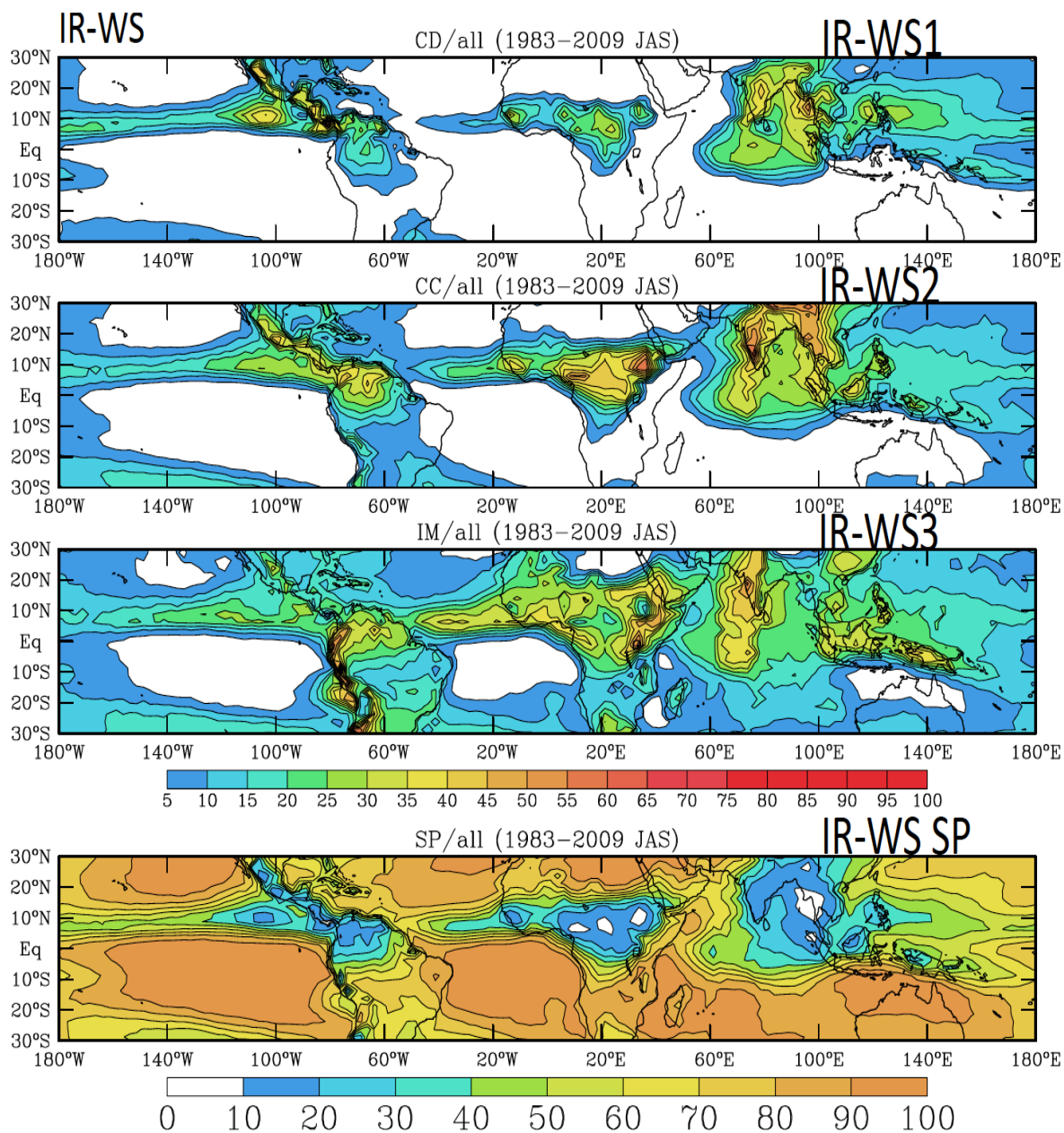
Figure 11. The geographic distribution of IR-WS averaged for July–September. Percentages are with respect to the total frequency of all cloud occurrences. The first three in each of the panels are convectively active regimes, while the bottom panel presents suppressed regimes (Source: Mekonnen and Rossow 2011).

TMPA Land-Sea Mask

ISCCP IR-WS Land/Sea Mask
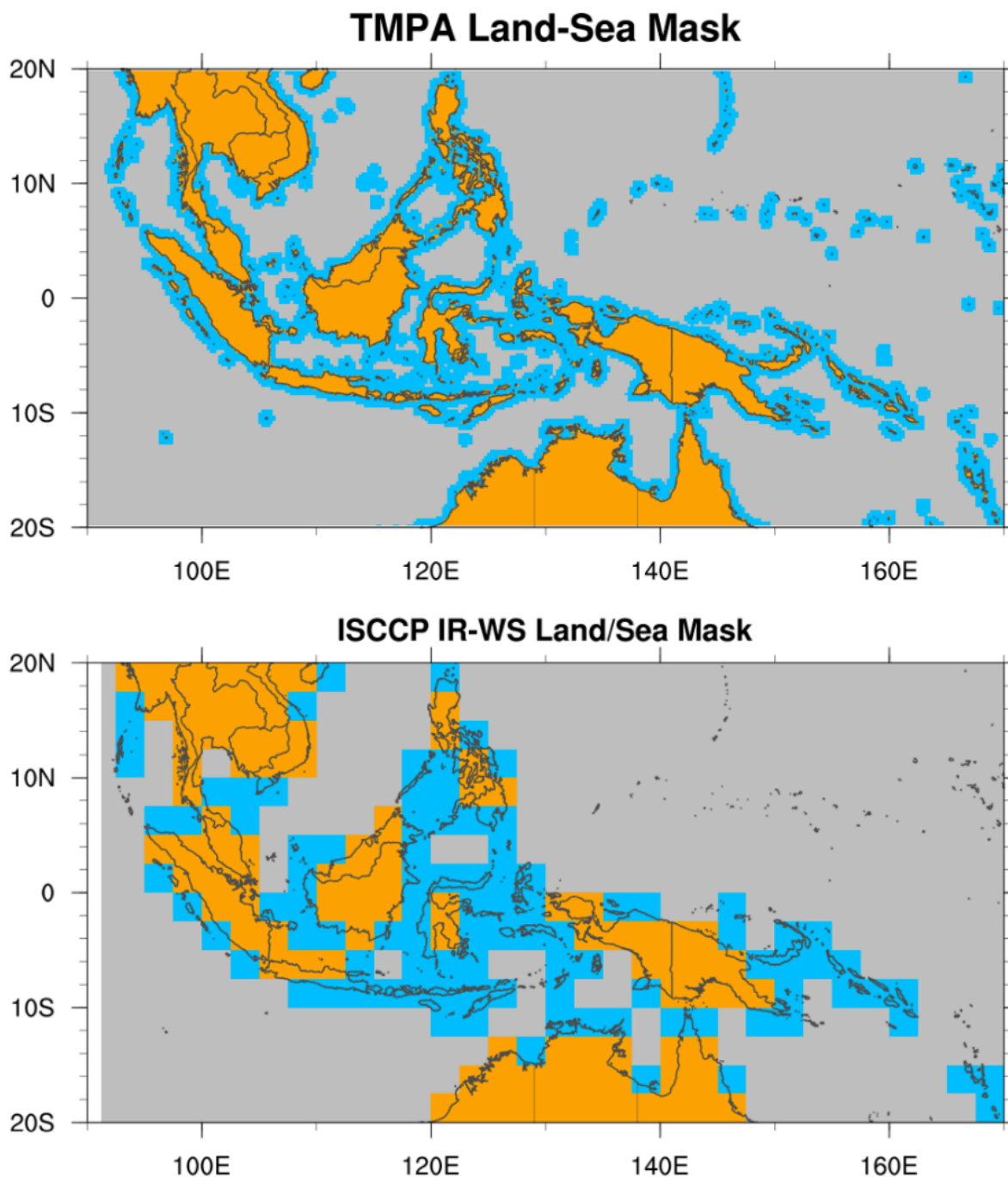
Figure 12. Land-Sea mask for *(a) TRMM and (b) ISCCP* weather state (Orange = Land, Blue = Coastal Sea, and Gray = Open Ocean). The main reason these two plots differ in pixel is because of the resolution difference between TMPA and ISCCP. TMPA resolution is 0.25^0 X 0.25^0 where as ISCCP resolution is 2.5^0 X 2.5^0.
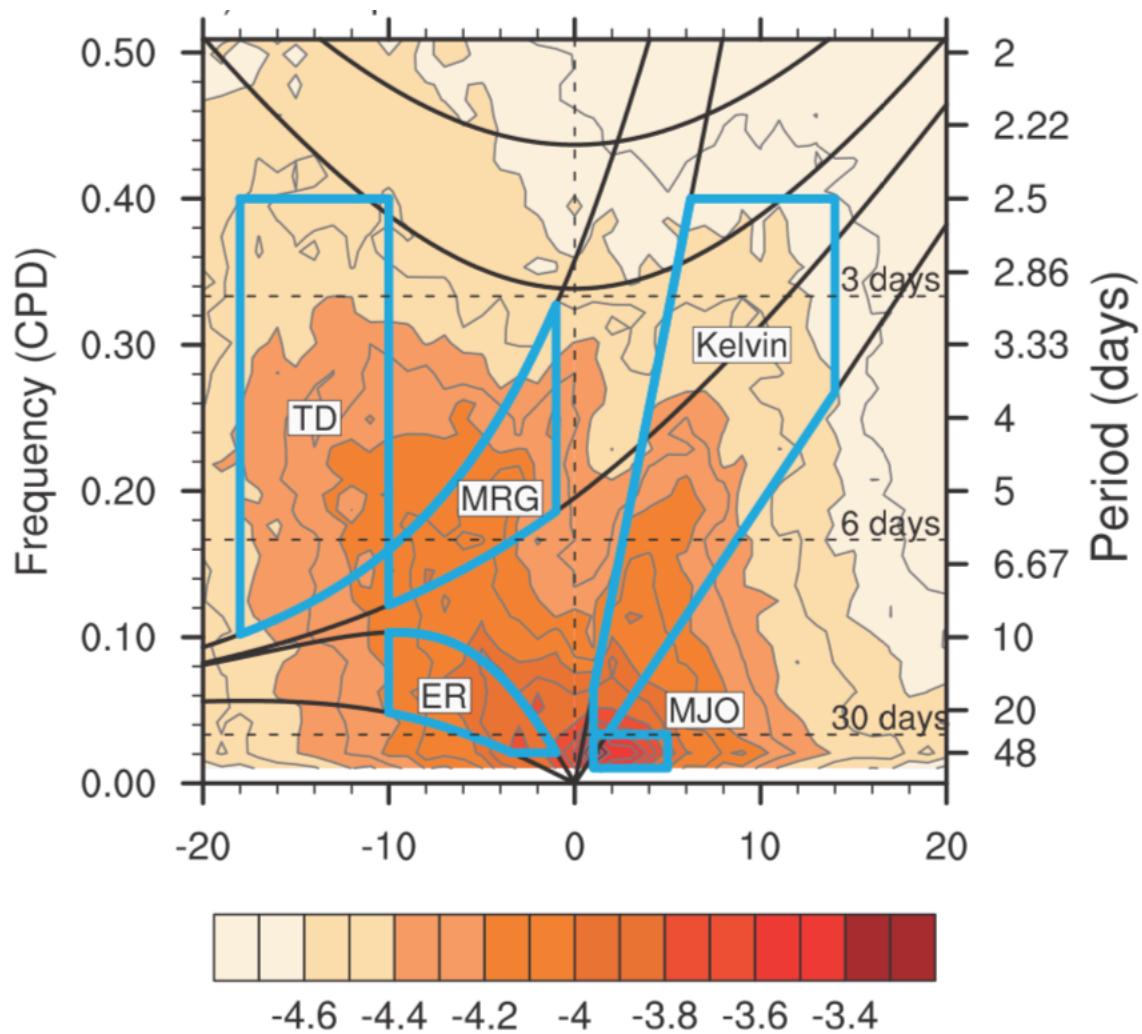
Figure 13. Wavenumber frequency spectrum for MJO, Kelvin wave, and ER waves. From Schreck et al. (2012)
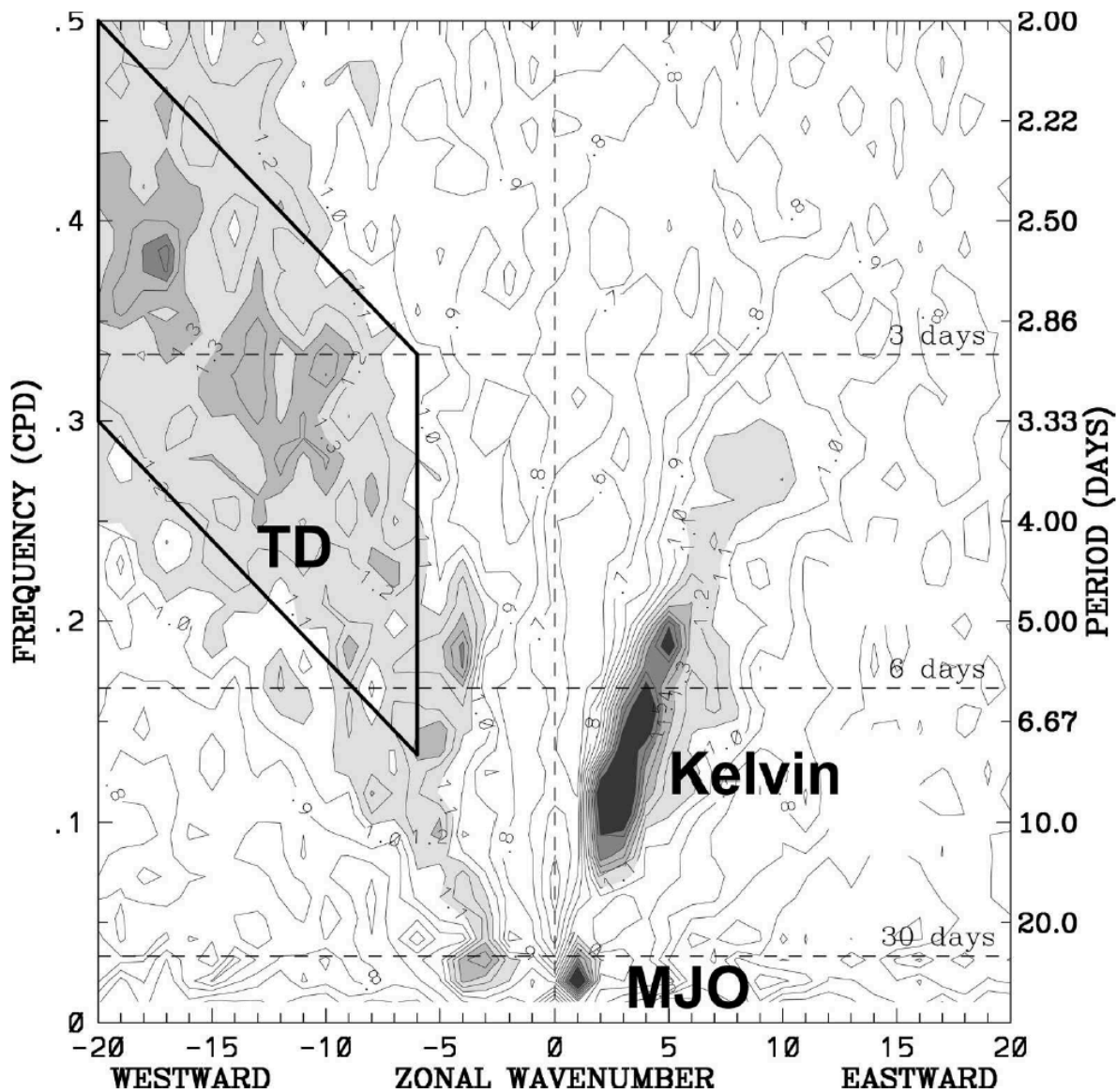
Figure 14. Wavenumber-frequency domain for Kelvin, MJO, and TD-type wave filtering. From

Kiladis et al. (2006)
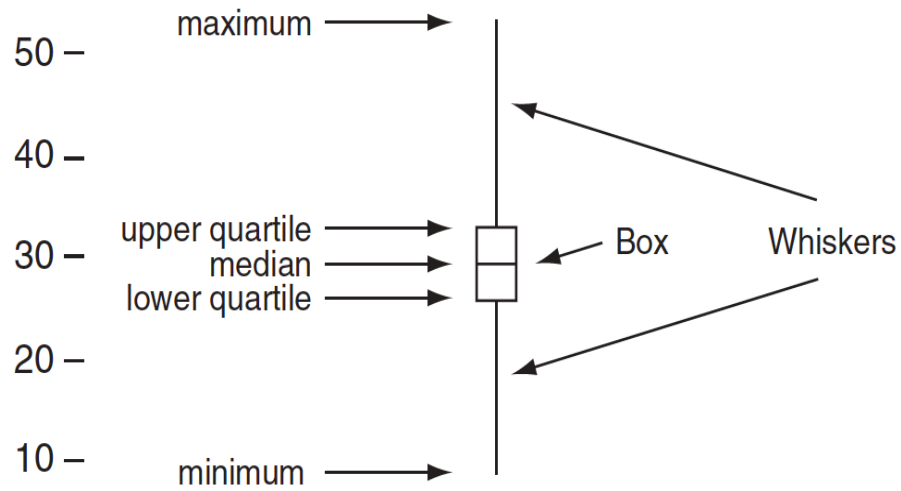
Figure 15. A simple boxplot, or box-and-whiskers plot. The upper and lower ends of the box are drawn at the quartiles, and the bar through the box is drawn at the median. The whiskers extend from the quartiles to the maximum and minimum data values. From D.S. Wilks (2011)

CHAPTER 3

Diurnal Cycle of Rainfall and Convection over the Maritime Continent using TRMM and ISCCP

3.1. Literature Review

The diurnal cycle of rainfall and convection over land and its adjacent coast may influence by terrestrial heating. The amplitude of the diurnal cycle over the ocean is not as pronounced as that over land due to the high heat capacity of the water body. An intense afternoon diurnal cycle may be attributed to the strong association between intense convection and organized weather systems of local to global scales (Chang et al. 1995). Due to complex terrain, the MC larger islands have strong land-sea breezes and contribute to the island heating that forces convective systems to move further away to offshore areas that conditional rain over the ocean (Yang and Slingo 2001; Sobel et al. 2011). Spatial variability of the diurnal cycle of rainfall and convection is associated with strong differential heating between land and water bodies. Observational studies show that deep convection that peaks in the afternoon over land appears to propagate to adjacent the coastal seas and offshore areas during nighttime (Fujita et al. 2011; Mori et al., 2004; Sato et al., 2009). The late afternoon or evening near-coastal convection can be understood as a response to solar heating of the land, turbulent transfer of heat moisture to coastal boundary layer, and lifting of an airmass (Mapes et al. 2003).

Past studies used different types of datasets to investigate the diurnal cycle of rainfall and convection in the tropics. Mori et al. (2004) used data from the Tropical Rainfall Measurement Mission (TRMM) Precipitation Radar (PR) for the MC. They found that convective rainfall peaks during the afternoon to evening and later propagates to coastal sea while the ocean regions convective rainfall peak during early morning hours. Sobel et al. (2011) investigated the diurnal cycle of rainfall over the MC and the Caribbean. They found that small islands, unlike larger

islands, play from non-existent to little significant in the intensification of rainfall and convection.

The diurnal cycle of precipitation features analyzed using the TRMM Precipitation Feature (PFs) dataset introduced by Nesbitt and Zipser (2003). They employed TRMM PFs dataset to study the diurnal cycle of rainfall varies with different features. Over land, rainfall is the minimum earlier in the day but peaks in the afternoon (Nesbitt and Zipser 2003). Afternoon rainfall is mostly associated with intense MCSs. But over the ocean and coastal areas, the diurnal cycle of rainfall has a small amplitude, minimum during the afternoon, maximum during the early morning, and maximum contribution from MCSs for its morning rainfall that also suggested by other studies (e.g., Liu and Zipser 2008; Liu and Zipser 2009).

A similar conclusion on the diurnal variability was also noted by other previous studies using different types of datasets. Nitta and Sekine (1994) and Ohsawa et al. (2001), using Blackbody Temperature (T_{BB}), reported that convection attains a maximum intensity during the late afternoon to evening hours over larger islands in the MC, while convection maximizes during early morning to morning hours over ocean areas including coasts near the large islands. Additionally, Chen and Houze (1997) used T_{BB} to investigate the diurnal cycle of convectively active and suppressed deep convection and found the active phase reached maximum during the afternoon to evening and early morning before dawn over land and ocean regions respectively.

Understanding the evolution of fluctuation of rainfall and convection has been a subject of various studies not only over the MC but also for various regions of the tropics because global circulation models struggle to represent diurnal cycle. Yang and Slingo (2001) analyzed the diurnal cycle of convection in tropics using cloud-top Brightness Temperature (T_B) datasets and found that the diurnal cycle is pronounced over continental regions during the afternoon to

evening hours. While the diurnal cycle has a strong signal over land, it is weaker over the open ocean. The role of diurnal cycle also investigated wave perturbations over Africa and the Pacific. Mekonnen and Rossow (2011, 2018) used the International Satellite Cloud Climatology Project (ISCCP) data to study the role of diurnal cycle in easterly wave initiation over North Africa. They found that intra-diurnal activity (defined by variability <= 1 day) peaks a few hours before the peak of rainfall and convective activity and suggested that diurnal cycle associated with intense orographic heating is crucial for the easterly wave initiation over East Africa. In this study, we investigate the diurnal cycle of rainfall and convection over the MC by classifying the region into land, coast, and ocean regions.

3.2. Results

3.2.1. Diurnal Cycle of Rainfall – TMPA

Figure 16 displays the diurnal cycle of rainfall. Over land, rainfall increases between 1800 LST and 2400 LST, but sharply decreases between 0900 LST and 1200 LST. The minimum rainfall over land occurs during afternoon time. Most of the rainfall observed over bigger islands of Sumatra and PNG (Figure 16). Over the coasts and oceans, rainfall increases between 0300 LST and 0900 LST and decreases after the local noon. Ocean areas north of Australia and south of larger islands (PNG, Borneo, Java) receive little rainfall during the day.

The decreasing rainfall over coast and ocean region is visibly significant to the southern part of the MC, especially in the afternoon to midnight. One of the reasons that might be the part of the MC, as mentioned earlier, is comprised of open ocean regions and have fewer terrains. Figure 16 shows that afternoon rainfall over high terrain moves over the coast and ocean later in the day. Overall, the diurnal cycle of rainfall peaks in the afternoon over land and decreases to a minimum of around 1200 LST. Rainfall peaks in the morning over the coast and ocean. These

diurnal cycle patterns agree with the finding of previous studies (e.g., Mori et al. 2004; Sato et al. 2009).

3.2.2. Diurnal Cycle of Convection – ISCCP

Figure 17 shows the diurnal cycle of deep convection based on IR-WS1. IR-WS1 is associated with large amounts of deep cumulus and cirrostratus clouds. The diurnal cycle of deep convective cloud regime (IR-WS1) attained maximum coverage over land and coastal sea regions at 2100 LST. The clouds of this weather regime are more frequent over Sumatra and Borneo with weaker signals over PNG, consistent with Jakob and Tselioudis, (2003).

IR-WS1 is less frequent over the ocean. Still, the western coastal sea areas of Sumatra, Java, the Malay Peninsula, and Borneo islands show some enhancement later in the evening between 2100 and 0300 LST. The maximum coverage of IR-WS1 over land and coastal sea areas occurs around the same time while over the ocean peaks at 1800 LST, especially over the western half of the MC. However, regions between Java, Borneo, Sumatra, and PNG shows a less pronounced diurnal cycle of IR-WS1 during the late evening to morning hours – less than 10% coverage. Land and coastal regions of the western MC show peak convection late in the afternoon, and, as expected, rainfall increases later in the day (c.f Figure 16). Both rainfall and deep convection are weaker over southern MC, western Pacific region, and central MC of between large islands.

Figure 18 shows the diurnal cycle of scattered convection (IR-WS2) that is thick anvil clouds and less vigorous deep convective and cirrostratus clouds. It is part of a convectively active cloud regime that usually follows IR-WS1. The diurnal cycle of IR-WS2 shows maximum coverage over the region most of the day with low coverage around noon. The IR-WS2 increase

from 1800 to 0600 LST and reaches maximum frequency at 0300 LST. Low frequency of occurrence also observed between 0900 and 1500 LST, especially over Borneo and PNG islands.

The IR-WS2 frequency over coastal regions peaks at the same time as it is over land, 0300 LST. As explained earlier, the reason might be data archived on a large-scale grid, and we will discuss this later by applying the land-sea mask to make the data compatible with that of TMPA and TRMM PFs. The maximum frequency of IR-WS2 at 2100 LST similar to IR-WS1 and increasing TMPA rainfall over the islands. The minimum coverage of the weather regime over the ocean and coastal sea areas is at 1200 LST.

IR-WS1 and IR-WS2 occur together (as anvil clouds are parts and parcel of a much larger and deep convective system: Figure 17 and 18), IR-WS2 showed up approximate to three hours later than IR-WS1. Therefore, we combine them into a single group (IR-WS12), which accounts for both MCSs type deep convection (IR-WS1) and its anvil clouds (IR-WS2). The IR-WS12 increases over land and coast areas between late afternoon through the evening with a peak at 2100 LST (Fig. 19). The maximum is around 70%, which indicates 70% of the IR-WS classified as IR-WS12 as opposed to one of the other IR-WSs. The fewest IR-WS12s (< 30%) over land and coast occur at around 1200 LST. IR-WS12 are more frequent over Sumatra and Borneo with a lower frequency over PNG, in agreement with Jakob and Tselioudis, (2003).

The maximum and minimum frequency of IR-WS12 follows a similar pattern with TMPA rainfall (c.f Fig. 16) temporally and spatially. But the IR-WS12 frequency over PNG is not intensified as other larger islands do during the same time with intense rainfall. The weather state has a weak diurnal cycle over the sea located between Sumatra, Borneo, Java, and PNG most of the day, where it receives less rainfall. Over the ocean, the IR-WS12 shows less

frequency than over land and coast areas with more intense convection concentrated over the western Pacific and eastern Indian oceans.

IR-WS3 is associated with non-organized shallow convection (isolated smaller-scale deep convective clouds), as shown in Figure 20 IR-WS3 peaks at 1200 LST over land and coasts when IR-WS12 and rainfall are minimal (c.f., Figs. 19 and 16). IR-WS3 decreases in the afternoon while large and well-organized convection and rainfall over land increases. Over ocean regions, IR-WS3 increases between 2100 LST and 1200 LST. Areas between the larger islands south of the equator and western MC show more frequency of IR-WS3 than rainfall and deep convection.

The diurnal cycle of the IR-WS3 regime has maximum frequency over large islands of Sumatra, Borneo, and PNG at 1200 LST. But, apart from noon hours, this regime had less coverage over land most of the day. IR-WS3 peaks observed over coastal around 1200 LST. The minimum coverage for land and coastal sea regions is at 1800 LST.

On the other hand, over the ocean regions, IR-WS3 shows a high frequency of occurrence around 0900 LST. Then later in the afternoon, it starts decaying later to its lowest frequency of occurrence at 1800 LST. The minimum frequency of IR-WS3 occurs when deep convection and rainfall is maximum over islands and coastal areas. IR-WS3 frequency peaks between 2100 LST and 1200 LST. But rainfall during this peak hour over the ocean has a lower rate, especially over the water body between large islands.

3.2.3. TMPA, ISCCP, and TRMM PFs Time Series Analysis

The diurnal cycles of rainfall, convection, and precipitation features are presented separately for land (black), coasts (red), or oceans (blue) in Figure 21. The left column shows the TMPA and IR-WSs discussed in Figs. 16 to 20. The right column shows aggregated rainfall from

TRMM-PR PFs subdivided by total volumetric rain (Fig. 21d), convective rainfall (Fig. 21e), and stratiform rainfall (Fig. 21f).

Rainfall and IR-WS12 (Figs. 21a, b) increase over land (black) from 1200 LST and 1800 LST and are lowest between 0900 LST and 1200 LST. Over land, IR-WS3 peaks early in the day around 0600 LST, while decreases between 1500 LST and 2100 LST. This cycle is opposite to rainfall and IR-WS12, but it is also much smaller in amplitude. Total and convective rainfall from PFs (Figs. 21d, e) shows similar fluctuations as TMPA rainfall and mesoscale convection (IR-WS12). The stratiform rainfall (Fig. 21f) delayed by about 3 hours.

In all six datasets, the diurnal cycles over coasts (red) and oceans (blue) are generally similar. They also have much smaller diurnal ranges compared with that over land. The diurnal cycle over land is associated with organized convection (IR-WS12), while the cycles over coasts and oceans dominated by isolated convection (IR-WS3). The diurnal variability over ocean regions are small but have maxima between 0300LST and 0600 LST and minima between 1500LST and 2100LST. The diurnal cycle over of deep convection over coast also leads over the oceans by a few hours. As expected, the diurnal cycle of rainfall over the ocean also appears to be more associated with stratiform rainfall (Fig. 21f), while the coasts and land are more dominated by convective rainfall (Fig. 21e). Also noteworthy is that the largest difference between TMPA (Fig. 21a) and the TRMM-PR PFs volumetric rain (Fig. 21d) occurs over the ocean. This difference between TMPA and TRMM-PR PFs makes sense as TMPA includes microwave estimates of rainfall over the oceans (Huffman et al. 2007).

Maximum IR-WS3 type of convection and PFs, including maximum rainfall over open ocean, occur early in the morning rainfall increases the morning hours but decreases after mid-day through the evening. Similarly, the precipitation features (Fig. 21d-f) peak in the morning,

followed by a sharp decrease closer to midnight. Except for precipitation features of convective and stratiform rainfall, all other variables (Fig. 21a-d) has a greater magnitude of rainfall and convection over coastal seas than over the open ocean. The minimum rainfall and precipitation features occur around midnight, while the minimum for IR-WS3 is around noon, and for IR-WS2 is around morning hours.

As shown in Figure 21, the afternoon rainfall over land is associated with intense deep convection characterized by IR-WS12 and consistent with increasing frequency of precipitation features. Additionally, rainfall over coastal areas appears to be linked with strong precipitation feature and late in the evening to early morning convective activity that propagates from the islands. However, convective activity is less pronounced over ocean areas compared to coastal seas. Precipitation features over coastal areas are more frequent compared to land and ocean.

The diurnal cycle of rainfall, convection, and precipitation feature discussed on a mean annual temporal scale. Figure 22 and 23 shows the comparison between diurnal cycle of rainfall and convection during boreal summer and winter seasons. The diurnal cycle of rainfall over coast and ocean does not show a change between two seasons. However, the MC landmasses afternoon rainfall is maximum during winter than the summer season (Fig. 22a and d). The organized convection (IR-WS12) over land, coast, and the ocean is significantly higher in winter than summer (Fig. 22b and e). On the other hand, scattered convection (IR-WS3) almost does not show seasonal variation.

Figure 23 a-f shows volumetric, convective, and stratiform precipitation features during boreal winter and summer seasons. All three PFs over land shows an enhanced feature during afternoon hours in winter than summer. Over coastal areas, volumetric and convective PFs (Fig.

23 a and b) increase early in the morning during winter than summer while stays the same over ocean regions (Fig. 23 a-f) for both seasons.

3.2.4. Diurnal Cycle of PFs: Convective Rainfall (RAINCONV2A25)

Compared to other PFs, Radar Precipitation Feature (RPF) has the highest contribution to total rainfall occurrence. Over the ocean, the percentage of small-size RPFs and their contribution is greater than over land (Liu et al. 2008). Figure 24 shows the diurnal cycle of convective rainfall from TRMM PFs dataset. The convective rainfall feature maximum occurred over the islands at 1500 LST, while the peak concentrated over the western part of the MC starting from noon (1200 LST) to early in the afternoon (around 1500 LST). Over coast and ocean regions peak early in the morning near 0300 LST and stays strong until noon. The convective rainfall peak hour is consistent with results in Nesbitt and Zipser (2003).

The TMPA rainfall peak period is three hours ahead of the convective rainfall, but the shallow type of weather state (IR-WS3) peaks over land and adjacent coastal regions at the same time. PFs are present over ocean areas throughout the day.

3.2.5. Diurnal Cycle of PFs: Stratiform Rainfall (RAINSTRAT2A25)

The MC exhibits a minimum fraction of stratiform rain (~25%), while other regions like the Pacific have a strong presence of stratiform rain (Schumacher and Houze 2003). Compared to rainfall (c.f Figure 16) and convection (c.f Figure 20), the precipitation features (c.f Figure 23) lags by three to six hours for rainfall and deep convective clouds (IR-WS1 or IR-WS12). However, it clearly shows that it has a similar peak time with IR-WS3 over land. The composite analysis of stratiform rain, in Figure 25, confirms similar timing with peak scattered convection. Coastal sea and open ocean reflect convective rain show some peak features over the

northeastern part of the MC. But the stratiform rain peak is weaker compared to the two convective and volumetric rain.

3.2.6. Diurnal Cycle of PFs: Volumetric Rainfall (RAINVOL2A25)

Volumetric rainfall determined from the near-surface rainfall output, and it depends on the stratiform and convective categorization of the PR data bin. (Nesbitt et al. 2000). Figure 26 shows the diurnal cycle of volumetric rainfall of precipitation features. The volumetric rain exhibited a strong frequency than convective and stratiform rains. The maximum feature starts increasing over Borneo and PNG around 1800 LST, and then later, around 2100 LST became peak precipitation feature over other islands of the MC.

Volumetric rain feature peaks at the same time with TMPA rainfall (Fig. 16) and deep convective (IR-WS1 or IR-WS12) weather states over land. Over the coastal seas and open ocean, the precipitation feature peaks early in the morning that is similar to peak time in IR-WS3 types.

3.3. Summary

This study highlighted the evolution and spatial distribution of the diurnal cycle over the Maritime Continent (MC). The Maritime Continent is a unique part of the globe where it is composed of several hundred for small to large islands and standing between the Pacific and Indian oceans. Its geographical location makes it very important to global atmospheric circulation as it exhibits diurnal to intraseasonal atmospheric variabilities. Over the mountainous larger islands, scattered convection (IR-WS3) peaks around midday when solar heating and orographic effects are largest. It transitions to well-organized convection (IR-WS12) and heavier rainfall in the afternoon and evening (~2100 LST), consistent with previous studies (e.g., Tromeur and Rossow 2010; Mekonnen and Rossow 2018).

The diurnal ranges are smaller over the coasts and ocean. Rainfall over the coast and ocean peaks in the early morning hours (~0300 LST), primarily in association with scattered convection (IR-WS3). The diurnal cycle of rainfall over the coasts and oceans show a phase to reflect stratiform rain than to convective rain.

Mori et al. (2004) and others have described convection over the MC initiating over land and then propagating to the coast and the oceans late in the afternoon. The diurnal cycle of rainfall (Fig. 16) demonstrated this evolution around the larger islands (Java, Borneo, and PNG), consistent with previous studies. Aggregating the region as a whole shows this pattern as well (Fig. 21a): rainfall peaks over land at 1900–2100 LST, coasts at 0300–0600 LST, and oceans at 0600–0900 LST. However, it is less apparent in the smaller diurnal ranges of the ISCCP IR-WSs. That could be due in part to the coarser horizontal resolution. A higher resolution IR-WS is under development and should be used to revisit these issues.

Diurnal cycle influenced by the existence of intraseasonal and synoptic fluctuations such as MJO, Kelvin waves, and ER waves. There are also studies suggesting that diurnal cycle may also modulate these equatorial bound intraseasonal and synoptic variabilities. Further investigation of these two-way influences may help improve weather prediction over the MC and beyond. The detailed influence of the MJO, Kelvin waves, and ER waves on diurnal cycle presented in the next chapter.
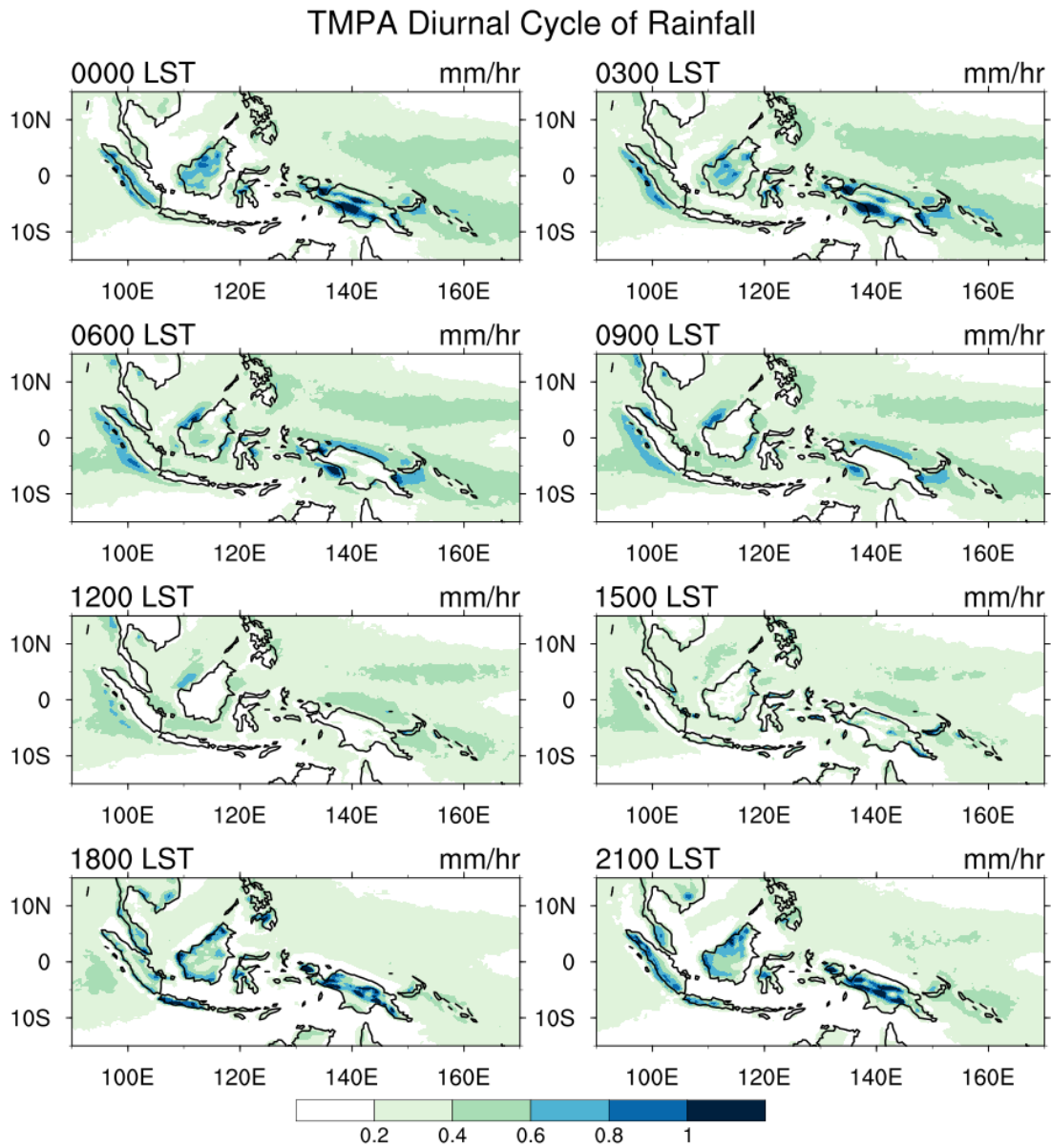
Figure 16. Mean diurnal cycle of rainfall using TMPA (mm/hr) from 0000 local standard time

(LST) to 2100 LST at 3-hr time intervals, averaged over December 1997 – December 2014.
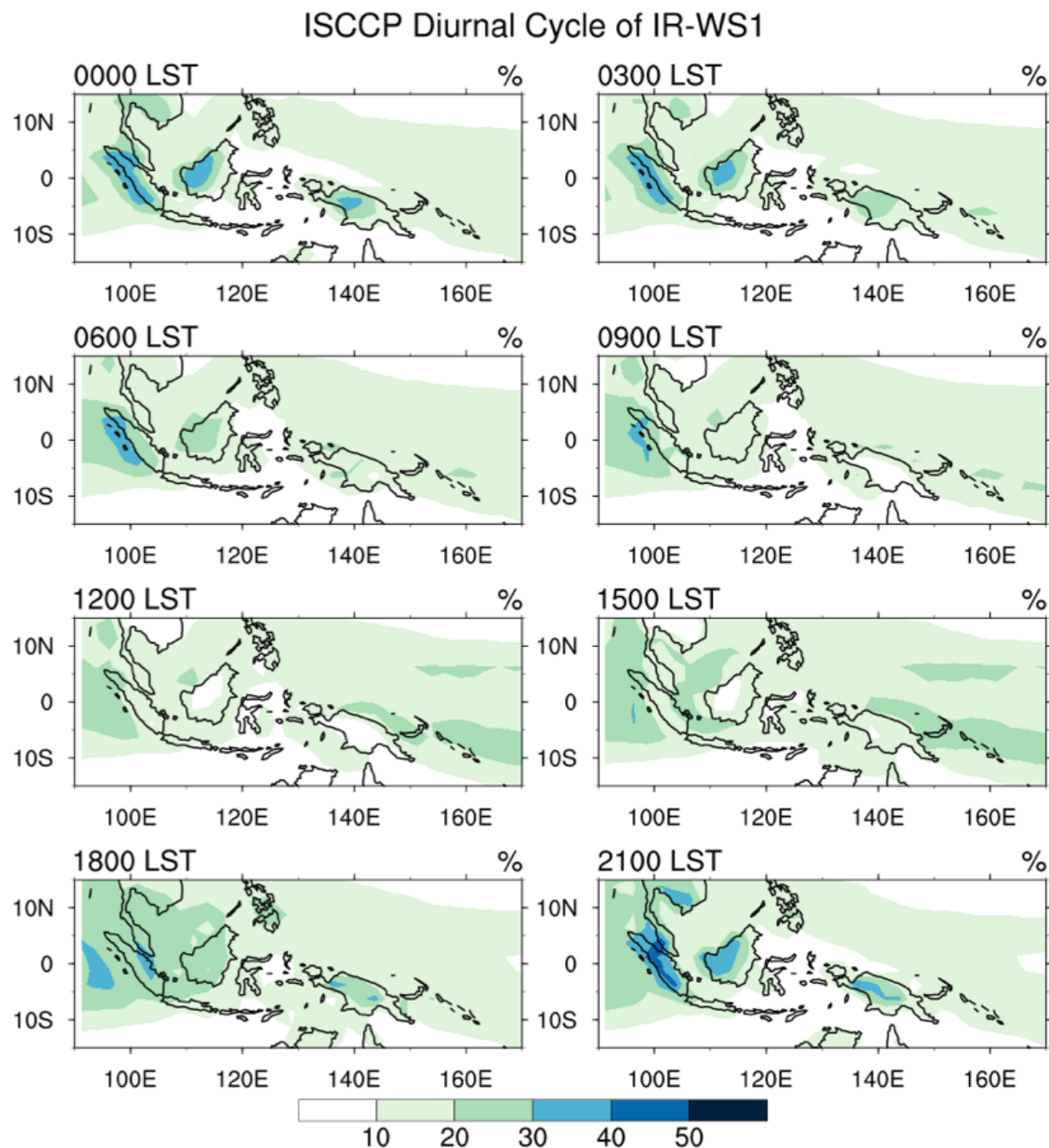
Figure 17. Mean diurnal cycle based on IR-WS1 (time averages). The averages are computed by summing all available IR-WS1 and divided by the number of days from August 1983 – June 2009. The frequency of occurrence is in percent (%) from 0000 to 2100 LST at 3-hr time intervals.
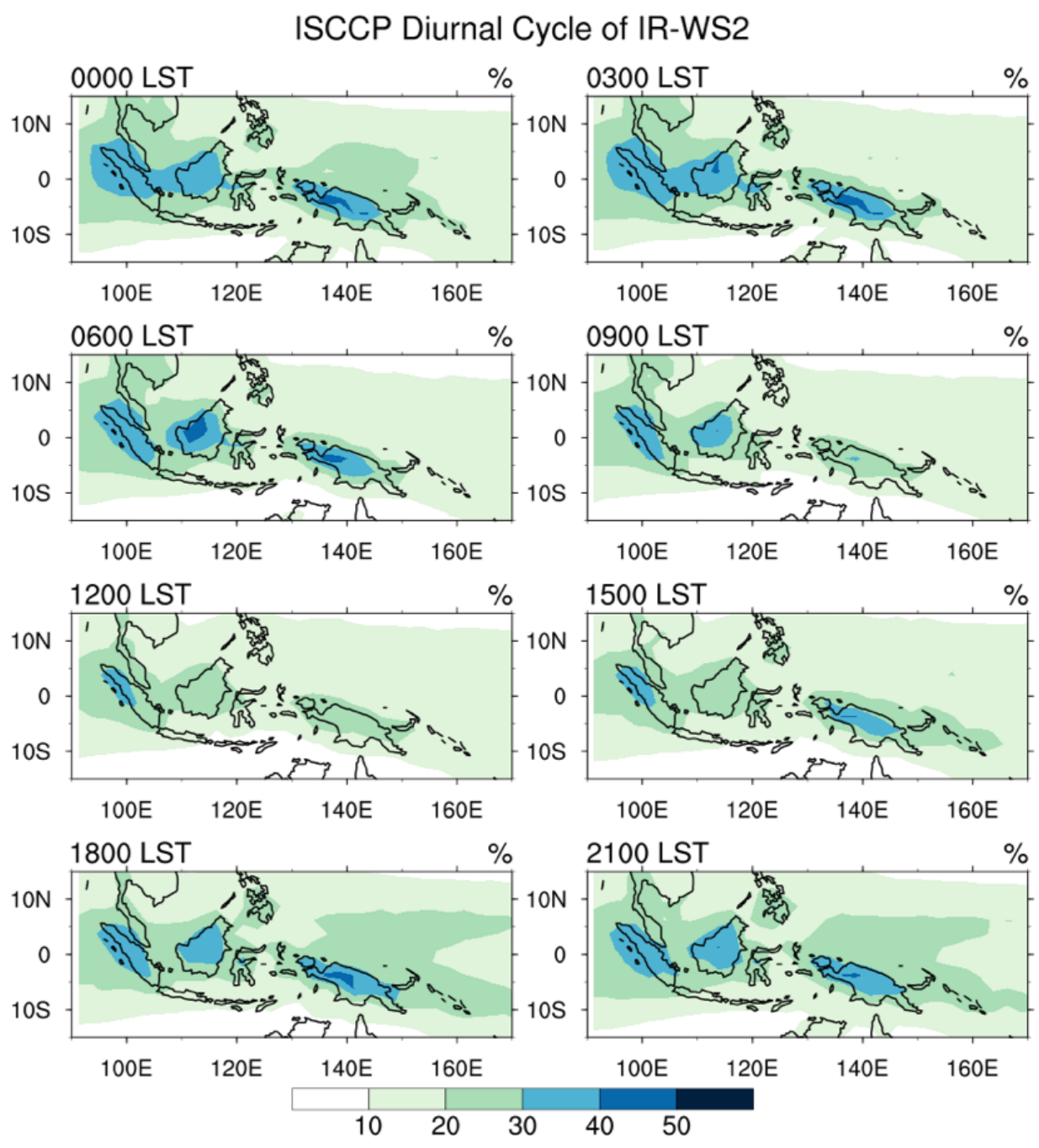
Figure 18. Same as Fig. 3-2, but for IR-WS2
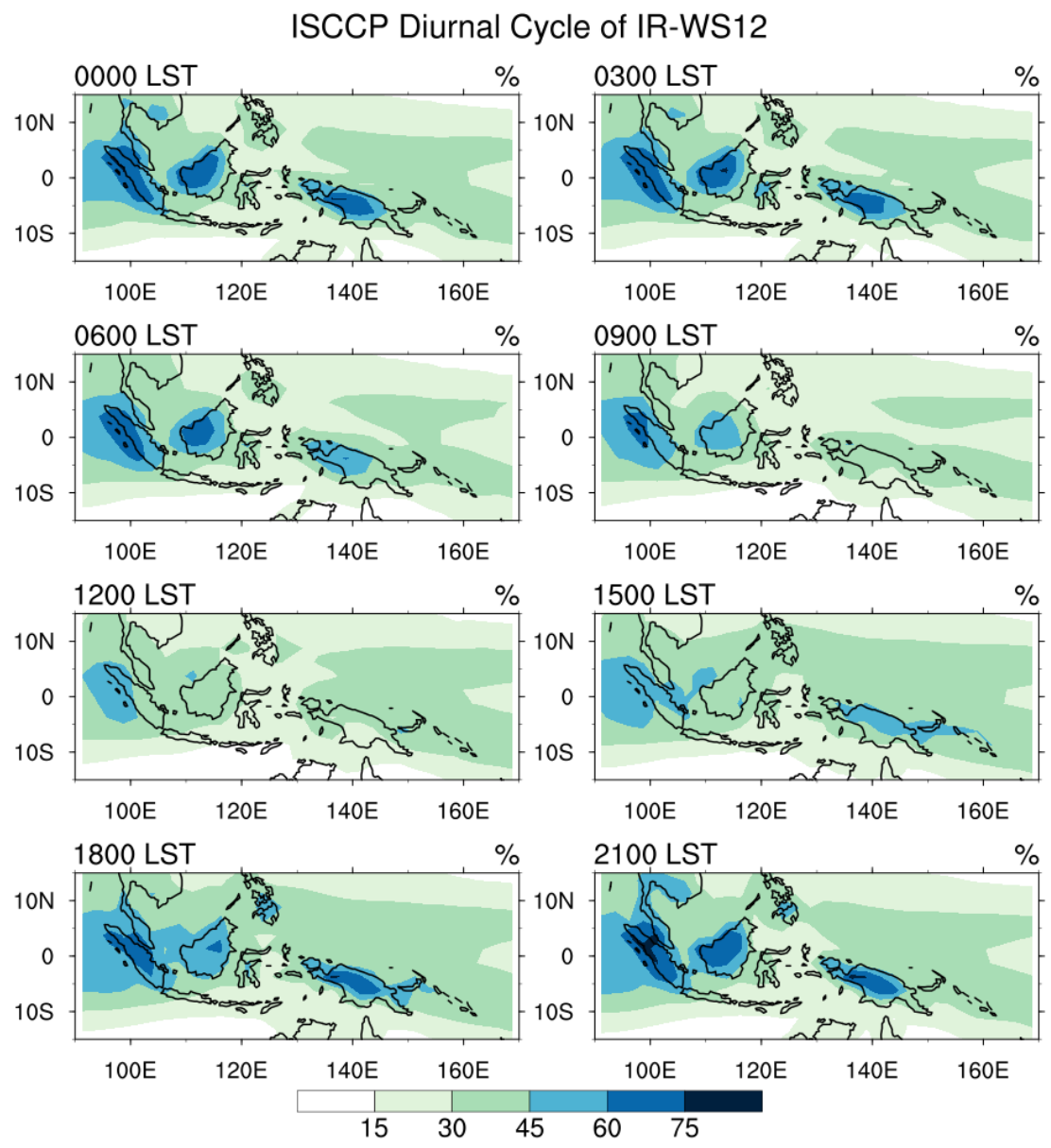
Figure 19. Same as Fig. 3.2, but for IR-WS12
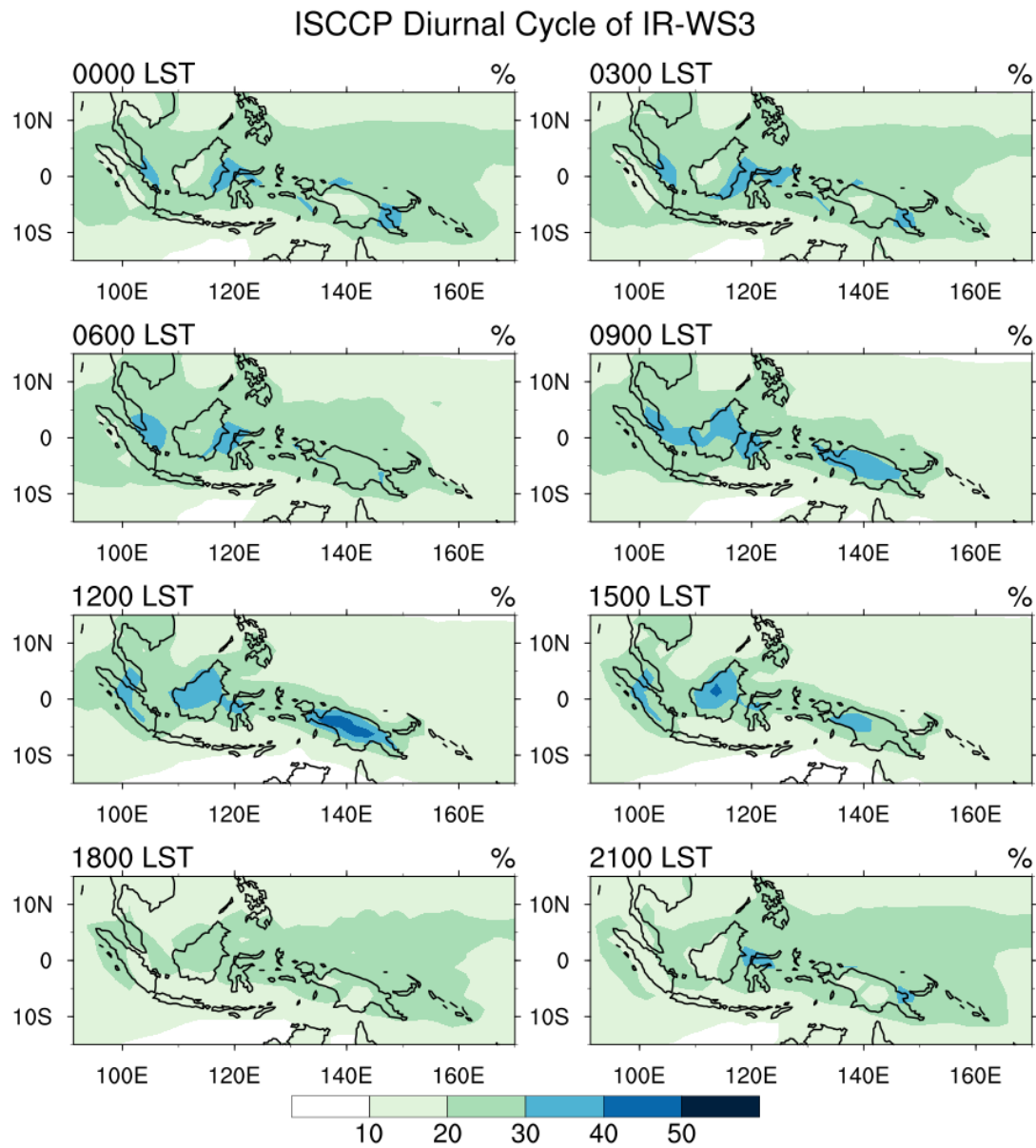
Figure 20. As in Fig. 3.2 but for IR-WS3.
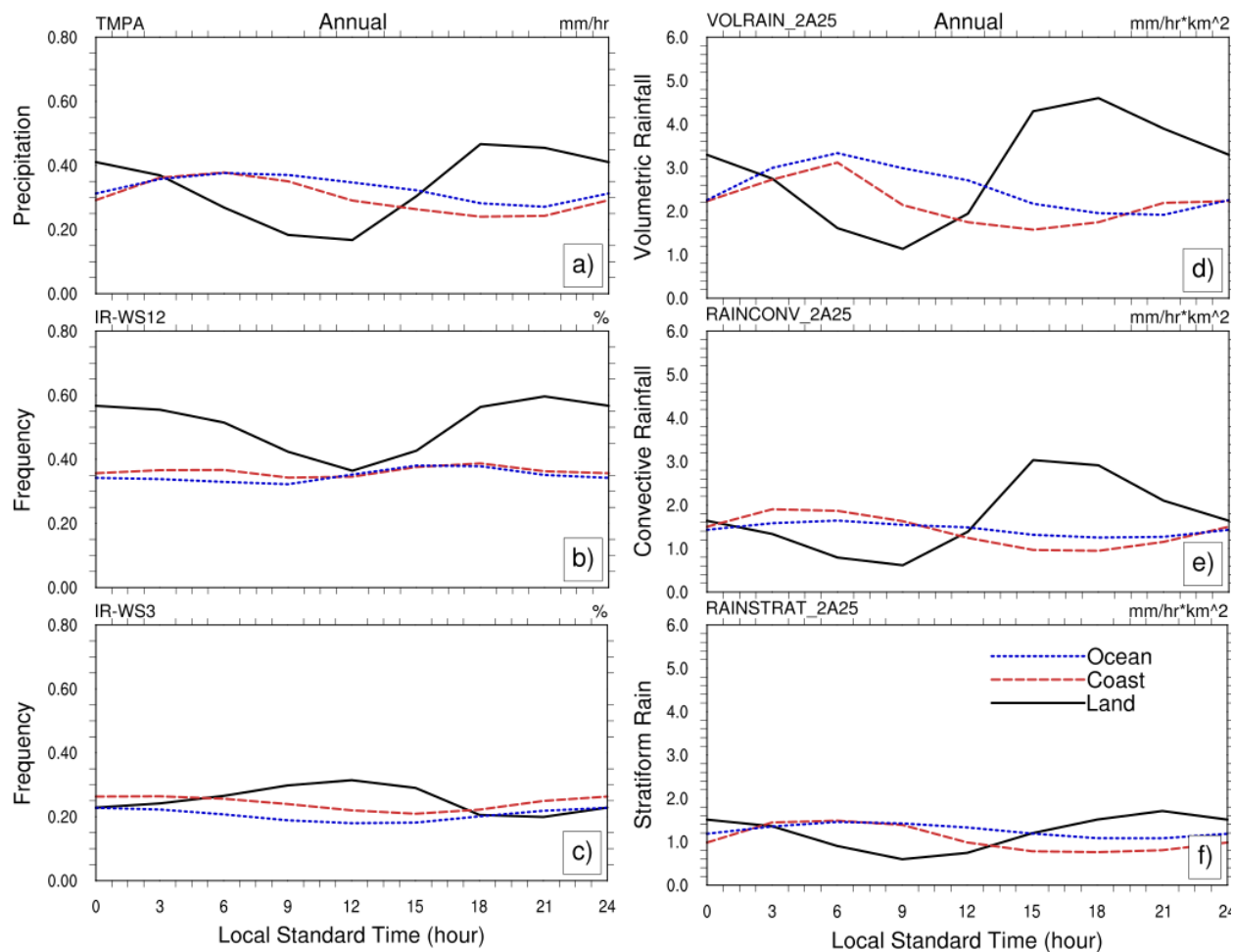
Figure 21. The mean time-series analysis of TMPA rainfall, ISCCP weather state (IR-WS12 and

IR-WS3), and TRMM PFs (Convective, Stratiform, and Volumetric rainfall features) from 0000

local standard time (LST) to 2100 LST at 3-hr time intervals. a) TMPA rainfall (mm/hr) b) IR-

WS12 (%) c) IR-WS3 (%) d) Volumetric rainfall (mm/km^{-1}hr^{-1}) e) Convective rainfall (mm/km^{-1}hr^{-1}) f) Stratiform rainfall (mm/km^{-1}hr^{-1}) and c). Black (Land), Red (Coastal Sea), and Blue

(Offshore).
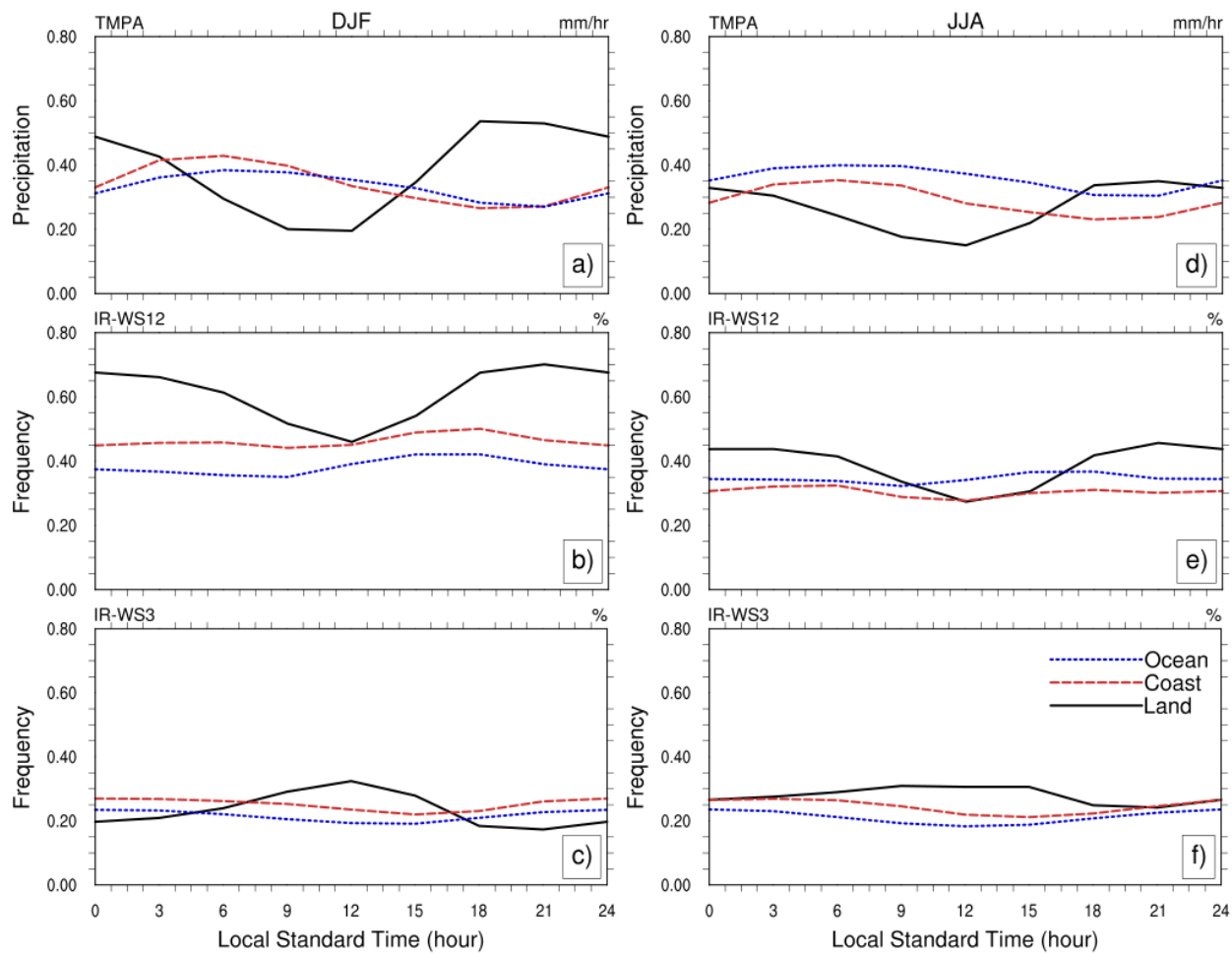
Figure 22. As in Fig. 21a–c, but for TMPA and IR-WS during DJF and JJA seasons
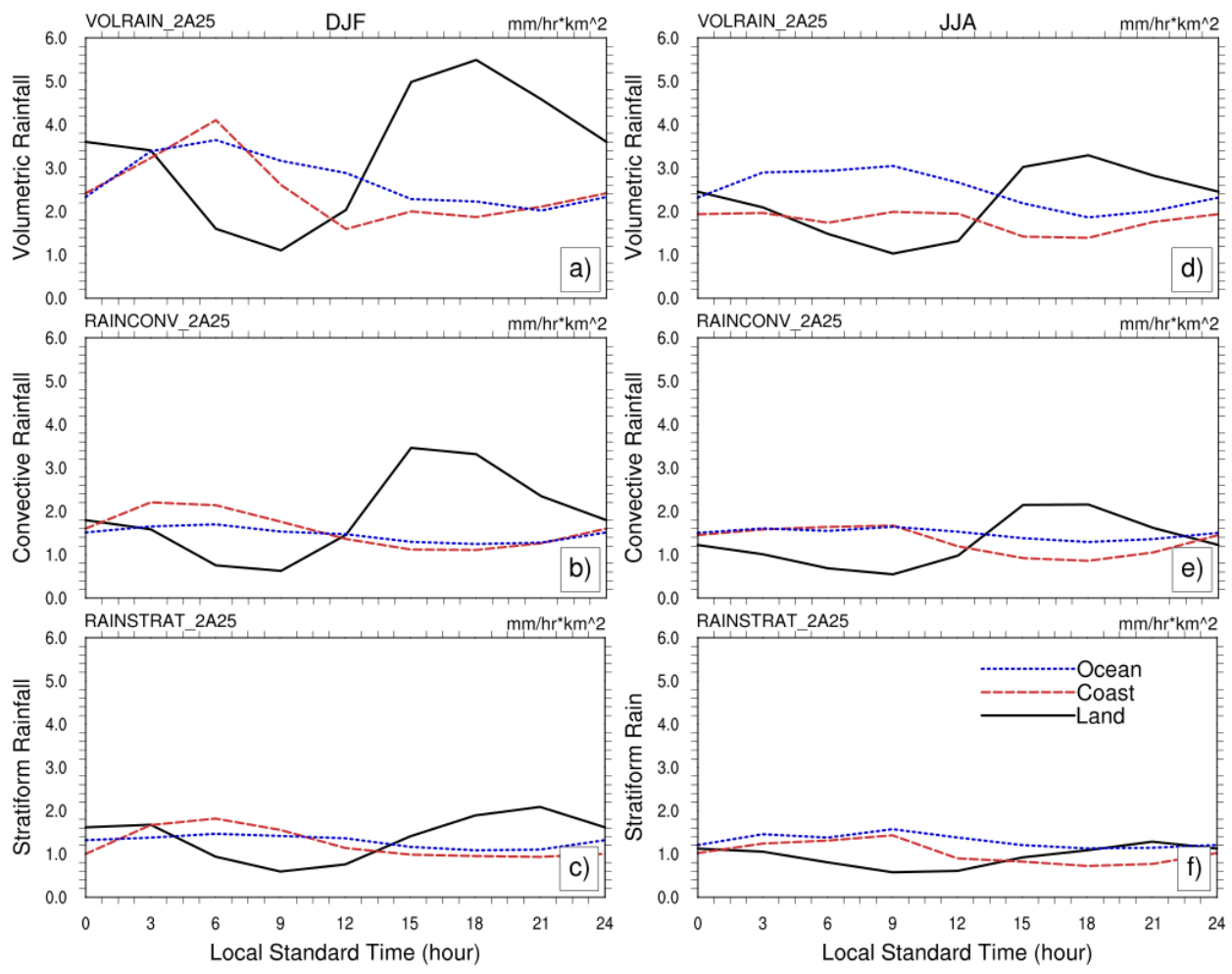
Figure 23. As in Fig. 21d–f, but for TRMM PFs during DJF and JJA seasons
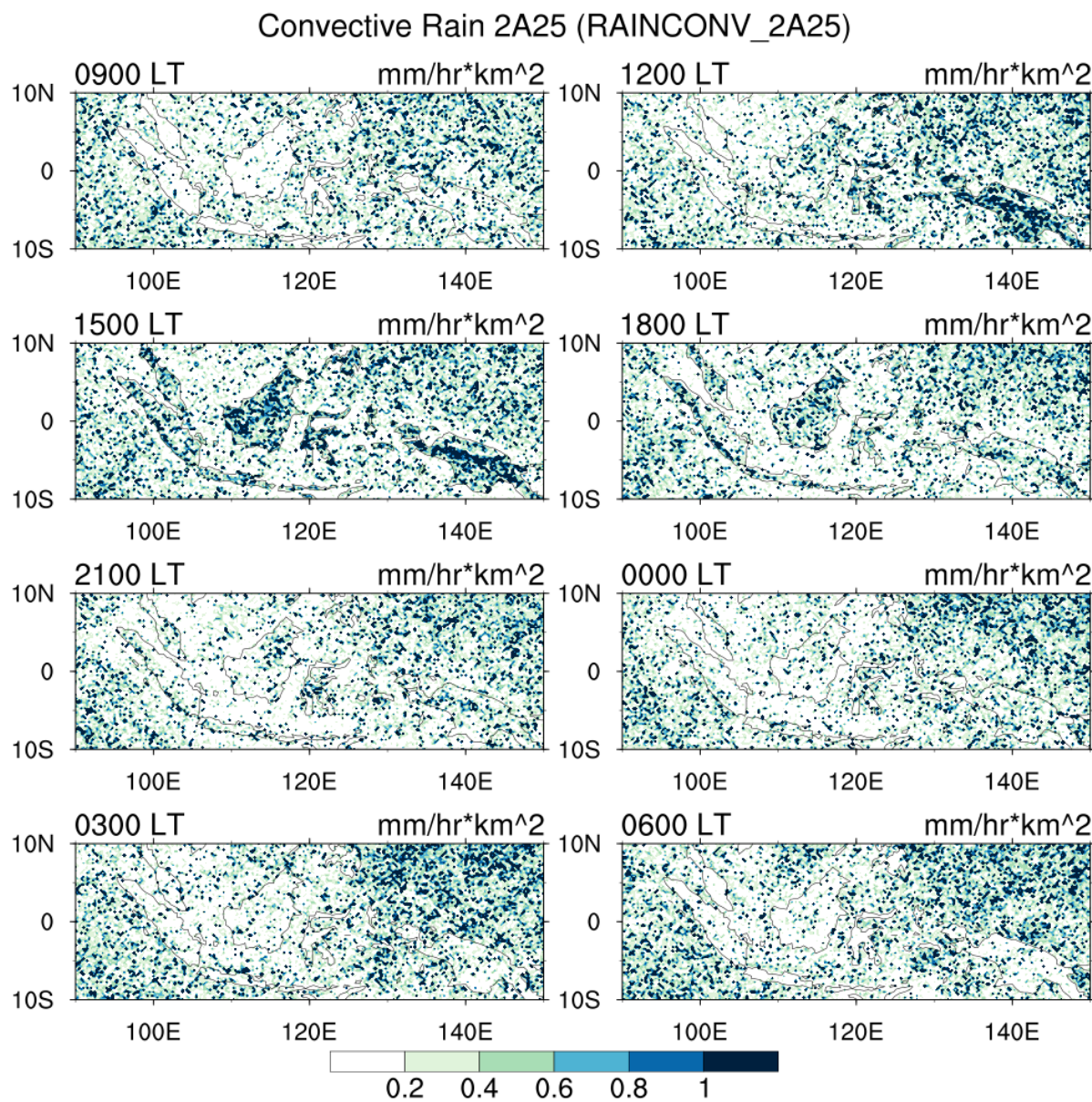
Figure 24. Mean diurnal cycle based of Convective Rainfall (mm/hr*km^2). The averages are computed by summing all available precipitation features and divided by the number of days from December 1997 - September 2014. The duration ranges from 0000 to 2100 LST at 3-hr time intervals.
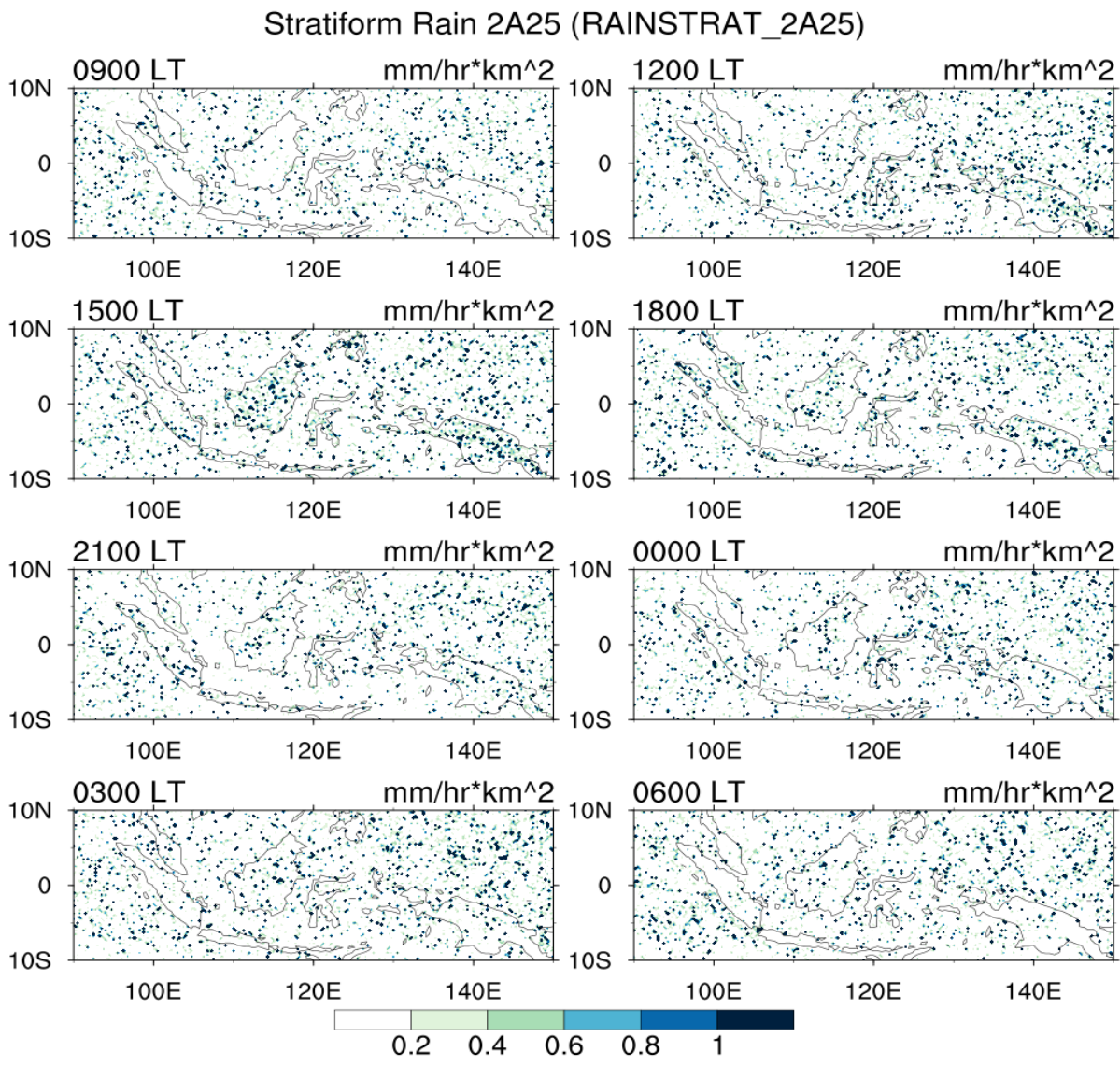
Figure 25. As in Fig. but for Stratiform Rainfall (mm/hr*km^2)
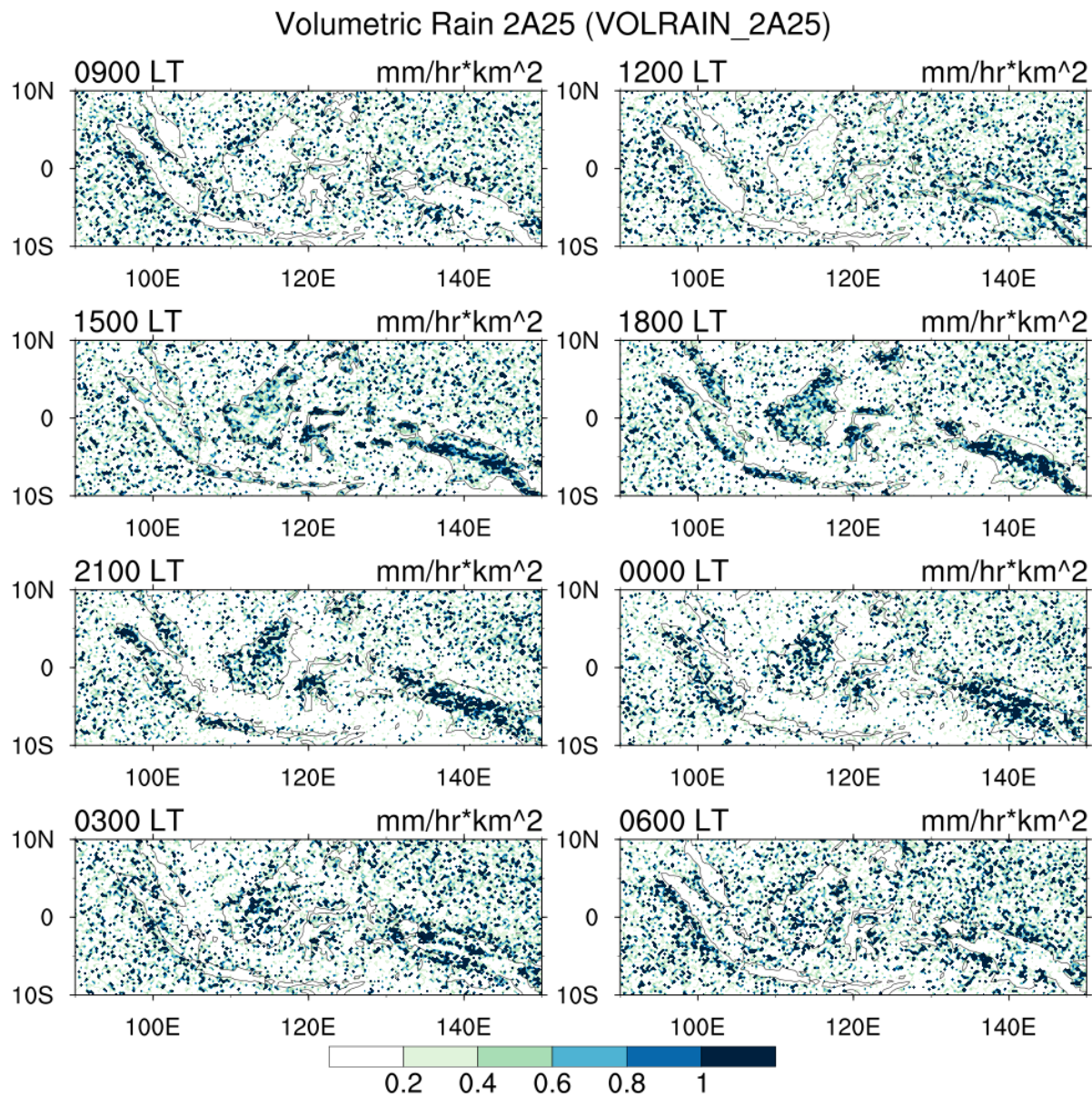
Figure 26. As in Fig. but for Volumetric Rainfall (mm/hr*km^2)

CHAPTER 4

Modulation of the Diurnal Cycle by the MJO, Kelvin waves and Equatorial Rossby Waves

4.1. Literature Review

It is well documented that the MJO and CCEWs have a significant influence on the thermodynamic environment of the convective system. But, wave modulation on the different types of convections (scattered and well-organized deep convection) and precipitation differs temporally and spatially (Van Der Linden et al. 2016). The MJO is a dominant component of tropical intraseasonal variability. It first identified as an intraseasonal variability with a 40–50 days wave period by Madden and Julian in a series of papers (1971, 1972) and later in 1994. A review paper by Zhang (2005) noted that the MJO is periodic in the range of 30 to 90 days. As summarized in chapter 1, the MJO is eastward propagating large scale disturbance of the tropical atmosphere-ocean system. Like a wave, the MJO characterized by amplitude and different phases (wave trough-ridge or enhanced and suppressed convection stages). The MJO characteristics and variability studied in various ways. Its amplitude and phases can identify the MJO perturbation isolated by using wave-number frequency filtering of geophysical field (e.g., OLR or Tb) or MJO events as it progresses eastward.

Wheeler and Hendon (2004) constructed a Multivariate MJO index using OLR and wind flow. The RMM indices show the development of non-MJO to MJO events propagates eastward with easterly and westerly anomalies that precede the onset of large-scale deep convection. The MJO events initiation is a period when transitioning of non-MJO phases to the MJO phase and typically may characterized as the onset of a large-scale, prolonged, and eastward propagating envelope of deep convective cloudiness over the Indian ocean (Wheeler and Hendon 2004). The MJO enhanced envelope developed over Indian Ocean, propagates eastward, and then dissipates as a suppressed over the western Pacific Ocean (Zhang 2005). The dynamic reorganization of

shallow convection into more mesoscale systems can trigger robust convective heating that results in an intensified large-scale wave motion of an MJO event. It is not an "on or off" kind of event; instead, it is a system with varied signal strength (Tromeur and Rossow 2010).

The MJO envelope propagates with an approximate wind speed of 5ms-1 in between Indian and western Pacific oceans (Zhang 2005). Studies show that some of the MJO events stall or terminate over the MC, but some slowly reach the Western Pacific (e.g., Majda and Yang 2016; Birch et al. 2016; Hendon and Salby 1994). While a slow propagation of the MJO has the potential to change the timing of the diurnal cycle, its termination may weaken the diurnal cycle (Innes and Slingo 2006). Studies also show that MJO terminates over the MC in association with the high terrain of large islands such as Borneo and Papua New Guinea (PNG) (Zhang 2005). Yokoi et al. (2017) argue that when the MJO reaches and passes, the MC heavy rainfall migrated to offshore during nighttime except for a shorter time onshore migration as the MJO passes through the region. This argument discussed by several researchers where mostly the nighttime offshore migration was observed in the west direction of the MC (e.g., Fujita et al. 2011). Figure 27 shows the MJO phases from initiation over the Indian Ocean to its dissipation over the western Pacific Ocean. The green shading denotes above-average rainfall, and the brown shading indicates below-average rain. The MJO consists of eight phases of propagation, which is categorized by one part as enhanced convective phases and the other phase as suppressed convective. The MJO convective phase (phase 1-4 events) exists over the Indian Ocean (western MC) and MC and suppressed phases (phases 5-8) western the Pacific Ocean. Convectively active MJO event phase that reached over the MC includes phases 3-5, and to some parts of the eastern MC phase, six is active (Gottschalck et al. 2010).

The MJO has a broader and significant influence on different global events such as the onset and active periods of the Indian monsoon (Chang et al. 2016), North American monsoon (Lorenz and Hartmann 2006), West African monsoon (Lavender and Matthews 2009) and also diurnal cycle of rainfall and deep convection over the MC (e.g. Neale and Slingo 2001; Virts et al. 2013). Some of the global systems influenced by the MJO includes El Nino Southern Oscillation (ENSO), storm track, tropical cyclone, Kelvin wave, tropical depression (TD-type) disturbances, equatorial Rossby wave, and monsoon systems (Schreck and Molinari 2011; Schreck et al. 2012; Weaver et al. 2011).

The prediction skill for intraseasonal variability like MJO has become a challenging task (Wheeler and Weickmann 2001). For example, Hung et al. (2013) simulated convectively coupled equatorial waves and MJO using several climate models and found that the models prediction capability is still not improved. They found one of the 20 climate models to be able to pinpoint a realistic eastward propagation of the MJO. Kim et al. (2009) used a diagnostic developed by the US Climate Variability and Predictability (CLIVAR) working group to diagnose the ability of 8 climate models to simulate the MJO. They recommended there needs to be a more realistic representation of the spectrum of variability in climate models to provide a better estimate of climate change extremes due to human activity.

Also, most global numerical models struggle to accurately forecast the multiscale interaction between diurnal cycle, the MJO, and CCEWs. Forecast inaccuracies are related to the lack of representation of the complex topography and diabatic heating profiles (Love et al. 2011; Majda and Yang 2016; Neale and Slingo 2001; Zhang et al. 2008). For instance, Majda and Yang (2016) argue that the interaction between the diurnal cycle of rainfall and the MJO is not well established. Janiga et al. (2018) analyzed prediction skill of the MJO, convectively coupled

equatorial waves at weeks 1-3 using Naval Earth System Model (NESM), ECMWF, and NCEP Climate Forecast System version 2 (CFSv2) models. They found that NSEM and ECMWF models show strong simulation skills for MJO-related signals, and CFSv2 is too slow and weak over the MC region. The statistical analysis of diurnal, synoptic, and intraseasonal variabilities discussed in this study can serve as a benchmark in improving numerical predictions over the MC.

Past studies used different datasets and methodologies to understand the MJO and Equatorial waves interact with each other and with tropical convection. Tromeur and Rossow (2010) and Tan and Jakob (2013) used ISCCP to identify the interaction between the MJO and deep tropical convection over the western Pacific and the MC. Thayer-Calder and Randal (2009) also studied the role of convective moistening in the MJO using Tropical Rainfall Measuring Mission (TRMM3B42) and European Center for Medium-Range Weather Forecasting (ECMWF) Re-Analysis (ERA-40). Straub and Kiladis (2003) used summer intraseasonal oscillation and OLR to understand the interaction between boreal summer intraseasonal oscillation and high-frequency tropical wave activity. They found shallow convection preceding deep heating and a vertical structure determined by both the shallow and deep modes. Schreck (2015) identify the convective anomaly of Kelvin waves and the MJO using TMPA.

Roundy and Frank (2004) reported the CCEWs (Kelvin and ER waves) might trigger by diabatic heating associated with organized deep convection. They also found that CCEWs modulate rainfall and convection in tropics. Over tropics, synoptic variability is a result of propagating disturbances with organized convective systems with spatial scale more substantial than the disturbance itself. One of the equatorially trapped waves is the Kelvin wave.

Lin (2007) defined the Kelvin wave as a type of low-frequency inertia-gravity wave trapped in a lateral boundary, such as mountain barrier. Kelvin wave has a distinct feature of being faster, occurs over a broader range of frequencies and wavenumbers, more global, and more concentrated to the equator compared to the MJO (Wheeler and Kiladis 1999). Convectively coupled Kelvin waves play a vital role in the generation of synoptic-scale rainfall variability (Schreck 2015). Considering the time of the year, Kelvin wave events observed at any time with the maximum frequency of events occur between February and August. The enhanced envelope of convection propagates eastward from equatorial Africa to the West Pacific Ocean at 15 m s-1 (Wheeler et al. 2000).

Like Kelvin wave, the ER occurs at any time of the year that propagates westward slowly at 5 m s-1. ER shows a characteristic of the dispersive wave, while Kelvin wave shows a non-dispersive wave behavior. ER wave also characterized by the geostrophic relationship between pressure and velocity fields (Matsuno 1966; Wheeler et al. 2000). Holton (1973) considers ER wave as of the most important for large-scale meteorological processes. Where ER is an absolute vorticity-conserving motion within inviscid barotropic fluid, dependent on the variation of the Coriolis parameter with latitude. However, in baroclinic atmosphere ER is a potential vorticity-conversing motion that depends on the isentropic gradient of potential vorticity.

4.2. Result and Discussion

The mere existence of MJO, Kelvin waves, and Equatorial waves cannot paint a full picture of how the diurnal cycle behaves over the MC alone. The consensus is that these tropical synoptic and intraseasonal variabilities can play a significant role in determining the diurnal cycle, but they are not the only factors. In this chapter, the interaction between diurnal cycle, the MJO, Kelvin waves, and Equatorial waves during the boreal winter season assessed. Morning

(0900LST) and afternoon (1800LST) hours selected for the analysis from the eight-time steps of the day (three hours interval) that these two periods of the day can explain the minimum and maximum better.

4.2.1. Diurnal Cycle of Rainfall

Fig. 28 shows the distribution of rainfall over land, coast, and sea. It is similar to fig. 6 in Worku et al. (2019) except that there only the mean values were discussed. Over land (fig. 28a) rainfall has higher dispersion in the afternoon (1800 LST) leading to midnight, and in the morning (0900 LST), rainfall dispersion is smaller. Rainfall over land gradually decreases from midnight to midday and then starts increasing in the afternoon. The dispersion and diurnal variability of rainfall over land are higher than both over the coast (fig. 28b) and ocean (fig. 28c). Over coast and ocean, the dispersion of rainfall indicates a smaller diurnal change with a slight increase in the morning hours, particularly over the coast.

Sakaeda et al. (2018) found two distinct diurnal rainfall peaks over western MC (Indian Ocean). These peaks are late afternoon rainfall peak in association with SST and surface fluxes and an early to late morning rainfall peak in association with increased low-tropospheric moisture. It is consistent with the diurnal cycle of rainfall and diurnal dispersion of rainfall discussed in figure 16 and figure 28, respectively.

The box plots show only small variations in the shape of the dispersions throughout the day. The range of values is larger over land in the afternoon, owing to the larger values of rainfall. The interquartile ranges (IQR), boxes, at the diurnal peak (1800 LST) do not overlap with those at the diurnal minimum (0900 LST), indicating the significance of the diurnal cycle over land. The ranges always overlap for the coast and ocean in which the diurnal variability is small.

4.2.2. Diurnal Cycle of Convection (IR-WS12 and IR-WS3)

Fig. 29 shows box plots of the diurnal variation of well-organized deep convection (IR-WS12) and scattered, less well-organized deep convection, (IR-WS3) over the MC. Well-organized deep convection is occurring over land, while non-organized scattered convection is more frequent over coast and ocean (Houze et al. 2015). Well-organized deep convection dispersion is higher than scattered convection over land, coast, and sea. Over land well-organized deep convection dispersion is higher in the afternoon leading to early morning hours and smaller around 1200 LST. Scattered convection over land shows larger dispersion at noon. But over coast and sea, both well-organized deep convection and shallow convection shows a dispersion with very smaller to negligible diurnal change. Nitta and Sekine (1994) finding of diurnal variability of convection shows organized deep convection peaks in the afternoon over land and the morning over coast and ocean, consistent with the result above.

The box plots show small variation in the shape of dispersions throughout the day all over the MC. Over land range of dispersion of well-organized deep convection is larger in the afternoon while scattered convection (IR-WS3) is smaller. The IQR for organized convection diurnal peak at 2100 LST does not overlap with minimum diurnal convection at 1200 LST. But like rainfall in fig. (28), Coast and sea show IQR values often overlap. Shallow convection also shows an overlap of IQR over coast and sea while over land the diurnal maximum (1200 LST) and minimum (1800 LST) do not overlap. The variability of well-organized deep and shallow convection over land is significant than the coast and sea. The maximum and minimum rainfall and well-organized deep convection often occurred over land around at 1800 LST and 0900 LST, respectively, and vice versa for shallow convection. Over coast and sea rainfall is a peak at 0900 LST and a minimum at 1800 LST (Worku et al. 2019).

4.2.3. MJO phases relationship with Rainfall and Convection

Rainfall enhances between MJO phase 3 and 6 over the MC (Gottschalck et al. 2010). The propagation of MJO over the MC is not as smooth as portrayed in idealized models. Rather the mountainous islands block the propagation that convection and wind anomalies dissipated around these islands. Rainfall and convection enhanced during phases 3 and 4 with an enhanced envelope of convection over the MC (Wu and SU 2009). Figure 30 illustrates the interaction between rainfall and MJO phases during 0900 (left) and 1800 LST (right). The presence of MJO over land does not affect morning rainfall; rather, it moderately affects afternoon rainfall. The afternoon rainfall enhanced during MJO phase 3. Over coast and ocean, the MJO effect on rainfall is significant than land. Rainfall peaks during phase 4.

The impact of MJO on rainfall over the coast and sea is larger in the morning than afternoon. It is clear from fig. 30 that MJO exerted a small impact on rainfall over land, but a larger impact on coast and sea. The MJO effect on the mean diurnal cycle of rainfall at different phases depicted in figure 31. Compared to the mean diurnal cycle of rainfall in fig. 22a afternoon rainfall exhibits significant enhancement over land during MJO phases 3 and 4. Coastal and ocean regions morning rainfall reaches maxima when MJO phase 4 passes over the MC. The MJO modulates rainfall and convection over the coast and ocean significantly compared to land (Sakaeda et al. 2017). The MJO presence over the MC affects not only rainfall but well-organized deep and non-organized shallow convections.

Figure 32 shows the modulation of well-organized deep convection (IR-WS12) by both active and suppressed phases MJO during 0900 and 1800 LST. Well-organized deep convection enhanced over land and coast in the morning and afternoon during MJO phase 4. But over sea organized convection peaks during MJO during phase 5. The dispersion of convection is not

symmetric, like rainfall. Throughout the MC MJO phases, 1 and 8 suppresses organized

convection. The variability of organized convection is slightly higher in the afternoon than in the

morning. Modulation of deep convection by the MJO explained by analyzing the fluctuation of

the diurnal mean frequency of convection. Figure 33 presents the impact of each MJO phase on

the frequency of occurrence of deep convection. Diurnal cycle of IR-WS12 in fig. 22b presented

that at 1200 LST, the mean diurnal frequency is similar to over land, coast, and sea. It slightly

modified due to the presence of MJO over the region. The IR-WS12 frequency of occurrence

over land increased in MJO phases 3, 4, and 5.

On the contrary, it decreases during MJO phases 1, 2, 7, and 8. The deep convection

frequency increased over coastal regions when MJO is at phase 4 and 5 but stays the same or

decreased in the rest of the phases. Deep convection frequency is more significant than ocean

convection as opposed to fig. 22b result. According to Tromeur and Rossow (2010), well-

organized deep convection produces 3 and 4 times more precipitation compared to scattered

convection over the MC.

Figure 34 presents the modulation of non-organized shallow convection (IR-WS3) by

MJO (both suppressed and active phases) during 0900 and 1800 LST. Shallow convection

dispersion is higher over land than other regions. The MJO phase 1 and 6 slightly enhances the

convection over land both during morning and afternoon, and they suppressed somewhat in

Phase 4. However, the coast and sea do not show any coherent variations. The presence of MJO

affects not only the distribution of shallow convection but also the mean diurnal cycle of the

frequency of occurrences. Figure 35 shows that different MJO phases modulate the diurnal cycle

of the mean frequency of occurrence of IR-WS3. The frequency of IR-WS3 enhanced or stay the

same around noon over land during MJO phases 1, 2, 7, and 8. But IR-WS3 frequency decreases

in all other phases. Similar to figure 33, coastal shallow convection frequency shows a greater increase than ocean regions.

4.2.4. MJO, Kelvin waves, and Equatorial Rossby waves interaction with rainfall and convection (1800 LST)

The wet, decreasing, dry, and increasing wave phases of MJO, Kelvin waves, and ER waves interaction with rainfall over land, coast, and sea during 1800 LST discussed in fig. 36. The dispersion of rainfall enhanced when MJO is in wet, increasing, and decreasing wave phases. But rainfall is suppressed when MJO is in the dry wave phase. The variation is significant where IQR does not overlap and less significant where it does. The MJO box plot shows that wet and dry phases IRQ do not overlap while decreasing and increasing phases overlap. But the boxplot for Kelvin and ER waves shows wet, increasing, dry, and decreasing phases overlap over land, coast, and sea.

The wave phases impact on the mean diurnal rainfall presented in figure 37. Afternoon rainfall over land enhances during wet MJO wave phase while suppressed in increasing phase and stays the same as in figure 22a in decreasing and dry phases. Over coast and sea, dry and increasing phases suppress rainfall while wet and decreasing phases enhance rainfall.

Figure 38 presents the modulation of rainfall by Kelvin wave that afternoon rainfall over land enhances in wet and decreasing Kelvin wave phases and stay the same as in fig. 22a during dry and increasing phases. Coastal morning rainfall shows enhancement in all wave phases while ocean rainfall is unaffected. Figure 39 presents ER wave phases that don't modulate afternoon rainfall over land as MJO and Kelvin wave phases did. ER wave also doesn't have a significant effect on coastal and ocean region morning rainfall. The MJO, Kelvin waves, and ER waves modulation of the diurnal cycle are not limited to rainfall only; rather, it modulates well-organized deep convection and non-organized shallow convection.

The wet, decreasing, dry, and increasing wave phases of MJO, Kelvin, and ER waves interaction with well-organized deep convection (IR-WS12) at 1800 LST discussed in fig. 40 over land, coast, and sea. The deep convection enhanced during wet and decreasing MJO wave phases over the MC but suppressed by dry and increasing wave phases. Kelvin waves wet and decreasing phases enhances deep convection over land with significant variation than over coast and sea. ER waves triggered the opposite effect of what MJO did on deep convection. ER wave enhanced the deep convection during dry and increasing phases and suppressed it during wet and decreasing phases all over the MC. The boxplot shows IQR of enhanced and suppressed organized convection do overlap for Kelvin wave phases but do not overlap during MJO and ER wave phases. The wave phases with small to no overlap indicate the significant variation between maxima and minima, while overlap shows insignificant variation.

On the other hand, the MJO wave phases modulation effect on the diurnal mean of frequency of occurrence depicted in figure 41. IR-WS12 frequency of occurrence decreases over land, coast, and ocean during wet and dry wave phases but increases during decreasing and increasing wave tendencies. The diurnal mean of frequency of occurrence of IR-WS12 over coast increases compares to over ocean region in all wave phases. As shown in figure 42, unlike the MJO wave phases, Kelvin wave phases don't increase the frequency of occurrence of deep convection over land. Slightly it decreases it during wet and decreasing phases and stays the same as in figure 22b in dry and increasing phases. Unlike MJO and Kelvin wave modulation of IR-WS12 by ER wave (figure 43) show increasing in frequency of occurrences during wet and decreasing wave phases and frequency of occurrence decreases in dry and increasing wave phases. The deep convection over coast does not change much (same as in fig. 22b) during dry and increasing wave phases but increases in wet and decreasing phases. Over the ocean, the deep

convection frequency of occurrence decreases during dry and increasing wave phases and increases during decreasing wave phase while unaffected in wet wave phase.

The wet, decreasing, dry, and increasing wave phases of MJO, Kelvin, and ER waves interaction with scattered convection at 1800 LST over land, coast, and sea discussed in figure 44. Over land MJO dry and increasing wave phases enhanced scattered convection slightly better than wet and decreasing wave phases, and the opposite is true for ER wave phases. The rest of the wave phases change is not significant to affect the shallow convection variation. Apart from the modulation of non-organized shallow convection distribution, the diurnal mean of frequency of occurrence modulation by wave phases depicted in figure 45. Over land presence of dry and increasing MJO wave phases decreases shallow convection frequency of occurrence while wet and decreasing wave phases do not affect it. Coastal scattered convection frequency shows increment in all wave phases. Dry and increasing wave phases increase scattered convection over the ocean. Coastal convection increases more than ocean convection during all wave phases.

Figure 46 shows the modulation of scattered convection by Kelvin waves. The scattered convection frequency over land decreases in all wave phases. However, over coast and ocean IR-WS3 frequency increases in all wave phases. Again, scattered convection over coast shows more frequency increment than over the ocean. Figure 47 depicts the modulation of IR-WS3 by the presence of ER waves. The scattered convection frequency over land increases during dry and increasing wave phases and decreases during wet and decreasing phases. Coastal scattered convection frequency increases more than ocean convection.

4.3. Summary

Diurnal cycle of rainfall during boreal winter shows higher dispersion variation over land than over coast and ocean regions. Land regions exhibit higher distribution late in the afternoon

leading to early morning hours and fewer distributions morning through noon. However, coast and ocean display a small variation in the distribution of rainfall throughout the day. The distribution of rainfall confirms the maximum and minimum diurnal mean values of rainfall, as stated by Worku et al. (2019).

Well-organized deep convection (IR-WS12) shows a similar distribution pattern as rainfall does over land. Deep convection has a higher distribution late in the afternoon leading to the early morning than noon hours. There is no significant variation of deep convection almost all day over coast and ocean regions. On the other hand, the distribution of non-organized shallow convection (IR-WS3) over land is higher during noon hour than at other times of the day. Coastal and ocean areas display an insignificant change in the distribution of shallow convection.

The impact of equatorial bound intraseasonal variabilities on the diurnal cycle of rainfall and convection evidenced. During MJO phases 3 to 6 over the MC landmasses, rainfall increases to a peak at 1800 LST, but dramatically smaller at 0900 LST during all MJO phases. It is quite a different rainfall distribution scenario when MJO phases analyzed over the coast and ocean. Coastal and ocean regions rainfall enhanced at 0900 LST than 1800 LST during MJO phase 4. All over the region, when MJO is at phases 1 and 8, rainfall seems suppressed and reaches minima throughout the diurnal range.

Well-organized deep convection over MC landmasses indicates an enhancement of distribution frequency during MJO phases 3 to 6. A frequency distribution is higher during phase 4 over land and coast while during phase 5 over ocean regions. The frequency of dispersion of deep convection is higher over land than coast and ocean during both morning and afternoon

hours. Same as rainfall distribution, MJO phases 1 and 8 suppressed deep convection than other phases.

Unlike rainfall and well-organized deep convection, the dispersion of non-organized shallow convection displays a smaller change in between MJO phases over coast and ocean both in the morning and afternoon. Contrary to that, over land-masses shallow convection frequency distribution peaks during phases 1 and 8 while it is smaller during phase 4.

The wave phase of MJO, Kelvin waves, and ER waves exerted influence on the diurnal variation of rainfall and convection. Rainfall and convection over the MC have strong activity in the afternoon than morning hours, as Worku et al. (2019) suggested, then we chose to study wave phase at 1800 LST alone. Rainfall distribution over the MC is larger when the MJO is at wet and decreasing wave phase but smaller when the phase is dry. Kelvin waves and ER waves phase displays a similar effect on rainfall over the MC except for slight enhancement over land during wet and decreasing phases.

Well-organized deep convection may enhance during MJO dry and increasing wave phases but suppressed during wet and decreasing phases over the region. Kelvin wave phases show insignificant change of deep convection distribution. ER show an increased convection during wet and decreasing wave phases. Scattered convection has a similar distribution pattern during all wave phases in the MC. But the wave phases seem to enhance the shallow convection over land during wet and decreasing phases.

One of the primary motivations for this study is understanding of the complex interactions between the MC's diurnal cycle, the MJO, and equatorial waves. In a future study, we will examine how the diurnal cycles are shown here vary by the phase of the MJO and

equatorial waves. We suggest that improved knowledge of these interactions may lead to further

model development focused on this critical part of the global climate system.
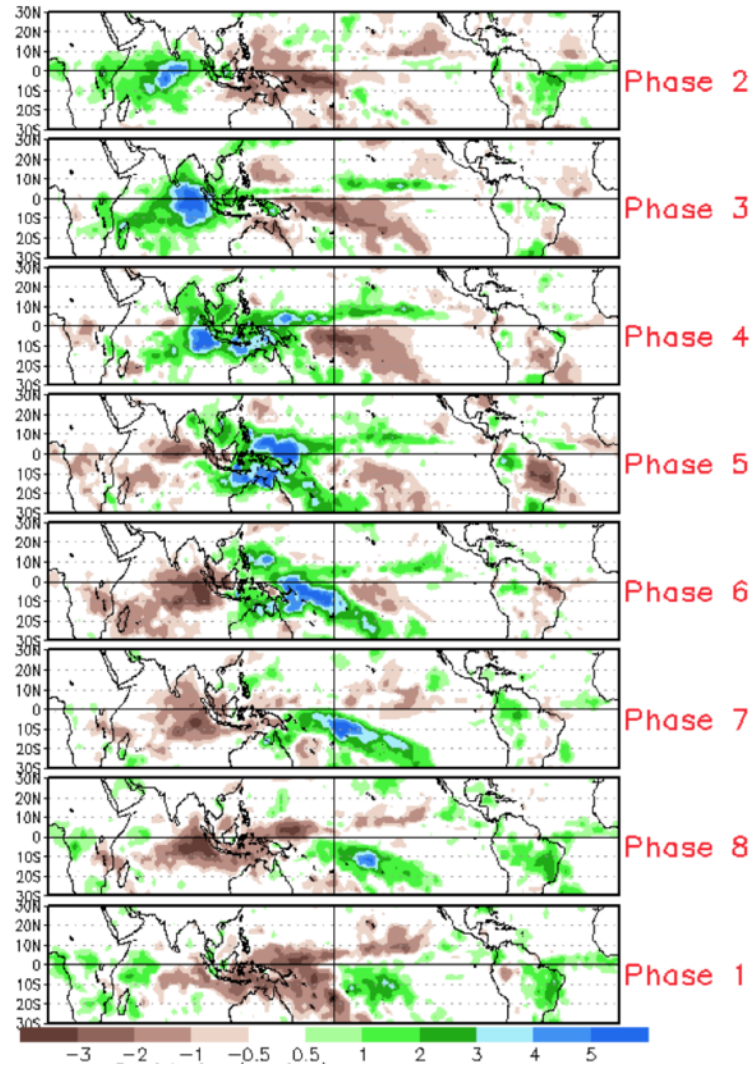
Figure 27. Difference from average rainfall for all MJO events from 1979 - 2012 for November - March for the eight phases described in the text. From Gottschalck et al. (2010)
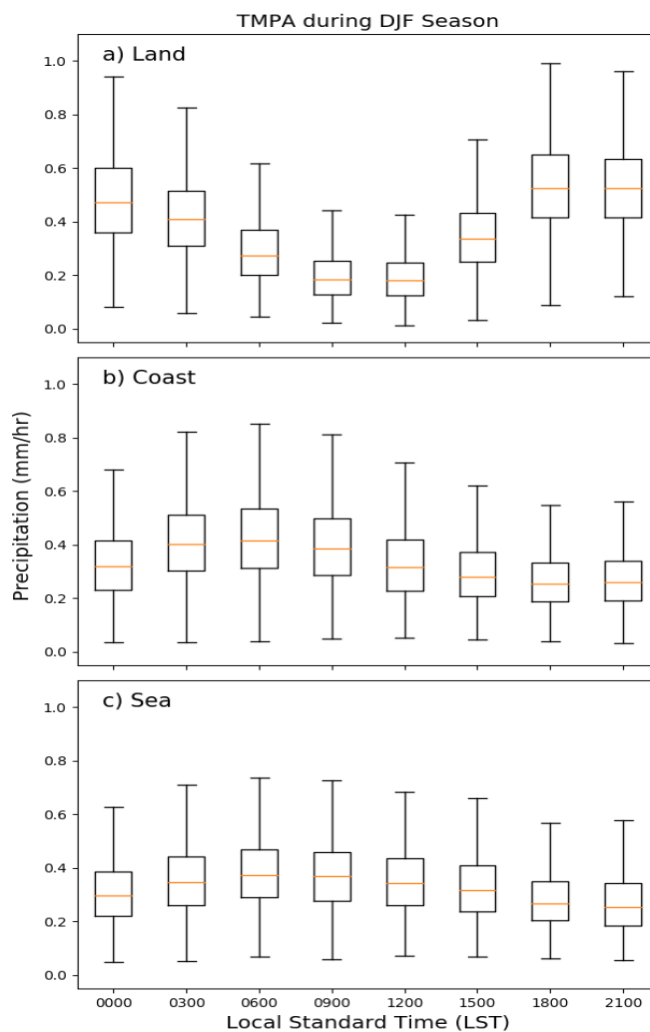
Figure 28. Box and whisker plot of TMPA Rainfall over the Maritime Continent. The orange

line in the box or Inter-quartile Range (IQR) represents 50% of data distribution. The line above

(below) the box is called Whisker and represent maximum (minimum) values in the data

represented with dash sign at the end of line. Outlier values are not included here for plot

cleanness. The variability of rainfall is larger over land where it peaks late in the afternoon and

minimum during noon LST. Over coast and sea rainfall variability is smaller.
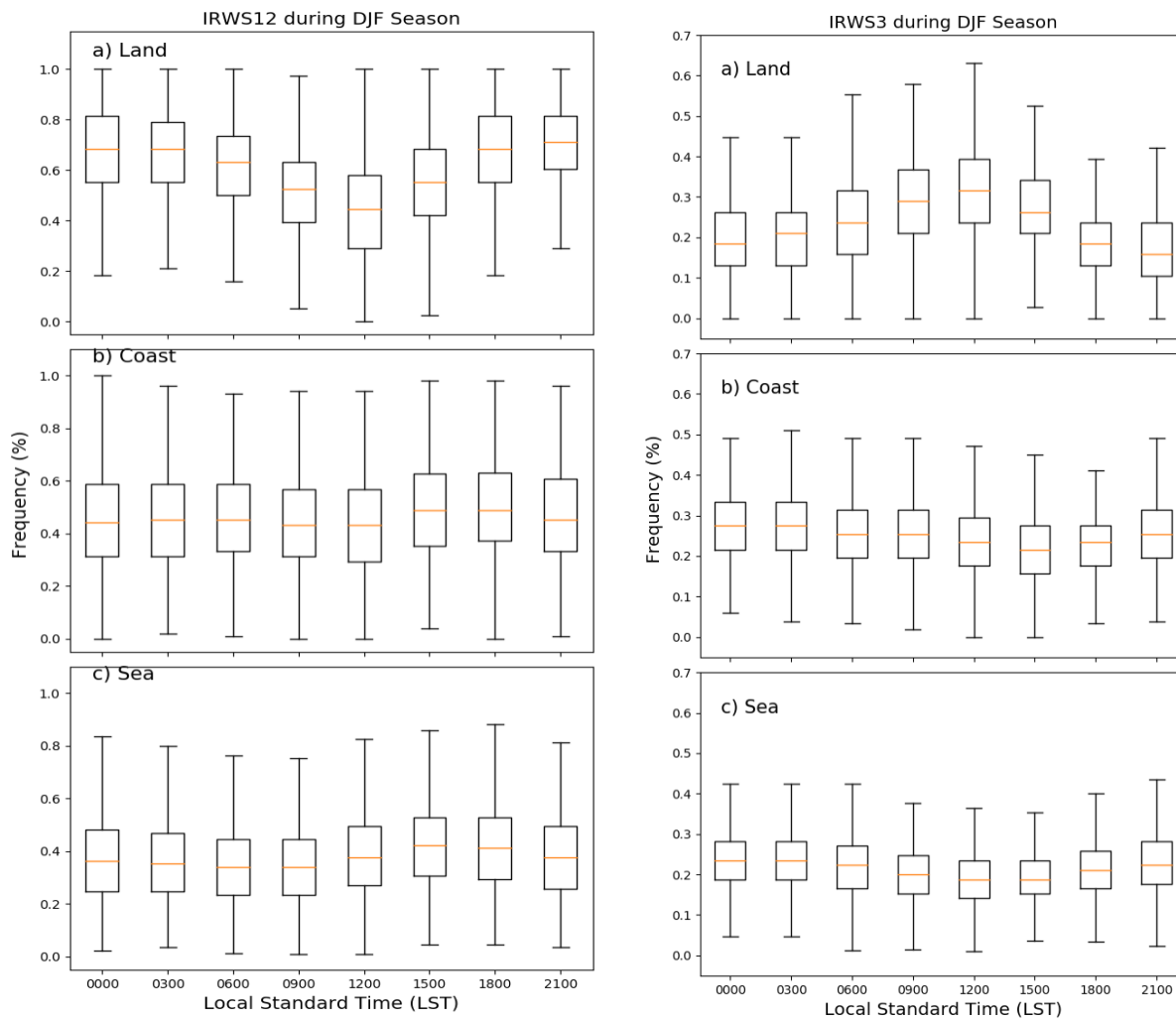
Figure 29. Box and whisker plots of well-organized deep convection (IR-WS12) and shallow

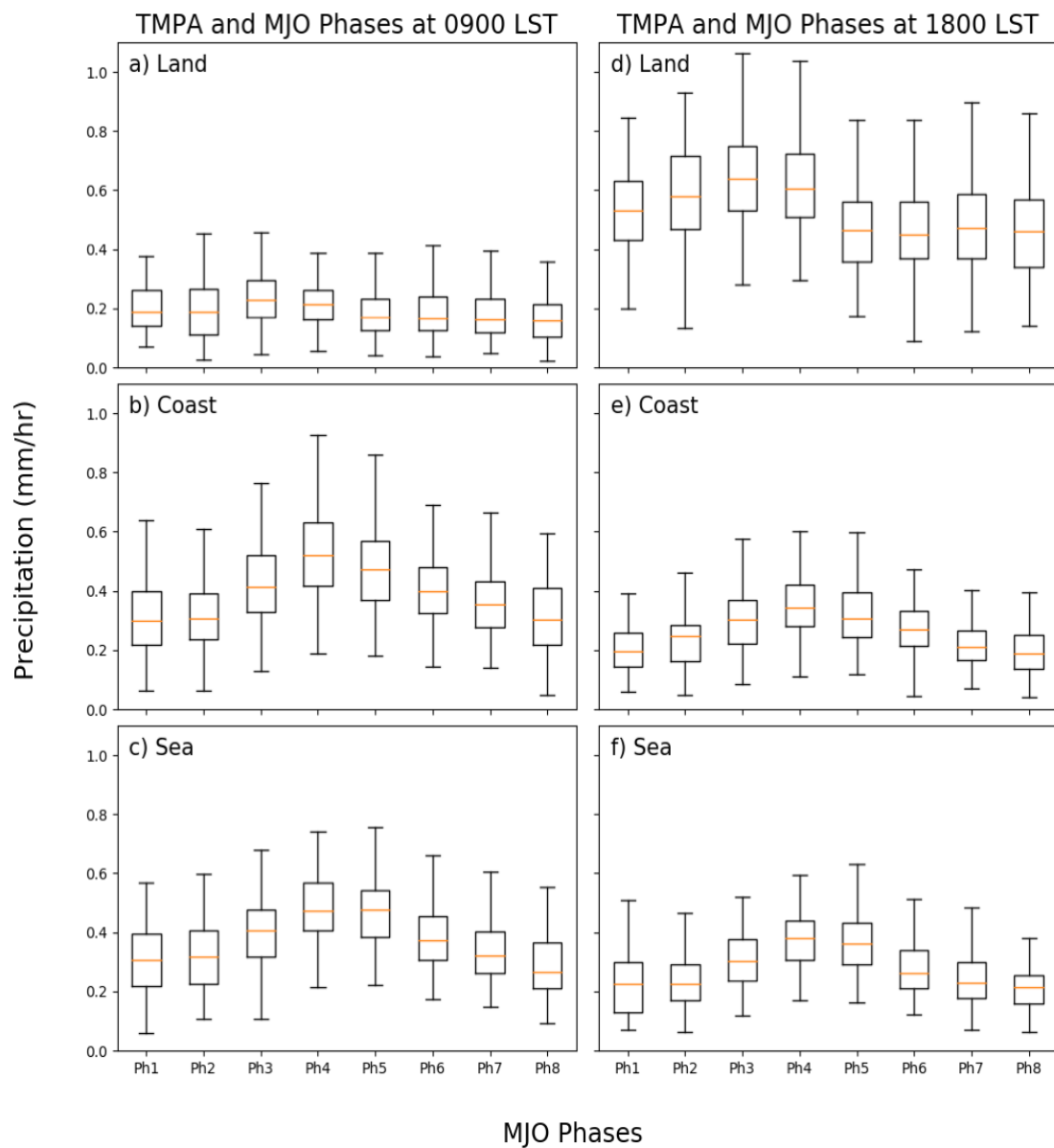convection (IR-WS3) during DJF over the Maritime Continent.

Figure 30. Box and whisker plots of TMPA and MJO Phases over the Maritime Continent during
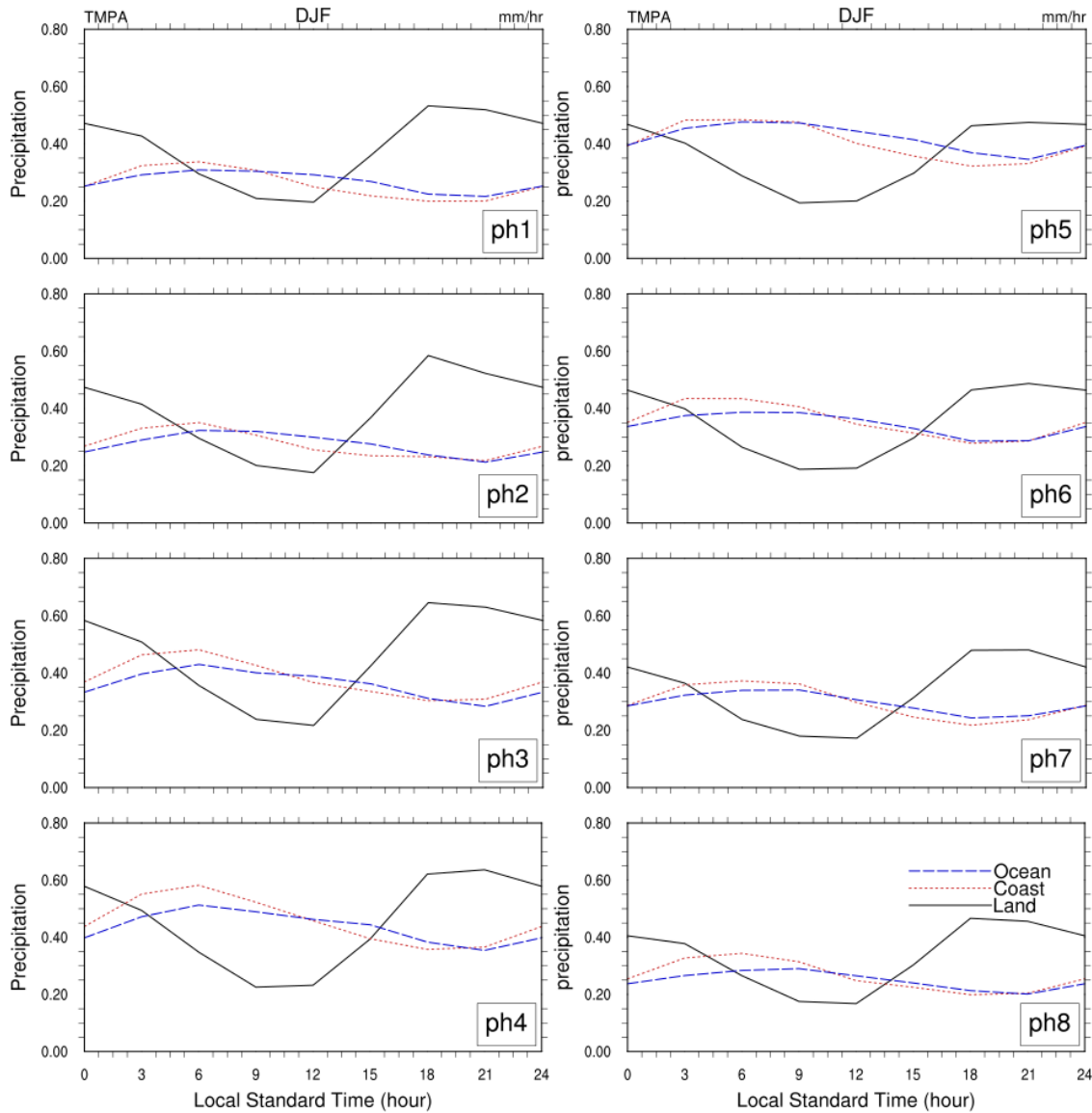
DJF at 0900 and 1800 LST.

Figure 31. The diurnal mean TMPA rainfall during MJO phase 1-8 over land, cost, and sea of

the MC. Rainfall over land shows a more pronounced change as the MJO phase changes than

over coast and sea.
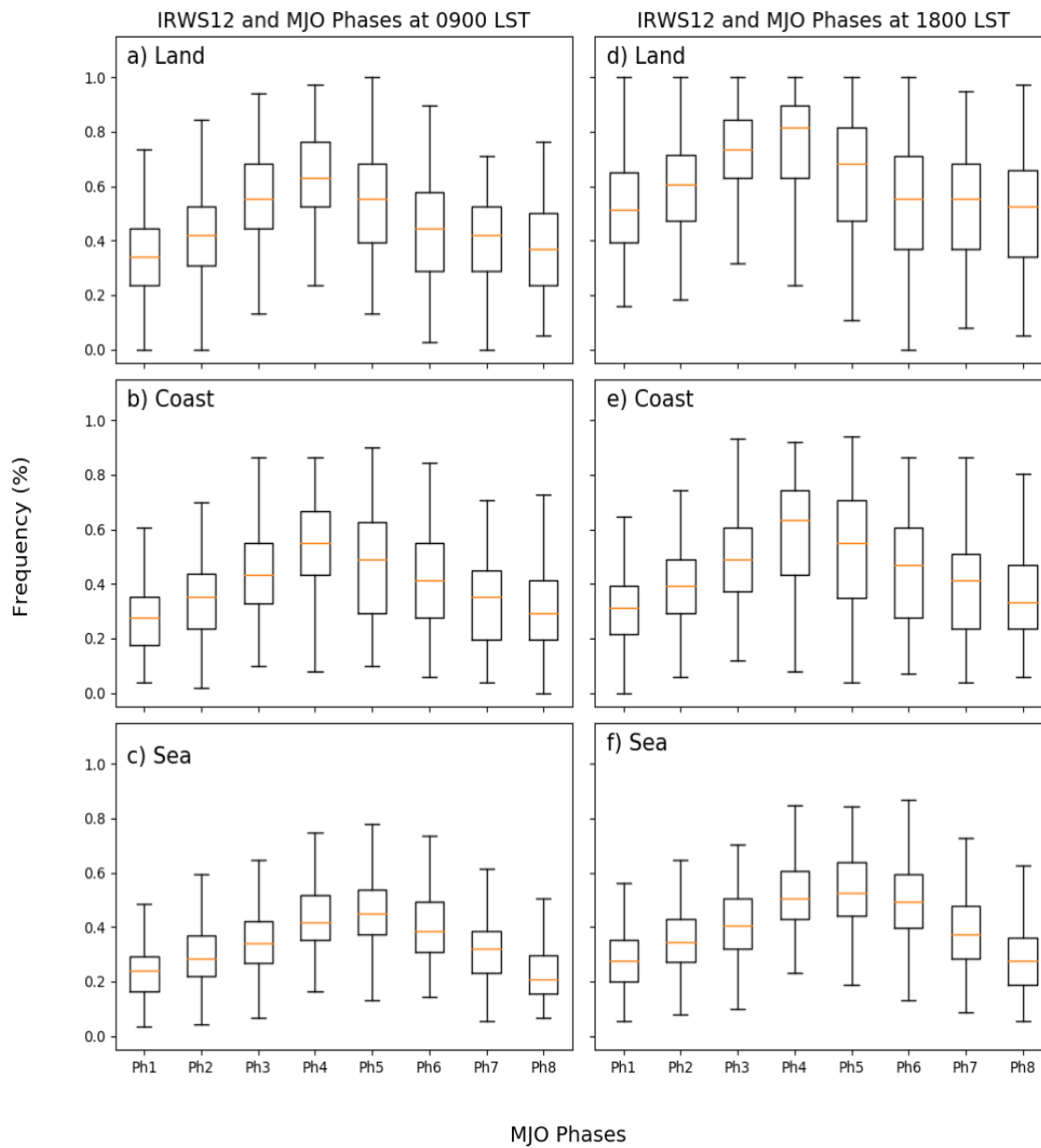
Figure 32. Box and Whisker plots of well-organized deep convection (IR-WS12) and MJO

Phases over the Maritime Continent during DJF at 0900 and 1800 LST.
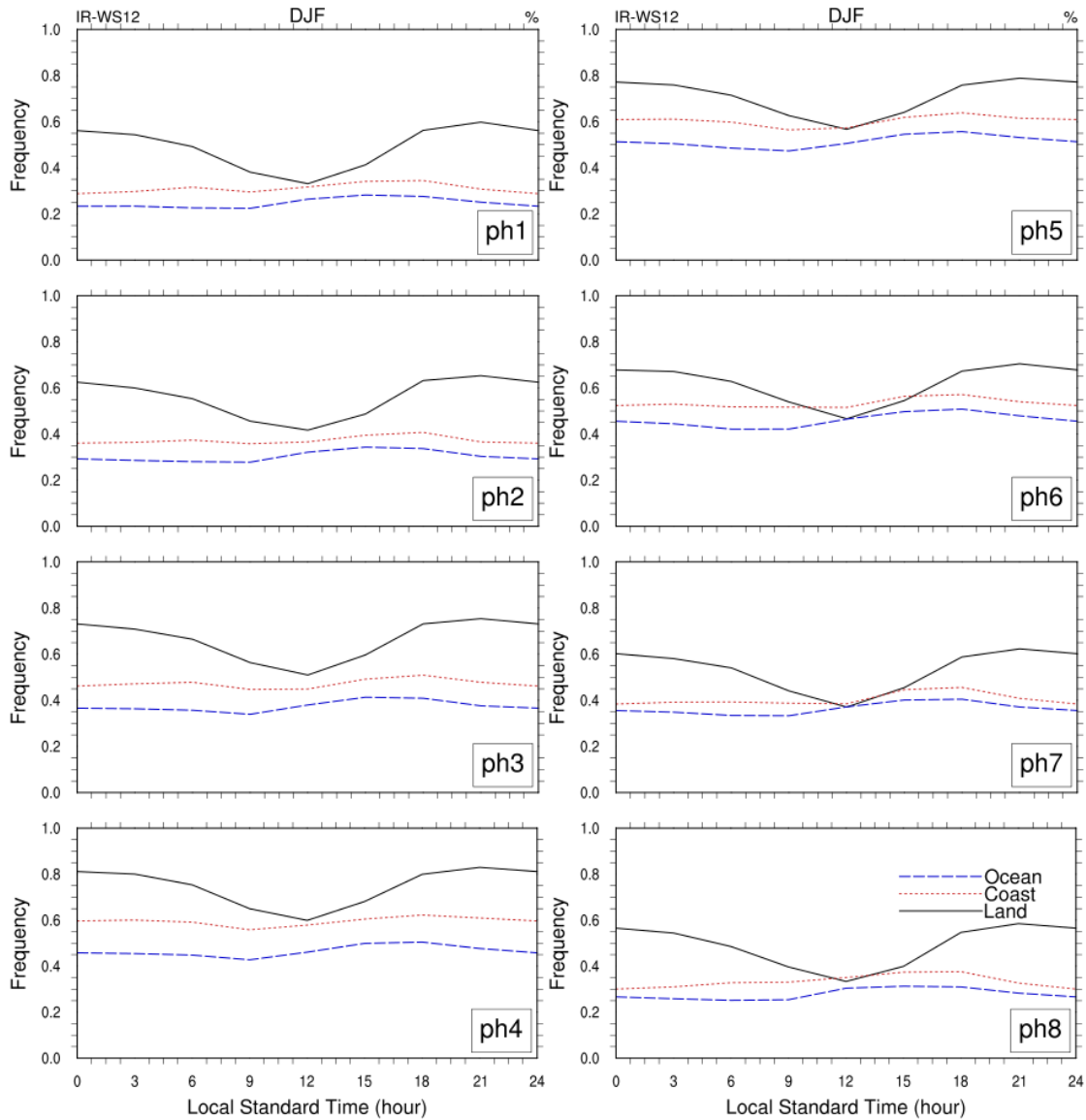
Figure 33. As in Fig. 31, but for IR-WS12
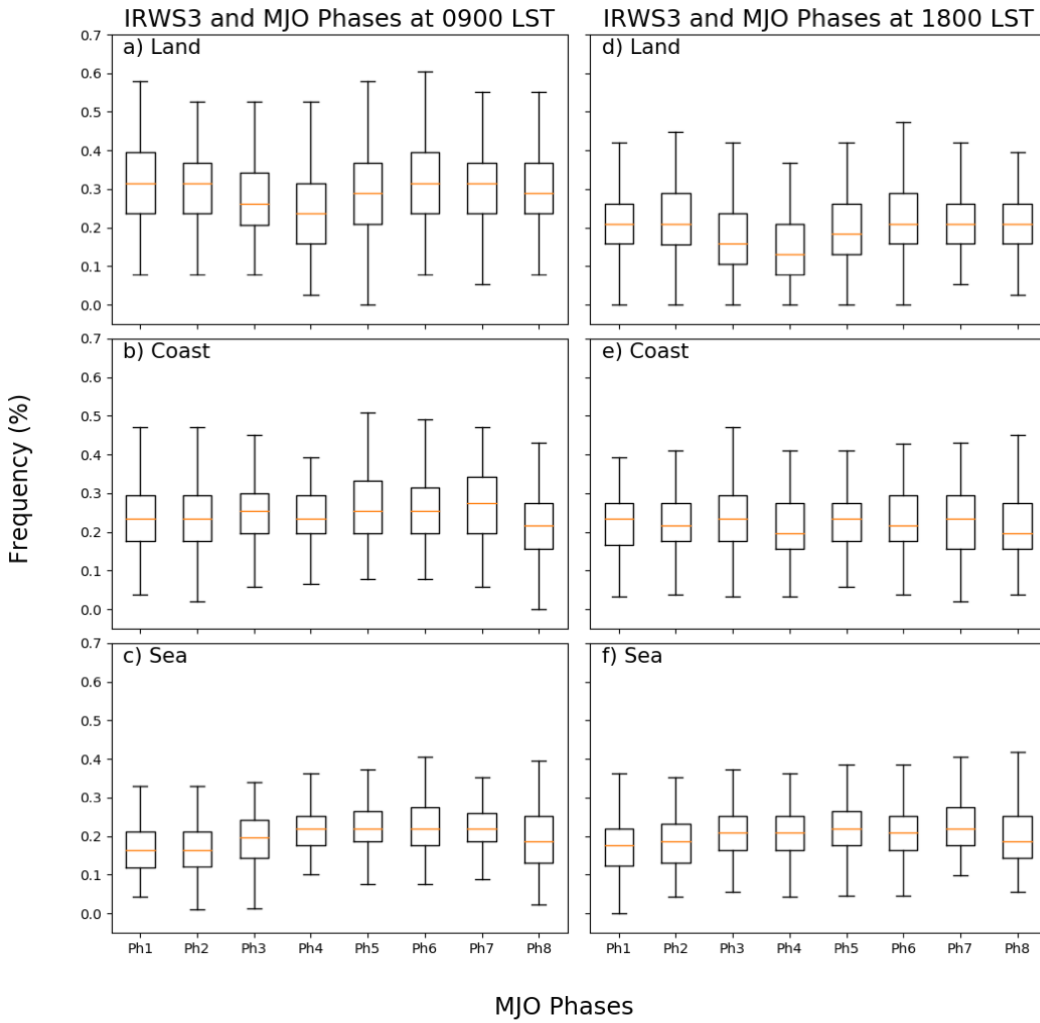
Figure 34. Box and whisker plots of shallow convection (IR-WS3) and MJO Phases over the

Maritime Continent during DJF at 0900 and 1800 LST.
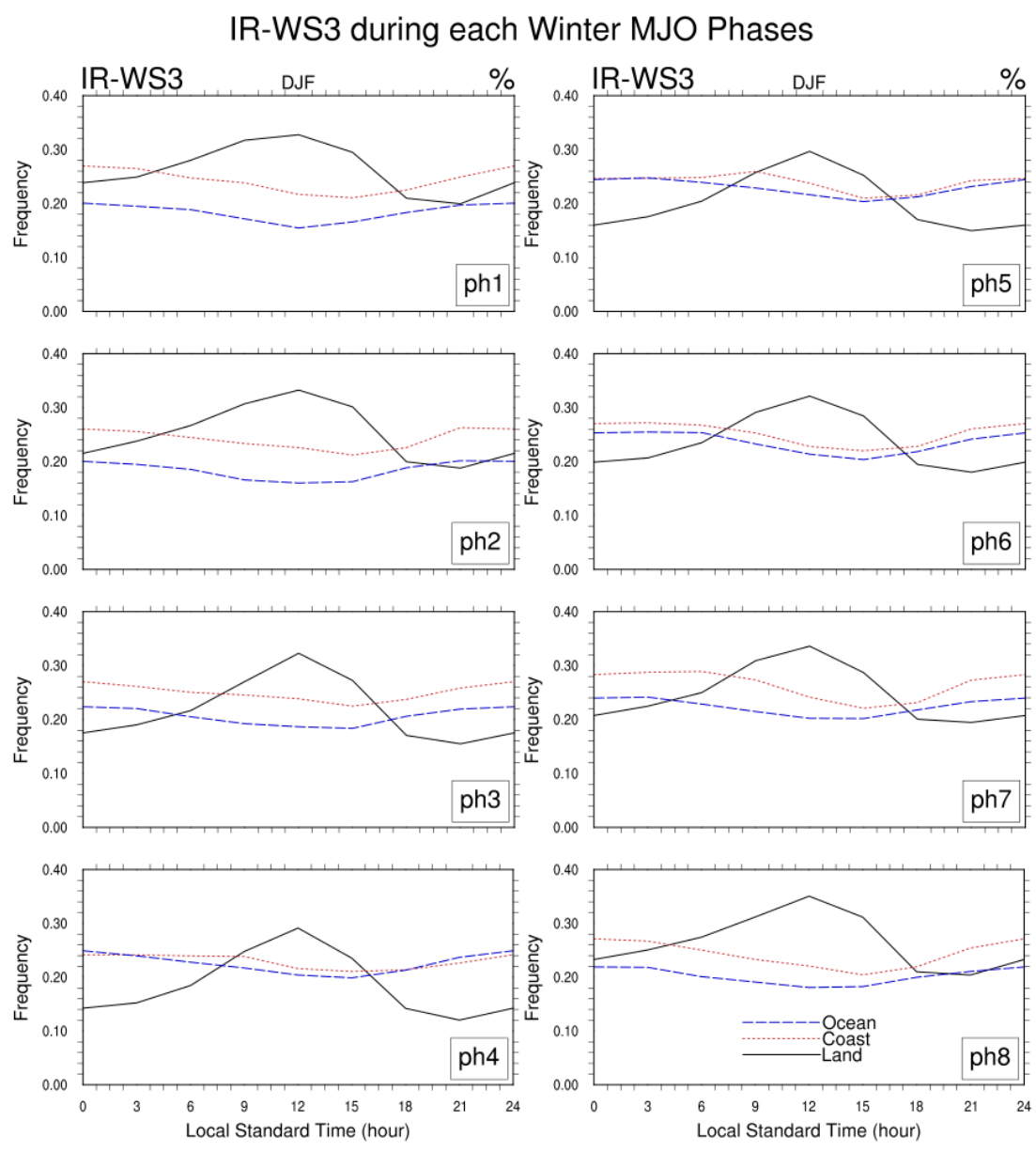
Figure 35. As in Fig. 31, but for IR-WS3
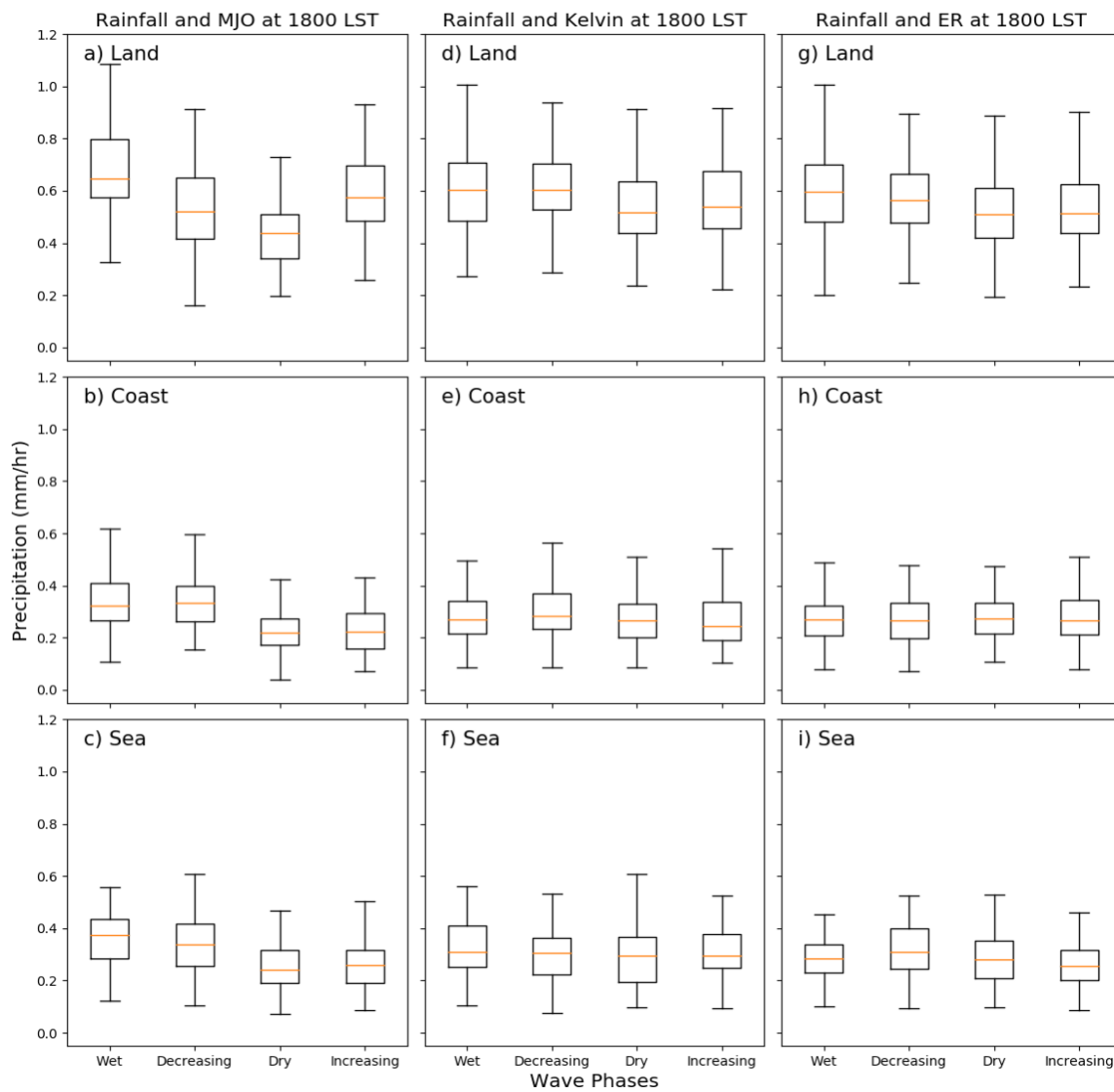
Figure 36. Box plots of MJO, Kelvin wave, and ER wave phases interaction with TMPA at 1800 LST during DJF over the Maritime Continent.
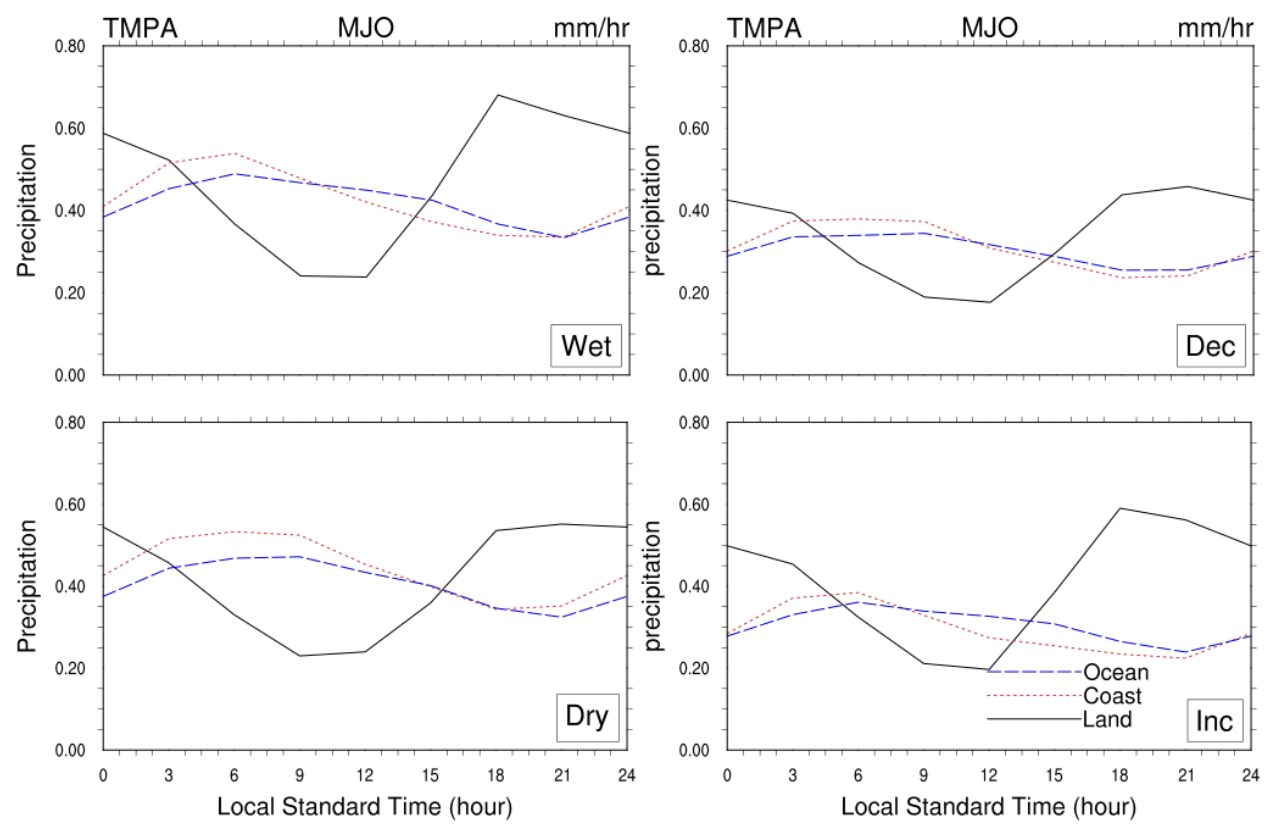
Figure 37. The diurnal mean rainfall during MJO's wet, dry, increasing and decreasing wave

phases. Wet and decreasing phases show an enhancement of rainfall while dry and increasing

phases show suppressed rainfall.
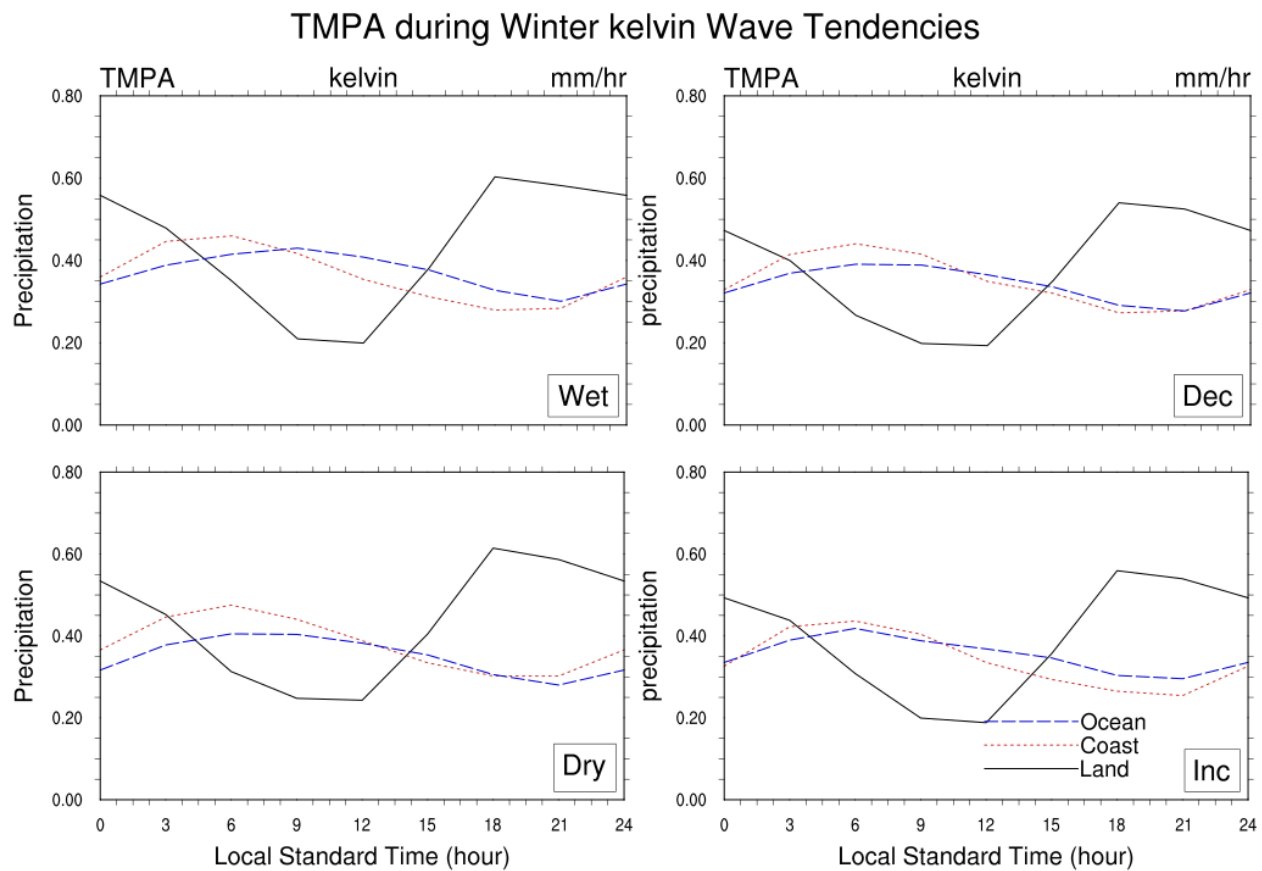
Figure 38. As in Fig. 37, but for rainfall during Kelvin wave phases
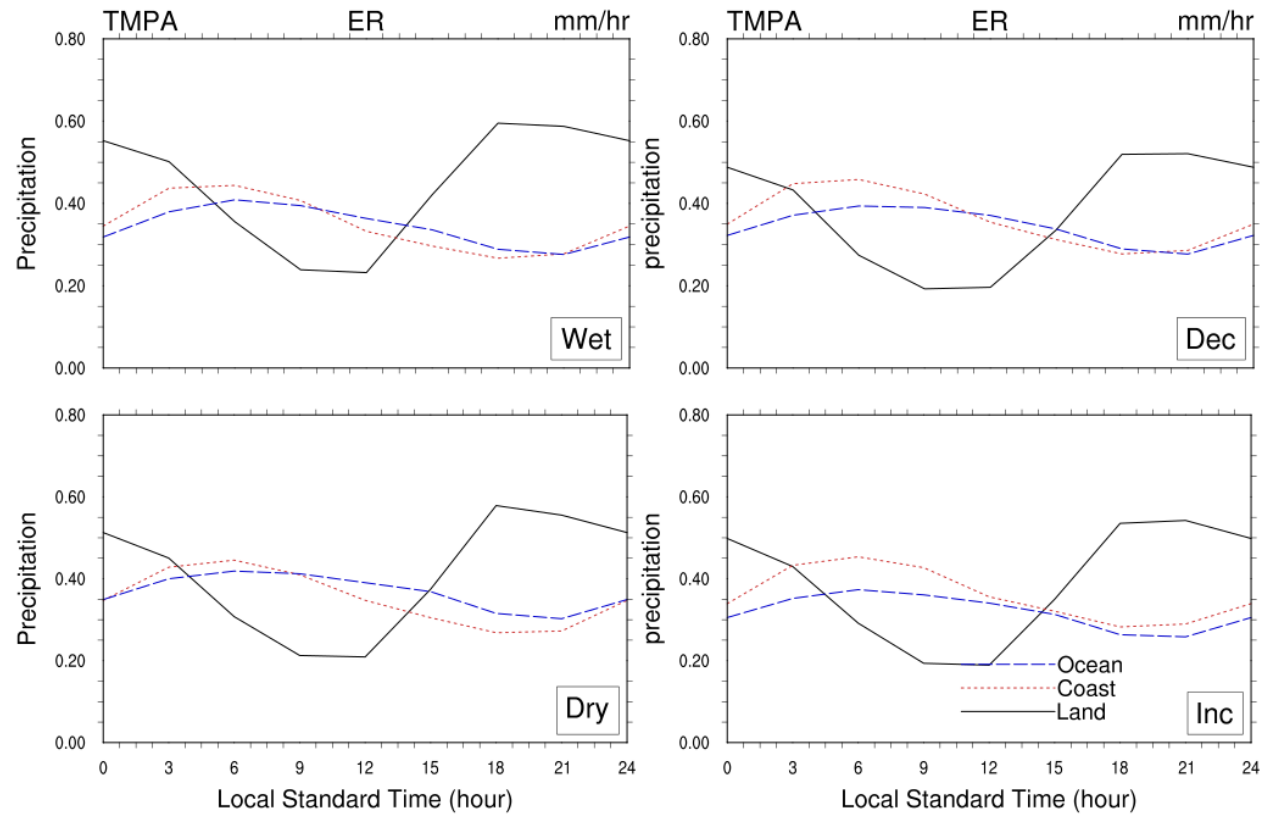
Figure 39 As in Fig. 37, but for rainfall during ER wave phases
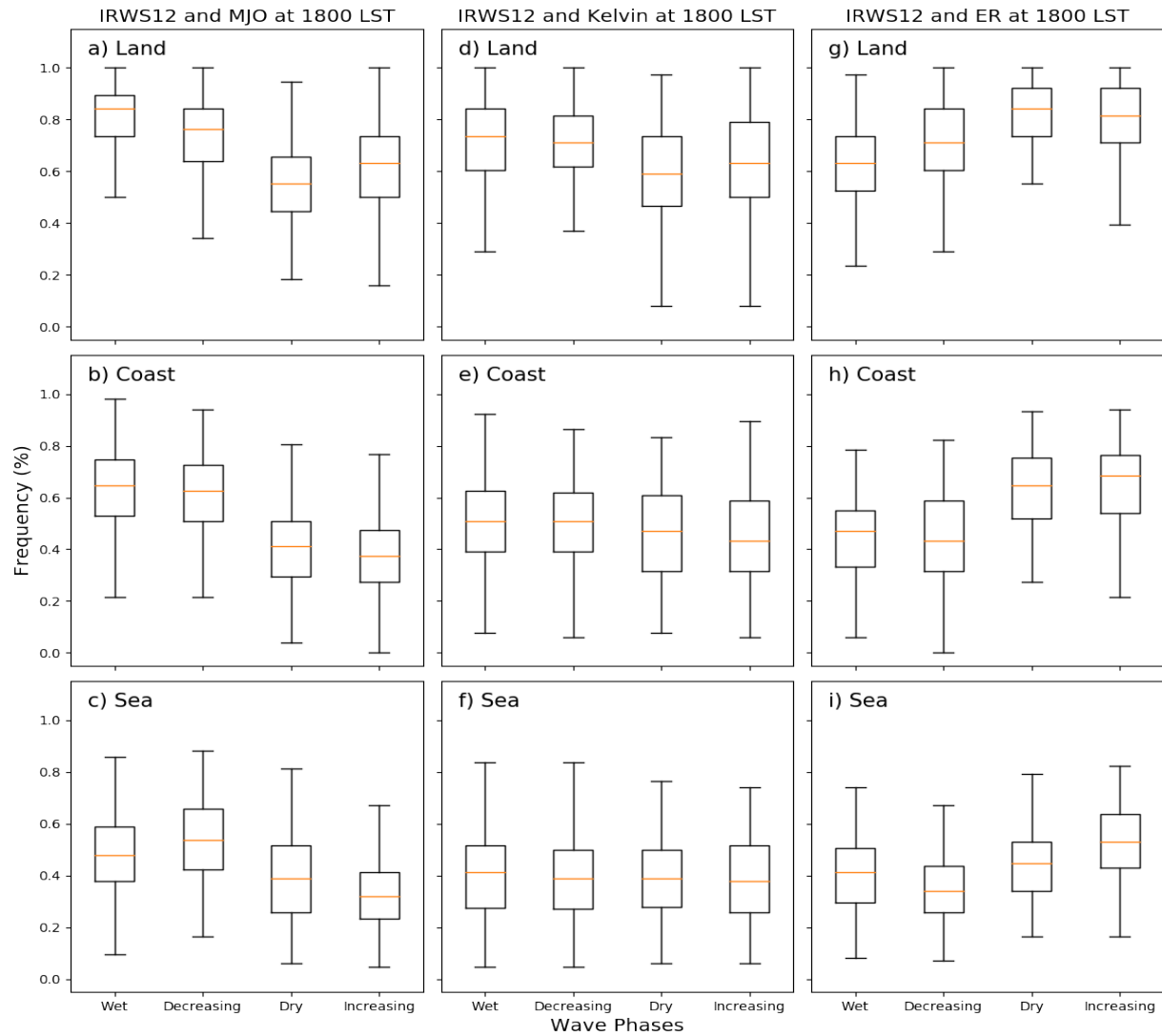
Figure 40. Box plots of MJO, Kelvin wave, and ER wave phases interaction with well-organized

convection (IR-WS12) at 1800 LST during DJF over the Maritime Continent.
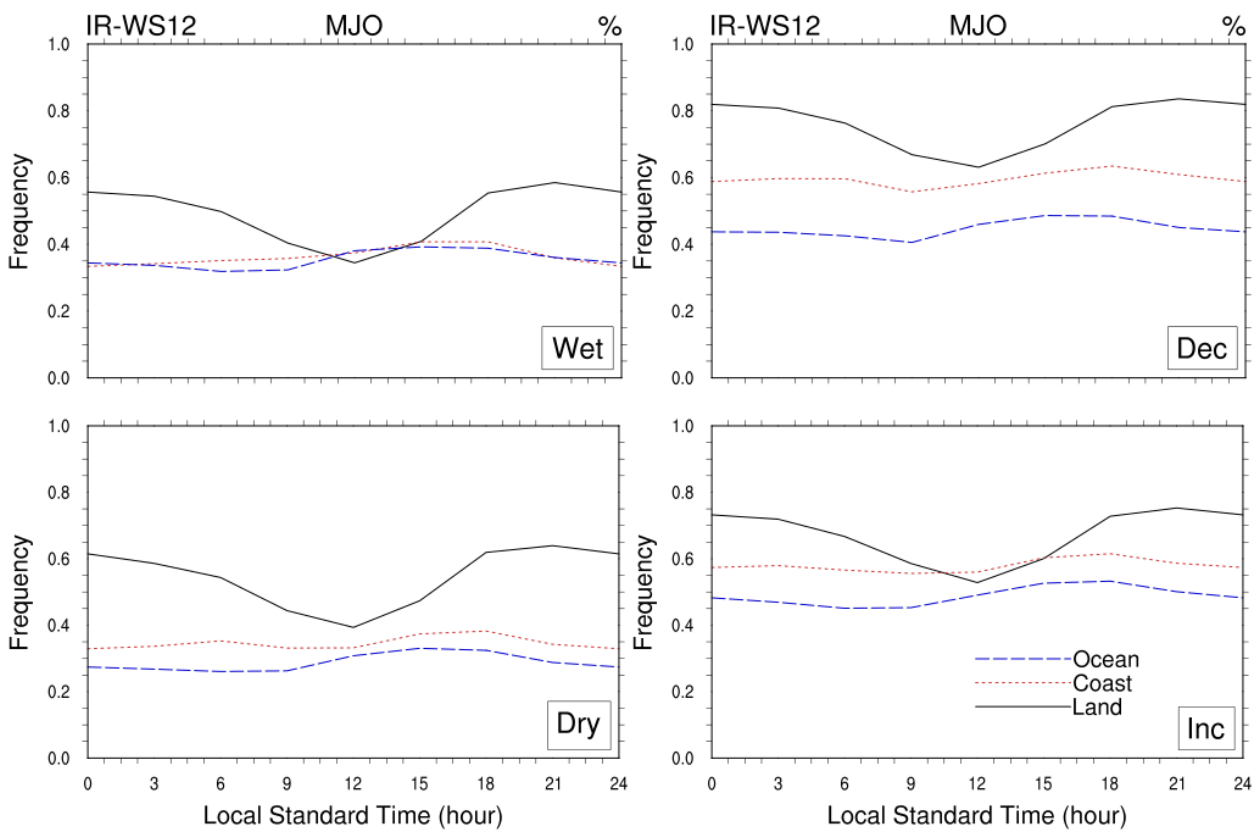
Figure 41. The diurnal mean IR-WS12 during MJO wet, dry, increasing and decreasing wave phases.
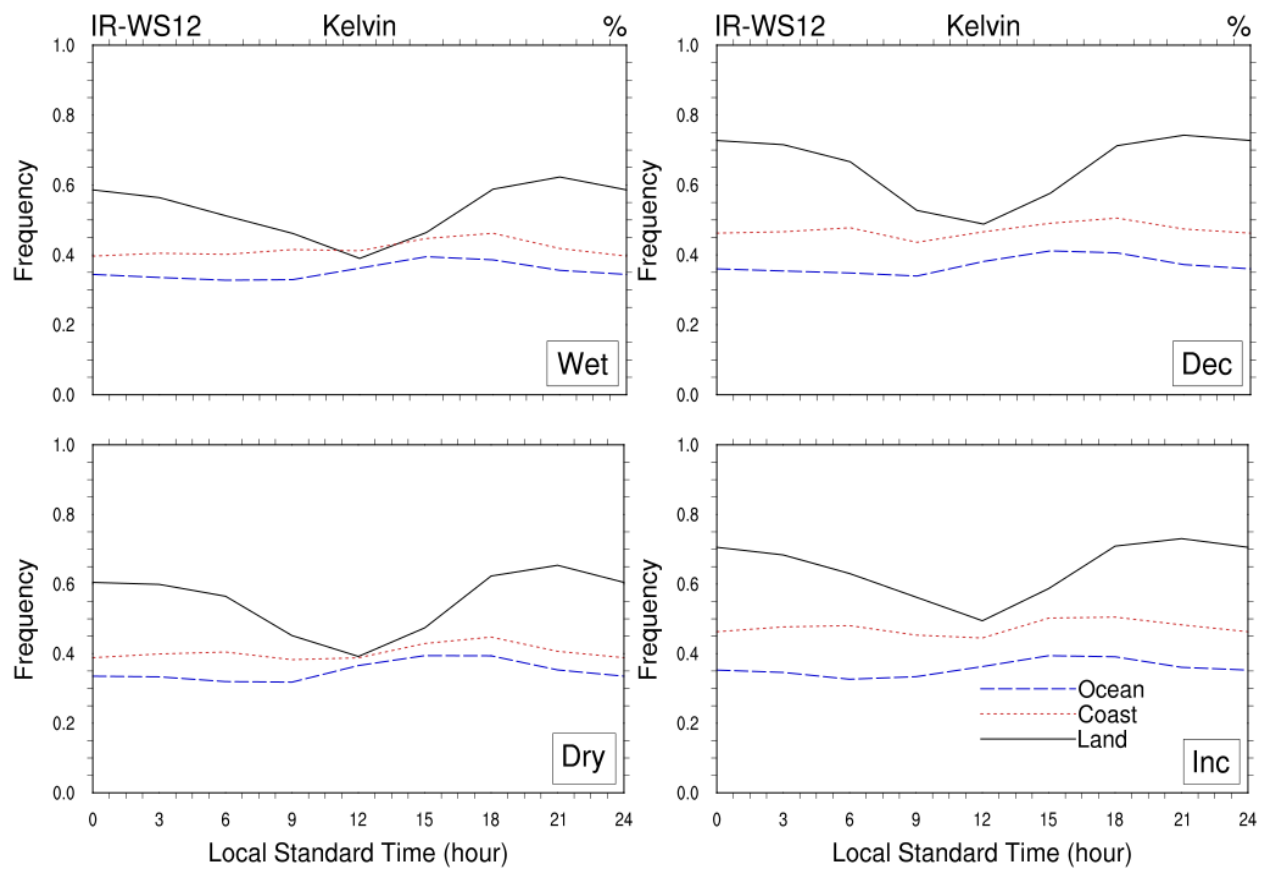
Figure 42. As in Fig. 41, but for IR-WS12 during Kelvin wave phases
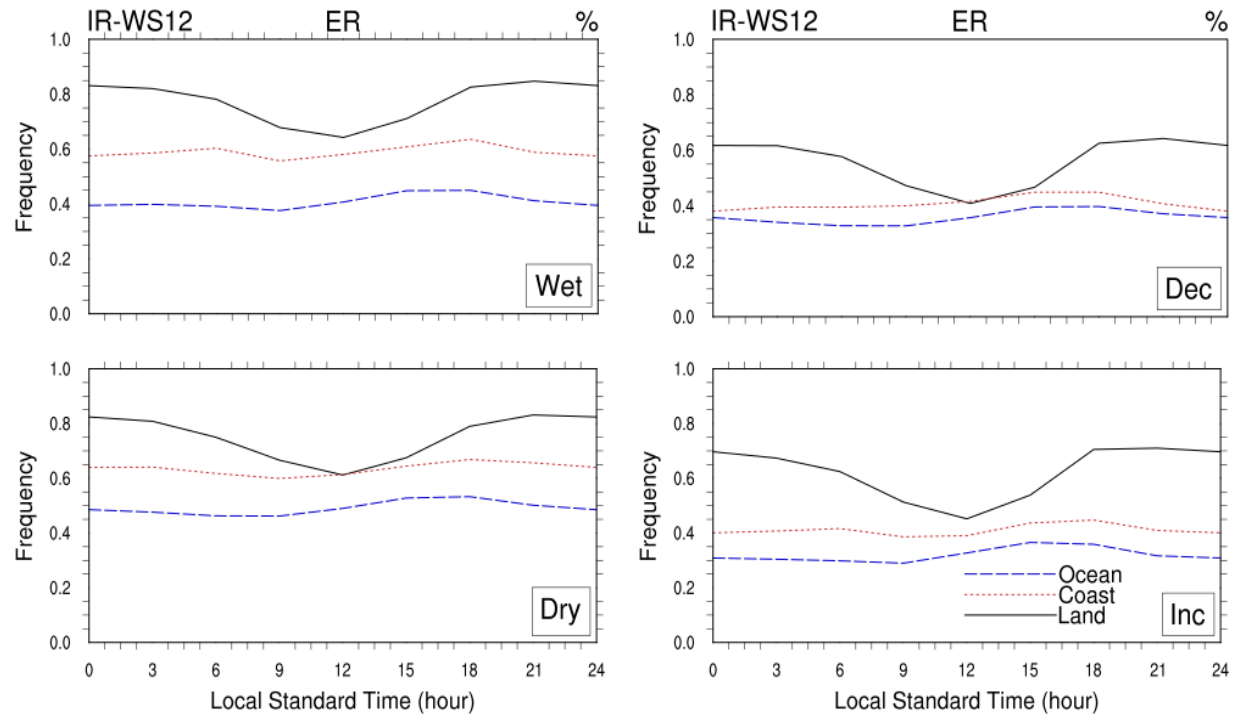
Figure 43. As in Fig. 41, but for IR-WS12 during ER wave phases
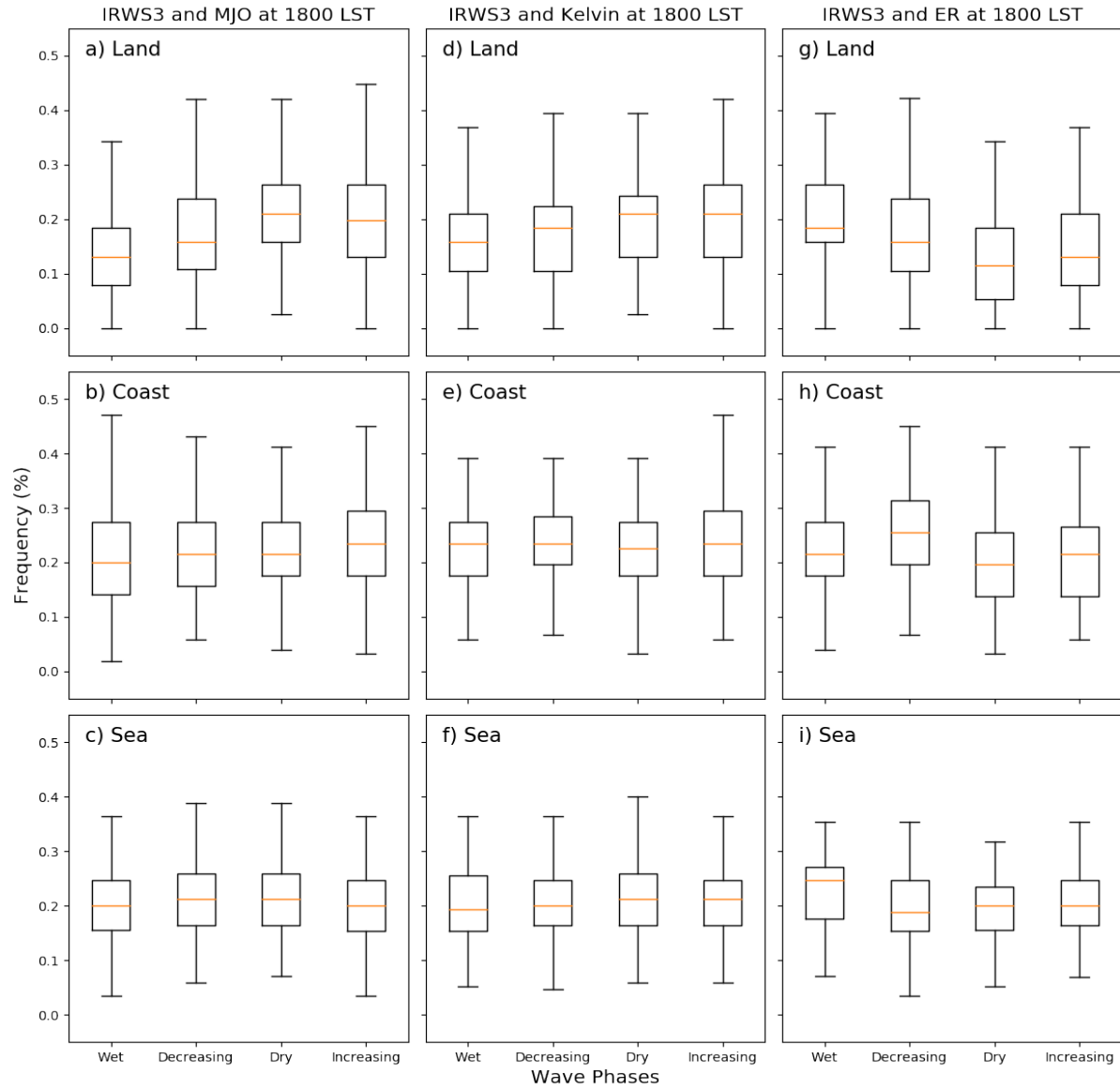
Figure 44. Box plots of MJO, Kelvin wave, and ER wave phases interaction with shallow convection (IR-WS3) at 1800 LST during DJF over the Maritime Continent.
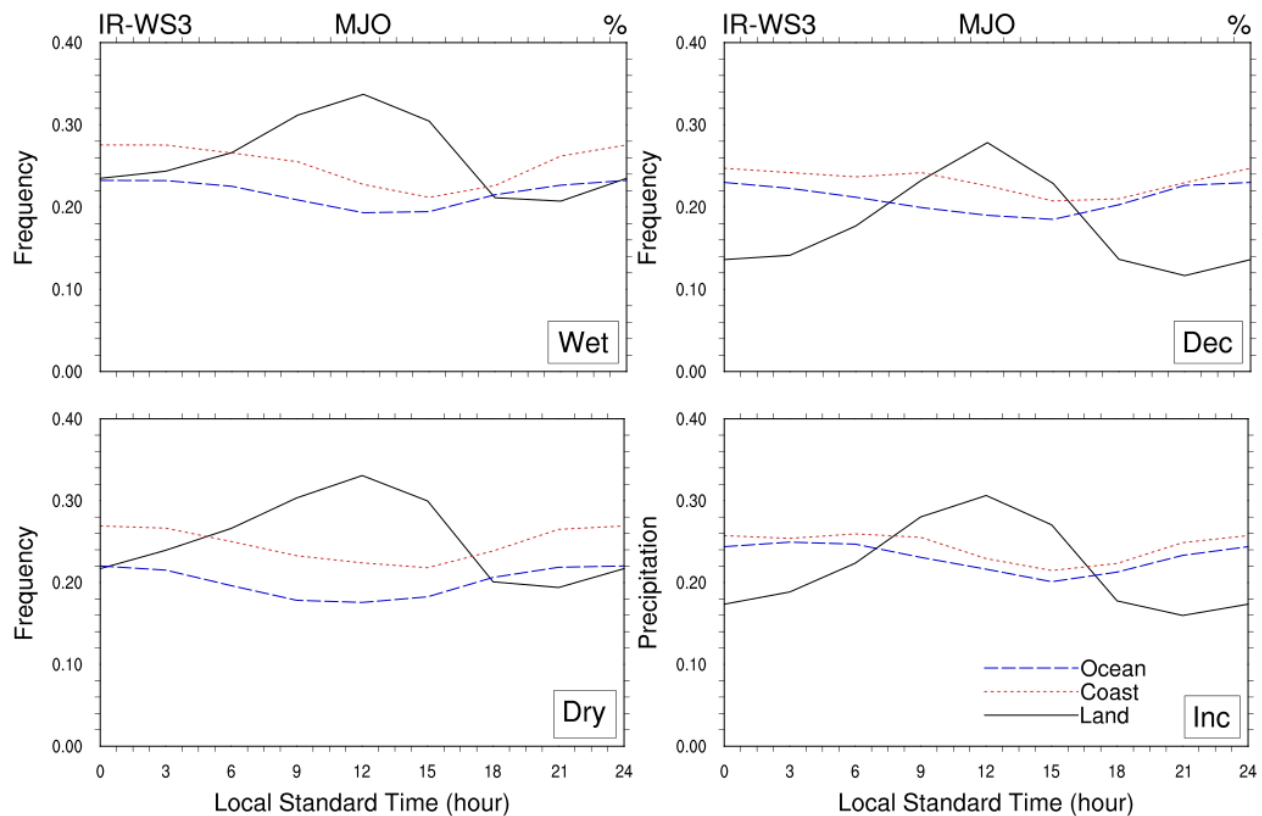
Figure 45. The diurnal mean IR-WS3 during MJO wet, dry, increasing and decreasing wave
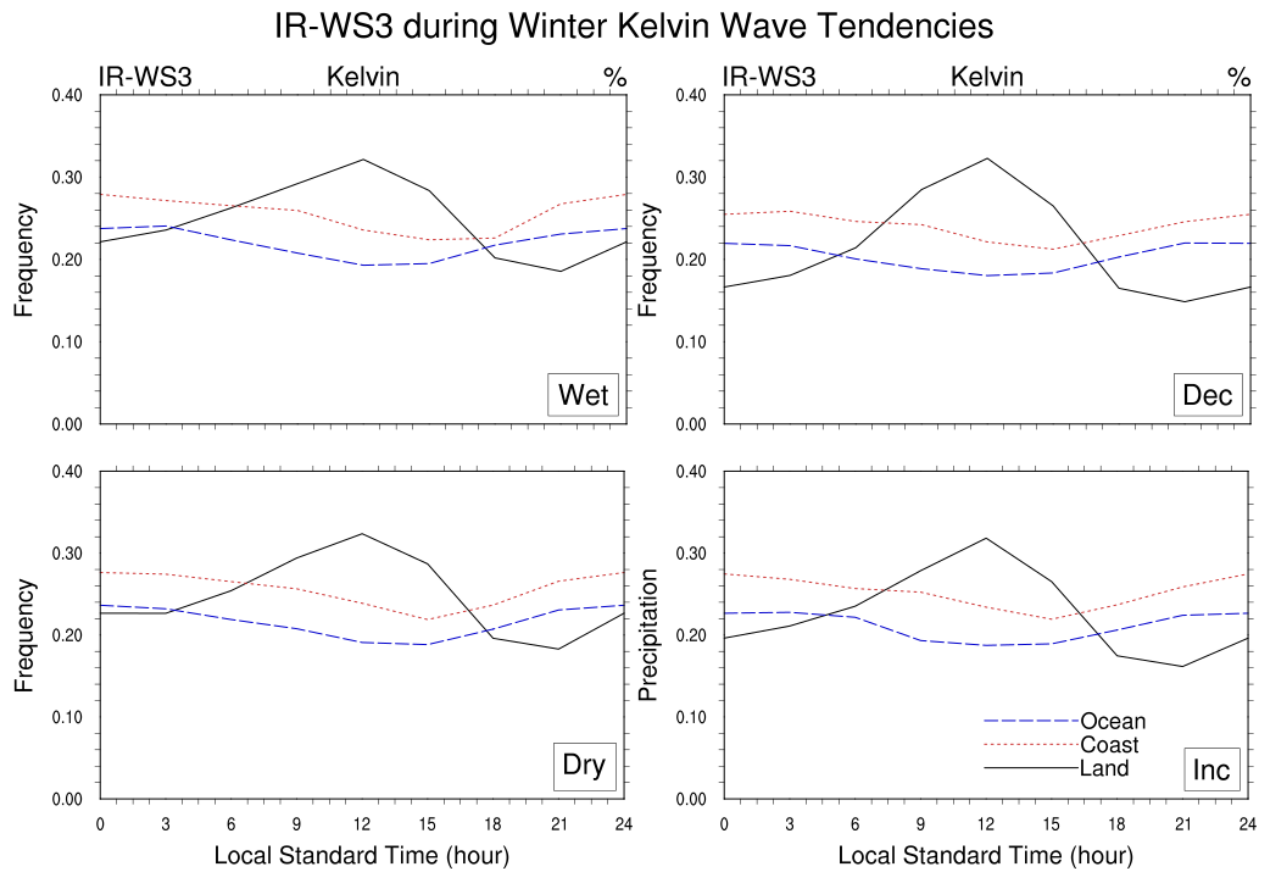
phases.

Figure 46. As in Fig. 41, but for IR-WS3 during Kelvin wave phases
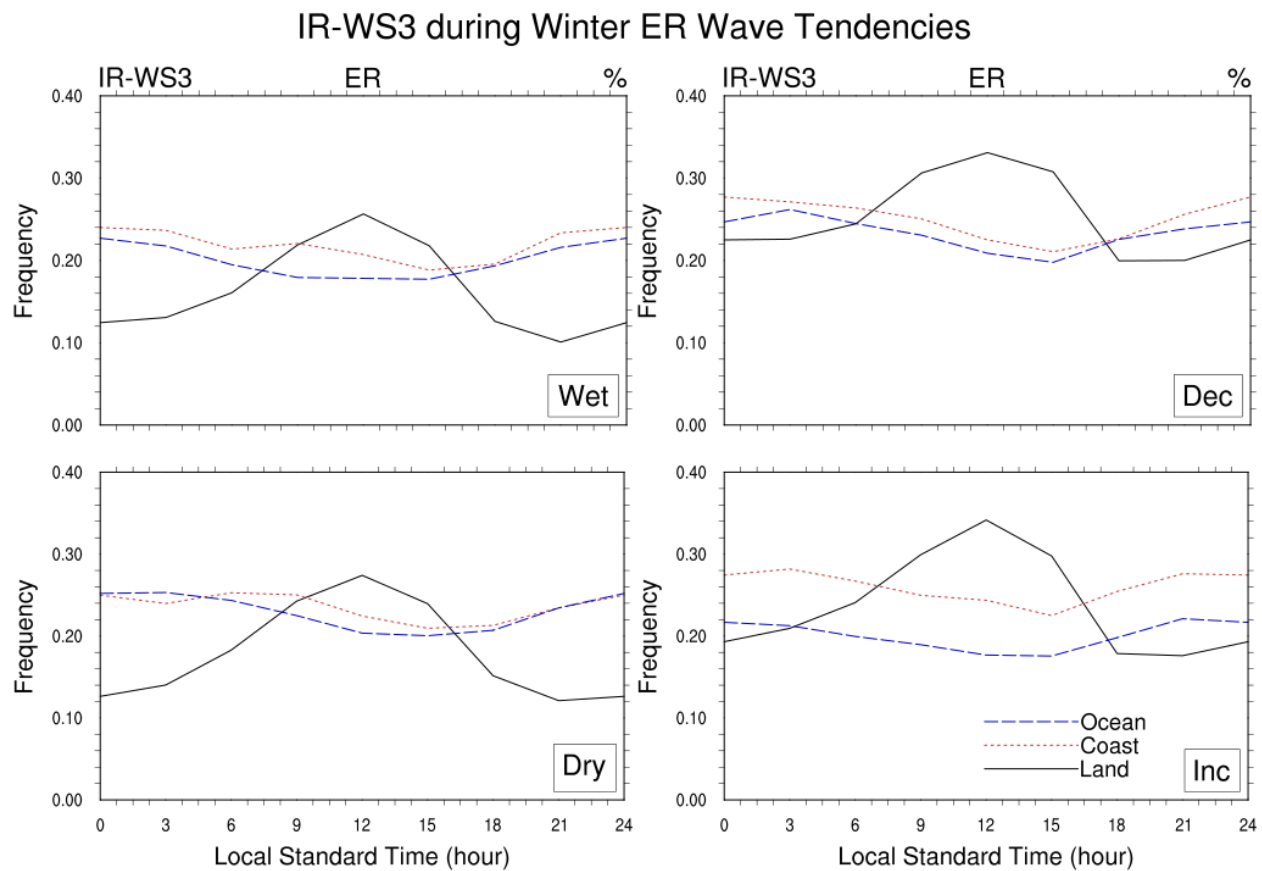
Figure 47. As in Fig. 41, but for IR-WS3 during ER wave phases

CHAPTER 5
Conclusion and Recommendation

The diurnal cycle of rainfall and convection over the MC is considered to be one of the strongest in tropics. Diurnal variability of rainfall is higher over land than offshore regions, rainfall peaks late in the afternoon and in the morning over land and ocean regions, respectively. The afternoon peak over land attributed to noon surface heating. Similarly, well-organized deep convection peaks approximately the same time as rainfall in the afternoon (over land) and the morning (over offshore). However, non-organized scattered convection peaks over land around noon local time, when deep convection and rainfall is less. The scattered convection shows a substantial frequency of occurrence over coast and ocean regions early in the morning. Understanding what determines the diurnal variability of rainfall and convection in addition to topography, is essential in improved numerical weather prediction. Previous studies suggest the diurnal cycle may influence by equatorial bound intraseasonal and synoptic modes of tropical variabilities.

Large scale tropical atmospheric wave modes influence the amplitude and phase of the diurnal cycle over the MC. These wave modes are intraseasonal variability (MJO) and synoptic-scale variability (Kelvin and ER waves). The MJO does not modulate rainfall over land in the morning, but it moderately modulates it in the afternoon. Over coast and ocean, rain slightly enhanced during MJO phase 4 in the morning. Well-organized deep convection (IR-WS12) somewhat increases in frequency in the afternoon over land and coast during phase 4. However, over coast and ocean scattered convection (IR-WS3) does not have significant variability in the morning and afternoon. Rather it shows slightly higher frequency during phases 1 and 8 in the morning and phases 2 and 6 in the afternoon.

The wave phases influence on rainfall and convection presents an interesting story. The MJO wet wave phase exerted significant enhancement to rainfall over the MC than other phases of Kelvin and ER waves. Over land deep convection enhanced by dry and increasing wave phases of the MJO and Kelvin waves while it influenced by wet and decreasing phases of ER. The MJO and ER wave enhanced deep convection over the coast and ocean as did on land. However, deep convection over coast and ocean seems not influenced by Kelvin wave phases. Scattered convection does not influence by the MJO, Kelvin wave, and ER wave phases like rainfall and convection over the MC. The MJO phases and wave phases show rainfall and convection significantly enhanced over coast compare to land and ocean regions.

In the interest of improving a sub-seasonal to seasonal prediction of rainfall, convection, and different scale variabilities, it is essential to understand the interaction between these variabilities. The modulation of the diurnal cycle by the MJO and CCEWs presence over the MC explained in this study. Further, there needs to be a study on the impact of the diurnal cycle on the MJO and CCEWs.

References

Barnes, H. C., & Houze Jr, R. A. (2013). The precipitating cloud population of the Madden-Julian Oscillation over the Indian and west Pacific Oceans. *Journal of Geophysical Research: Atmospheres, 118*(13), 6996-7023.

Birch, C., Webster, S., Peatman, S., Parker, D., Matthews, A., Li, Y., & Hassim, M. (2016). Scale interactions between the MJO and the western Maritime Continent. *Journal of Climate, 29*(7), 2471-2492.

Chang, A., Chiu, L., & Yang, G. (1995). Diurnal cycle of oceanic precipitation from SSM/I data. *Monthly Weather Review, 123*(11), 3371-3380.

Chang, C.-P., Lu, M.-M., & Lim, H. (2016). Monsoon convection in the maritime continent: interaction of large-scale motion and complex terrain. *Meteorological Monographs, 56*, 6.1-6.29.

Chen, S. S., & Houze, R. A. (1997). Diurnal variation and life-cycle of deep convective systems over the tropical Pacific warm pool. *Quarterly Journal of the Royal Meteorological Society, 123*(538), 357-388.

Collier, J. C., & Bowman, K. P. (2004). Diurnal cycle of tropical precipitation in a general circulation model. *Journal of Geophysical Research: Atmospheres, 109*(D17).

Fujita, M., Yoneyama, K., Mori, S., Nasuno, T., & Satoh, M. (2011). Diurnal convection peaks over the eastern Indian Ocean off Sumatra during different MJO phases. *Journal of the Meteorological Society of Japan. Ser. II, 89*, 317-330.

Gottschalck, J., Roundy, P. E., Schreck III, C. J., Vintzileos, A., & Zhang, C. (2013). Large-scale atmospheric and oceanic conditions during the 2011–12 DYNAMO field campaign. *Monthly Weather Review, 141*(12), 4173-4196.

Gottschalck, J., Wheeler, M., Weickmann, K., Vitart, F., Savage, N., Lin, H., . . . Nakagawa, M. (2010). A framework for assessing operational Madden–Julian oscillation forecasts: A CLIVAR MJO working group project. *Bulletin of the American Meteorological Society, 91*(9), 1247-1258.

Hagos, S. M., Zhang, C., Feng, Z., Burleyson, C. D., De Mott, C., Kerns, B., . . . Martini, M. N. (2016). The impact of the diurnal cycle on the propagation of M adden-J ulian O scillation convection across the M aritime C ontinent. *Journal of Advances in Modeling Earth Systems, 8*(4), 1552-1564.

Hendon, H. H., & Salby, M. L. (1994). The life cycle of the Madden–Julian oscillation. *Journal of the Atmospheric Sciences, 51*(15), 2225-2237.

Hoaglin, D. C., Mosteller, F., & Tukey, J. W. (2009). *Fundamentals of exploratory analysis of variance* (Vol. 367): John Wiley & Sons.

Holton, J. R. (1973). An introduction to dynamic meteorology. *American Journal of Physics, 41*(5), 752-754.

Holton, J. R., & Lindzen, R. S. (1968). A note on Kelvin waves in the atmosphere. *Mon. Wea. Rev, 96*(6), 385-386.

Houze Jr, R. A., Rasmussen, K. L., Zuluaga, M. D., & Brodzik, S. R. (2015). The variable nature of convection in the tropics and subtropics: A legacy of 16 years of the Tropical Rainfall Measuring Mission satellite. *Reviews of Geophysics, 53*(3), 994-1021.

Huffman, G. J., Bolvin, D. T., Nelkin, E. J., Wolff, D. B., Adler, R. F., Gu, G., . . . Stocker, E. F. (2007). The TRMM multisatellite precipitation analysis (TMPA): Quasi-global, multiyear, combined-sensor precipitation estimates at fine scales. *Journal of hydrometeorology, 8*(1), 38-55.

Hung, M.-P., Lin, J.-L., Wang, W., Kim, D., Shinoda, T., & Weaver, S. J. (2013). MJO and convectively coupled equatorial waves simulated by CMIP5 climate models. *Journal of Climate, 26*(17), 6185-6214.

Inness, P. M., & Slingo, J. M. (2006). The interaction of the Madden–Julian oscillation with the maritime continent in a GCM. *Quarterly Journal of the Royal Meteorological Society: A journal of the atmospheric sciences, applied meteorology and physical oceanography, 132*(618), 1645-1667.

Jakob, C., & Tselioudis, G. (2003). Objective identification of cloud regimes in the tropical western Pacific. *Geophysical Research Letters, 30*(21).

Janiga, M. A., J. Schreck III, C., Ridout, J. A., Flatau, M., Barton, N. P., Metzger, E. J., & Reynolds, C. A. (2018). Subseasonal forecasts of convectively coupled equatorial waves and the MJO: Activity and predictive skill. *Monthly Weather Review, 146*(8), 2337-2360.

Janiga, M. A., & Thorncroft, C. D. (2016). The influence of African easterly waves on convection over tropical Africa and the east Atlantic. *Monthly Weather Review, 144*(1), 171-192.

Joseph, S., Sahai, A., & Goswami, B. (2009). Eastward propagating MJO during boreal summer and Indian monsoon droughts. *Climate Dynamics, 32*(7-8), 1139-1153.

Kikuchi, K., & Wang, B. (2008). Diurnal precipitation regimes in the global tropics. *Journal of Climate, 21*(11), 2680-2696.

Kiladis, G. N., Thorncroft, C. D., & Hall, N. M. (2006). Three-dimensional structure and dynamics of African easterly waves. Part I: Observations. *Journal of the Atmospheric Sciences, 63*(9), 2212-2230.

Kiladis, G. N., Wheeler, M. C., Haertel, P. T., Straub, K. H., & Roundy, P. E. (2009). Convectively coupled equatorial waves. *Reviews of Geophysics, 47*(2).

Kim, D., Sperber, K., Stern, W., Waliser, D., Kang, I.-S., Maloney, E., . . . Khairoutdinov, M. (2009). Application of MJO simulation diagnostics to climate models. *Journal of Climate, 22*(23), 6413-6436.

Kim, J.-E., & Alexander, M. J. (2013). Tropical precipitation variability and convectively coupled equatorial waves on submonthly time scales in reanalyses and TRMM. *Journal of Climate, 26*(10), 3013-3030.

Kummerow, C., Barnes, W., Kozu, T., Shiue, J., & Simpson, J. (1998). The tropical rainfall measuring mission (TRMM) sensor package. *Journal of atmospheric and oceanic technology, 15*(3), 809-817.

Lavender, S. L., & Matthews, A. J. (2009). Response of the West African monsoon to the Madden–Julian oscillation. *Journal of Climate, 22*(15), 4097-4116.

Lin, X., Randall, D. A., & Fowler, L. D. (2000). Diurnal variability of the hydrologic cycle and radiative fluxes: Comparisons between observations and a GCM. *Journal of Climate, 13*(23), 4159-4179.

Lin, Y.-L. (2007). *Mesoscale dynamics*: Cambridge University Press.

Liu, C., & Zipser, E. J. (2005). Global distribution of convection penetrating the tropical tropopause. *Journal of Geophysical Research: Atmospheres, 110*(D23).

Liu, C., & Zipser, E. J. (2008). Diurnal cycles of precipitation, clouds, and lightning in the tropics from 9 years of TRMM observations. *Geophysical Research Letters, 35*(4).

Liu, C., & Zipser, E. J. (2009). "Warm rain" in the tropics: Seasonal and regional distributions based on 9 yr of TRMM data. *Journal of Climate, 22*(3), 767-779.

Liu, C., Zipser, E. J., Cecil, D. J., Nesbitt, S. W., & Sherwood, S. (2008). A cloud and

    precipitation feature database from nine years of TRMM observations. *Journal of Applied*

    Meteorology and Climatology, 47(10), 2712-2728.

Lorenz, D. J., & Hartmann, D. L. (2006). The effect of the MJO on the North American

    monsoon. *Journal of Climate, 19*(3), 333-343.

Love, B. S., Matthews, A. J., & Lister, G. M. (2011). The diurnal cycle of precipitation over the

    Maritime Continent in a high-resolution atmospheric model. *Quarterly Journal of the*

    Royal Meteorological Society, 137(657), 934-947.

Madden, R. A., & Julian, P. R. (1971). Detection of a 40–50 day oscillation in the zonal wind in

    the tropical Pacific. *Journal of the Atmospheric Sciences, 28*(5), 702-708.

Madden, R. A., & Julian, P. R. (1972). Description of global-scale circulation cells in the tropics

    with a 40–50 day period. *Journal of the Atmospheric Sciences, 29*(6), 1109-1123.

Madden, R. A., & Julian, P. R. (1994). Observations of the 40–50-day tropical oscillation—A

    review. *Monthly Weather Review, 122*(5), 814-837.

Majda, A. J., & Yang, Q. (2016). A multiscale model for the intraseasonal impact of the diurnal

    cycle over the Maritime Continent on the Madden–Julian oscillation. *Journal of the*

    Atmospheric Sciences, 73(2), 579-604.

Mapes, B. E., Warner, T. T., & Xu, M. (2003). Diurnal patterns of rainfall in northwestern South

    America. Part III: Diurnal gravity waves and nocturnal convection offshore. *Monthly*

    Weather Review, 131(5), 830-844.

Matsuno, T. (1966). Quasi-geostrophic motions in the equatorial area. *Journal of the*

    Meteorological Society of Japan. Ser. II, 44(1), 25-43.

Mekonnen, A., & Rossow, W. B. (2011). The interaction between deep convection and easterly waves over tropical North Africa: A weather state perspective. *Journal of Climate, 24*(16), 4276-4294.

Mekonnen, A., & Rossow, W. B. (2018). The interaction between deep convection and easterly wave activity over Africa: Convective transitions and mechanisms. *Monthly Weather Review, 146*(6), 1945-1961.

Mohr, K. I., & Zipser, E. J. (1996). Mesoscale convective systems defined by their 85-GHz ice scattering signature: Size and intensity comparison over tropical oceans and continents. *Monthly Weather Review, 124*(11), 2417-2437.

Mori, S., Hamada, J.-I., Sakurai, N., Fudeyasu, H., Kawashima, M., Hashiguchi, H., . . . Matsumoto, J. (2011). Convective systems developed along the coastline of Sumatera Island, Indonesia, observed with an X-band Doppler radar during the HARIMAU2006 campaign. *Journal of the Meteorological Society of Japan. Ser. II, 89*, 61-81.

Mori, S., Jun-Ichi, H., Tauhid, Y. I., Yamanaka, M. D., Okamoto, N., Murata, F., . . . Sribimawati, T. (2004). Diurnal land–sea rainfall peak migration over Sumatera Island, Indonesian Maritime Continent, observed by TRMM satellite and intensive rawinsonde soundings. *Monthly Weather Review, 132*(8), 2021-2039.

NCL. (2015). The NCAR Command Language (Version 6.3. 0)[Software].

Neale, R., & Slingo, J. (2003). The Maritime Continent and its role in the global climate: A GCM study. *Journal of Climate, 16*(5), 834-848.

Nesbitt, S. W., & Zipser, E. J. (2003). The diurnal cycle of rainfall and convective intensity according to three years of TRMM measurements. *Journal of Climate, 16*(10), 1456-1475.

Nesbitt, S. W., Zipser, E. J., & Cecil, D. J. (2000). A census of precipitation features in the tropics using TRMM: Radar, ice scattering, and lightning observations. *Journal of Climate, 13*(23), 4087-4106.

Nitta, T., & Sekine, S. (1994). Diurnal variation of convective activity over the tropical western Pacific. *Journal of the Meteorological Society of Japan. Ser. II, 72*(5), 627-641.

Ohsawa, T., Ueda, H., Hayashi, T., Watanabe, A., & Matsumoto, J. (2001). Diurnal variations of convective activity and rainfall in tropical Asia. *Journal of the Meteorological Society of Japan. Ser. II, 79*(1B), 333-352.

Ramage, C. S. (1971). *Monsoon meteorology*. Retrieved from

Reed, R. J., & Recker, E. E. (1971). Structure and properties of synoptic-scale wave disturbances in the equatorial western Pacific. *Journal of the Atmospheric Sciences, 28*(7), 1117-1133.

Riley, E. M., Mapes, B. E., & Tulich, S. N. (2011). Clouds associated with the Madden–Julian oscillation: A new perspective from CloudSat. *Journal of the Atmospheric Sciences, 68*(12), 3032-3051.

Rossow, W. B., Mekonnen, A., Pearl, C., & Goncalves, W. (2013). Tropical precipitation extremes. *Journal of Climate, 26*(4), 1457-1466.

Rossow, W. B., & Schiffer, R. A. (1991). ISCCP cloud data products. *Bulletin of the American Meteorological Society*.

Rossow, W. B., & Schiffer, R. A. (1999). Advances in understanding clouds from ISCCP. *Bulletin of the American Meteorological Society, 80*(11), 2261-2288.

Rossow, W. B., Tselioudis, G., Polak, A., & Jakob, C. (2005). Tropical climate described as a distribution of weather states indicated by distinct mesoscale cloud property mixtures. *Geophysical Research Letters, 32*(21).

Roundy, P. E. (2008). Analysis of convectively coupled Kelvin waves in the Indian Ocean MJO. *Journal of the Atmospheric Sciences, 65*(4), 1342-1359.

Roundy, P. E., & Frank, W. M. (2004). A climatology of waves in the equatorial region. *Journal of the Atmospheric Sciences, 61*(17), 2105-2132.

Rui, H., & Wang, B. (1990). Development characteristics and dynamic structure of tropical intraseasonal convection anomalies. *Journal of the Atmospheric Sciences, 47*(3), 357-379.

Sakaeda, N., Kiladis, G., & Dias, J. (2017). The diurnal cycle of tropical cloudiness and rainfall associated with the Madden–Julian oscillation. *Journal of Climate, 30*(11), 3999-4020.

Sakaeda, N., Powell, S. W., Dias, J., & Kiladis, G. N. (2018). The diurnal variability of precipitating cloud populations during DYNAMO. *Journal of the Atmospheric Sciences, 75*(4), 1307-1326.

Sato, T., Miura, H., Satoh, M., Takayabu, Y. N., & Wang, Y. (2009). Diurnal cycle of precipitation in the tropics simulated in a global cloud-resolving model. *Journal of Climate, 22*(18), 4809-4826.

Schreck III, C. J. (2015). Kelvin waves and tropical cyclogenesis: A global survey. *Monthly Weather Review, 143*(10), 3996-4011.

Schreck III, C. J., & Molinari, J. (2011). Tropical cyclogenesis associated with Kelvin waves and the Madden–Julian oscillation. *Monthly Weather Review, 139*(9), 2723-2734.

Schreck III, C. J., Molinari, J., & Aiyyer, A. (2012). A global view of equatorial waves and tropical cyclogenesis. *Monthly Weather Review, 140*(3), 774-788.

Schreck III, C. J., Molinari, J., & Mohr, K. I. (2011). Attributing tropical cyclogenesis to equatorial waves in the western North Pacific. *Journal of the Atmospheric Sciences, 68*(2), 195-209.

Schreck III, C. J., Shi, L., Kossin, J. P., & Bates, J. J. (2013). Identifying the MJO, equatorial waves, and their impacts using 32 years of HIRS upper-tropospheric water vapor. *Journal of Climate, 26*(4), 1418-1431.

Schumacher, C., & Houze Jr, R. A. (2003). Stratiform rain in the tropics as seen by the TRMM precipitation radar. *Journal of Climate, 16*(11), 1739-1756.

Singh, M., & Bhatla, R. (2019). Modulation of active-break spell of Indian summer monsoon by Madden Julian Oscillation. *Journal of Earth System Science, 128*(3), 70.

Sobel, A. H., Burleyson, C., & Yuter, S. (2011). Rain on small tropical islands. *Journal of Geophysical Research: Atmospheres, 116*(D8).

Sorooshian, S., Gao, X., Hsu, K., Maddox, R., Hong, Y., Gupta, H. V., & Imam, B. (2002). Diurnal variability of tropical rainfall retrieved from combined GOES and TRMM satellite information. *Journal of Climate, 15*(9), 983-1001.

Straub, K. H. (2013). MJO initiation in the real-time multivariate MJO index. *Journal of Climate, 26*(4), 1130-1151.

Straub, K. H., & Kiladis, G. N. (2003). Interactions between the boreal summer intraseasonal oscillation and higher-frequency tropical wave activity. *Monthly Weather Review, 131*(5), 945-960.

Takayabu, Y. N., & Kimoto, M. (2008). Diurnal march of rainfall simulated in a T106 AGCM and dependence on cumulus schemes. *Journal of the Meteorological Society of Japan. Ser. II, 86*, 163-173.

Tan, J., & Jakob, C. (2013). A three-hourly data set of the state of tropical convection based on cloud regimes. *Geophysical Research Letters, 40*(7), 1415-1419.

Teng, H., & Wang, B. (2003). Interannual variations of the boreal summer intraseasonal oscillation in the Asian–Pacific region. *Journal of Climate, 16*(22), 3572-3584.

Thayer-Calder, K., & Randall, D. A. (2009). The role of convective moistening in the Madden–Julian oscillation. *Journal of the Atmospheric Sciences, 66*(11), 3297-3312.

Thompson Jr, R. M., Payne, S. W., Recker, E. E., & Reed, R. J. (1979). Structure and properties of synoptic-scale wave disturbances in the intertropical convergence zone of the eastern Atlantic. *Journal of the Atmospheric Sciences, 36*(1), 53-72.

Tromeur, E., & Rossow, W. B. (2010). Interaction of tropical deep convection with the large-scale circulation in the MJO. *Journal of Climate, 23*(7), 1837-1853.

Tukey, J. W. (1977). Some thoughts on clinical trials, especially problems of multiplicity. *Science, 198*(4318), 679-684.

UCAR/COMET. (2017). MJO, Equatorial Waves, and Tropical Cyclogenesis. Retrieved from https://www.meted.ucar.edu/tropical/synoptic/MJO_EqWaves/print.htm

UCAR/NCAR/CISL/VETS. (2017). The NCAR Command Language (Version 6.4.0) [Software], http://dx.doi.org/10.5065/D6WD3XH5.

Van Der Linden, R., Fink, A. H., Pinto, J. G., Phan-Van, T., & Kiladis, G. N. (2016). Modulation of daily rainfall in southern Vietnam by the Madden–Julian oscillation and convectively coupled equatorial waves. *Journal of Climate, 29*(16), 5801-5820.

Van Rossum, G., & Drake Jr, F. L. (1995). *Python reference manual*: Centrum voor Wiskunde en Informatica Amsterdam.

Virts, K. S., Wallace, J. M., Hutchins, M. L., & Holzworth, R. H. (2013). Diurnal lightning

variability over the Maritime Continent: Impact of low-level winds, cloudiness, and the

MJO. *Journal of the Atmospheric Sciences, 70*(10), 3128-3146.

Wang, B., & Liu, F. (2011). A model for scale interaction in the Madden–Julian oscillation.

Journal of the Atmospheric Sciences, 68(11), 2524-2536.

Weaver, S. J., Wang, W., Chen, M., & Kumar, A. (2011). Representation of MJO variability in

the NCEP Climate Forecast System. *Journal of Climate, 24*(17), 4676-4694.

Wheeler, M., & Kiladis, G. N. (1999). Convectively coupled equatorial waves: Analysis of

clouds and temperature in the wavenumber–frequency domain. *Journal of the

Atmospheric Sciences, 56*(3), 374-399.

Wheeler, M., Kiladis, G. N., & Webster, P. J. (2000). Large-scale dynamical fields associated

with convectively coupled equatorial waves. *Journal of the Atmospheric Sciences, 57*(5),

613-640.

Wheeler, M., & Weickmann, K. M. (2001). Real-time monitoring and prediction of modes of

coherent synoptic to intraseasonal tropical variability. *Monthly Weather Review, 129*(11),

2677-2694.

Wheeler, M. C., & Hendon, H. H. (2004). An all-season real-time multivariate MJO index:

Development of an index for monitoring and prediction. *Monthly Weather Review,

132*(8), 1917-1932.

Wilks, D. S. (2011). *Statistical methods in the atmospheric sciences* (Vol. 100): Academic press.

Willmott, C. J., Robeson, S. M., & Matsuura, K. (2007). Geographic box plots. *Physical

Geography, 28*(4), 331-344.

Worku, L. Y., Mekonnen, A., & Schreck III, C. J. (2019). Diurnal cycle of rainfall and convection over the Maritime Continent using TRMM and ISCCP. *International Journal of Climatology, 39*(13), 5191-5200.

Wu, C.-H., & Hsu, H.-H. (2009). Topographic influence on the MJO in the Maritime Continent. *Journal of Climate, 22*(20), 5433-5448.

Yang, G.-Y., & Slingo, J. (2001). The diurnal cycle in the tropics. *Monthly Weather Review, 129*(4), 784-801.

Yokoi, S., Mori, S., Katsumata, M., Geng, B., Yasunaga, K., Syamsudin, F., . . . Yoneyama, K. (2017). Diurnal cycle of precipitation observed in the western coastal area of Sumatra Island: offshore preconditioning by gravity waves. *Monthly Weather Review, 145*(9), 3745-3761.

Zhang, C. (2005). Madden-julian oscillation. *Reviews of Geophysics, 43*(2).